Exploring the Cell-Specific Role of Serotonin 2B in Regulating Fibrosis Following Myocardial Infarction

By

John Caleb Snider

Dissertation

Submitted to the Faculty of the

Graduate School of Vanderbilt University

in partial fulfillment of the requirements

for the degree of

DOCTOR OF PHILOSOPHY

In

Biomedical Engineering

October 31, 2020

Approved by:

W. David Merryman, PhD

Hind Lal, PhD

Antonis Hatzopoulos, PhD

Cynthia Reinhart-King, PhD

Todd Giorgio, PhD

ACKNOWLEDGEMENTS

I was only able to accomplish this work with the invaluable help of many mentors, coworkers, friends, family, and funding agencies. I want to acknowledge all of the coauthors on the manuscript adapted to for this dissertation. I would primarily like to acknowledge my advisor, Dave Merryman. He created a lab environment in which I was able to thrive. His enthusiasm and confidence encouraged me to persevere, and he granted me the independence to develop into a capable scientist. I want to acknowledge all of my fellow lab members which I had the pleasure of overlapping with. Y'all made the long hours and hard work enjoyable, kept the mood light, and provided scientific support and friendship throughout this journey.

I would like to acknowledge Vanderbilt University, the National Heart, Lung, and Blood Institute, the Fondation Leducq, and the American Heart Association for providing the funding and infrastructure to make this work possible. I would like to thank each member of my dissertation committee for the support and guidance provided throughout my studies.

I want to thank my parents for instilling in me the desire to learn. Because of those 3 years of self-guided study (homeschooling), I learned how to learn, and that equipped me with the foundation to be molded into an independent scientist. The love and support of my family never lacked or faded, I never lacked encouragement or the freedom to discover, and for that, I am exceedingly grateful.

Most importantly, I want to thank my wife, Beth. Even after getting the first year of graduate school preview, you still agreed to marry me. You were by my side this entire time. You loved, nurtured, and encouraged me. You also did more than your fair share of tolerating late nights, jargon-filled ramblings, and stress. You gave us Finley. You brought me joy. I love you.

"Men became scientific because they expected law in nature, and they expected Law in nature because they believed in a Legislator." – C. S. Lewis

TABLE OF CONTENTS

LIST OF TABLES

Table **Page**

LIST OF FIGURES

Figures **Page**

LIST OF ABBREVIATIONS

Abbreviations and Key Terms	Definition and relevance to thesis work
5-HT$_{2B}$	Serotonin 2B receptor
5-HT	Serotonin
ACEi	Angiotensin converting enzyme inhibitor
AFM	Atomic force microscopy
AngII	Angiotensin II
ARB	AT$_1$R blocker
AT$_1$R	Angiotensin II receptor type 1
BMPRII	Bone morphogenetic protein receptor II
BrdU	5-bromo-2-deoxyuridine – nucleotide analog to identify mitotic cells
BW723C86	5-HT$_{2B}$ agonist
BZ	Border zone – transition region between scar tissue and viable myocardium
CDF	Cumulative distribution function
CF	Cardiac fibroblast
DMSO	Dimethyl sulfoxide – used as solvent for drug studies
DOCA	Deoxycorticosterone – agent used to induce vascular injury
ECM	Extracellular matrix
EF	Ejection fraction
ERK	Extracellular regulated kinase
FACS	Fluorescence-activated cell sorting
FOV	Field of view
FS	Fractional shortening
GO	Gene ontology
GLS	Global longitudinal strain – metric of cardiac contractility
GPCR	G protein-coupled receptor
Htr2b	Gene encoding 5-HT$_{2B}$
IL	Interleukin
LV	Left ventricle
LVID	Left ventricular inner dimension
LV Vol	Left ventricular volume
MCM	MerCreMer, recombinase activated in the presence of tamoxifen
MI	Myocardial infarction
MMP	Matrix metalloproteinase
Nppb	Natriuretic peptide B – RNA encoding marker of cardiomyocyte injury
PAC	Proangiogenic cell
PAH	Pulmonary arterial hypertension
PASMC	Pulmonary artery smooth muscle cell
PDGF	Platelet-derived growth factor
PEG400	Polyethylene glycol 400 – used as solvent for drug studies

PH	Pulmonary hypertension
Postn	Gene encoding periostin, a myofibroblast marker
PSR	Picrosirius red stain – stain used to identify ECM (red) vs. cytoplasm (yellow)
qPCR	Quantitative polymerase chain reaction
ROS	Reactive oxygen species
RS	RS*127445* – 5-HT_{2B} antagonist
RVSP	Right ventricular systolic pressure
SB	SB204741 – 5-HT_{2B} antagonist
SERT	5-HT transporter
SHG	Second harmonic generation – imaging modality for identification of collagen fibers
SHR	Spontaneously hypertensive rat – model of hypertension-induced cardiomyopathy
Tcf21	Transcription factor 21 – resident CF marker
TGFβ	Transforming growth factor β
WGA	Wheat germ agglutinin – stain to identify cardiomyocyte cell walls
WT	Wild type

Chapter 1

Introduction and Motivation

1.1 Cardiovascular disease burden

Cardiovascular disease is pervasive throughout the United States, affecting approximately 10% of individuals according to a 2017 National Health Interview Survey. It is the leading cause of mortality, contributing to more deaths than cancer [1]. The economic burden of cardiovascular disease accounts for approximately 2% of the GDP of the United States [2]. A significant subset within cardiovascular disease is ischemic heart disease, which most notably presents as a myocardial infarction (**MI**). It is estimated that the annual incidence of MI in Americans is over 800,000 [1]. However, mortality from acute MI has dropped dramatically in the past 40 years due to improvements in percutaneous coronary intervention [3]. Percutaneous coronary intervention has emerged as the dominant clinical approach to treating acute ST-elevated MI, and it functions to restore blood flow through the occluded vessel responsible for the ischemic event. A catheter is placed into the occluded vessel, a balloon is inflated to increase vessel diameter, and a stent is placed to maintain the vessel opening. Door-to-balloon time is a metric used to track how long from the onset of vessel occlusion until the vessel is reopened. Increases in door-to-balloon time are associated with increased infarct size, morbidity and mortality [4]. The recommended time is less than 90 minutes, creating a significant hurdle in patients without close proximity to a hospital [5].

Concerted effort has gone into salvaging myocardial tissue following MI due to the lack of intrinsic regenerative capability of cardiomyocytes. This deficiency paired with a higher survival rate from primary MI has resulted in a significant increase in heart failure prevalence.

Heart failure carries a high mortality rate along with significant social and economic costs. The chronic nature of heart failure amplifies a decreasing quality of life due to the constant reliance on medication and decreased physical capabilities [6], [7].

1.2 Tissue response to MI

MI is an ischemic injury most commonly caused by the rupture of an atherosclerotic plaque which is subsequently lodged in a coronary vessel. Lack of blood flow and oxygen to cardiomyocytes causes irreversible cardiac damage within minutes of the occlusive event [8]. The wound healing response post-MI aims to effectively remove damaged tissue and replace it with a fibrotic scar, while maximizing ventricular wall integrity and cardiac contractile function. This process occurs though two overlapping phases: an inflammatory phase and a reparative/proliferative phase (outlined in **Figure 1.1**) [9]. Rapid cell death instigates a dramatic inflammatory response during the first few days following MI. Various hematopoietic cells initiate a finely coordinated response to clear damaged cells, cellular debris, and extracellular matrix (**ECM**). Granulation tissue is formed to act as a scaffold for neovascularization and scar deposition. [10]–[12]. Since most cells do not survive the ischemic event, resident cardiac fibroblasts (**CFs**) from the border zone (**BZ**) of the injury rapidly proliferate and infiltrate within 3 days of the initial insult [13]. Following debridement of necrotic cardiomyocytes by a rapid and robust inflammatory response, the granulation phase begins to stabilize and reinforce the left ventricle (**LV**) wall via formation of a collagen-dominated scar [10], [12]. The quality of initial scar formation plays a leading role in determining future outcomes. Insufficient matrix deposition can lead to LV rupture or aneurysm, while excessive scar formation can lead to tissue stiffening, scar expansion, and arrhythmias [14], [15]. Furthermore, replacement of contractile myocardium with a collagenous scar creates a local increase in mechanical strain at the BZ of surviving myocardium and scar tissue. To compensate for the biomechanical alterations, connective

tissue often expands beyond the original injury, creating a subsequent decline in tissue compliance and cardiac output [16], [17].

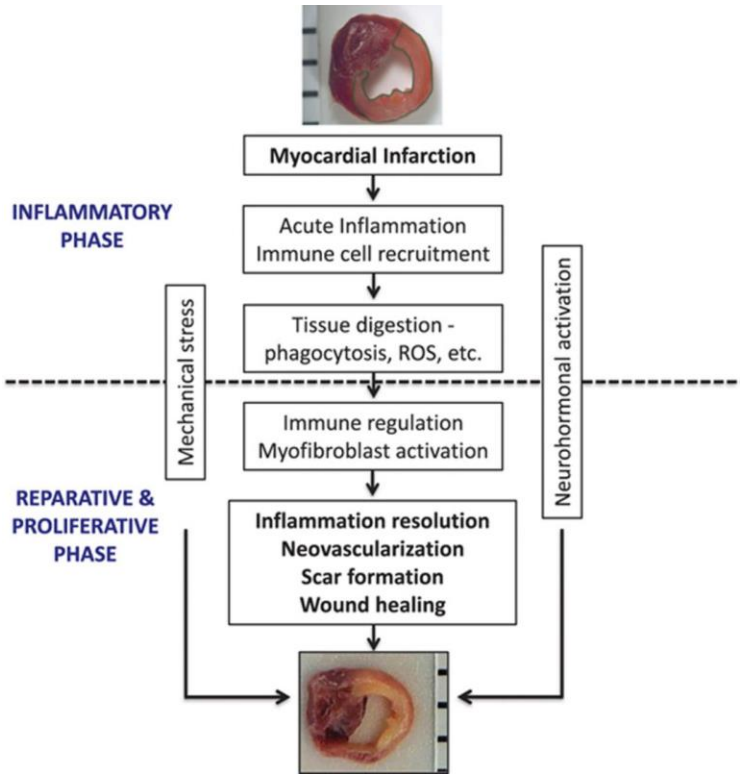

Figure 1.1. Schematic outlining the stages of healing following MI.
Reprinted with permission from Prabhu et al. [9]

1.3 Therapeutic shortcomings to address MI

Much research has gone into diverse approaches for optimizing healing after MI. Several trials have attempted to target the inflammatory response to MI. The CANTOS trial (Canakinumab Antiinflammatory Thrombosis Outcome Study) inhibited the cytokine interleukin (**IL**)-1β to reduce subsequent cardiovascular events [18]. While some short-term benefits were observed in this trial, a large body of evidence reveals that pharmacological approaches to modify inflammation have no clinical benefits [19]–[21]. Importantly, clinical practice guidelines recommend to avoid using steroids and nonsteroidal inflammatory agents in the acute and early

stages following MI, citing concerns over adverse outcomes [22]. Targeting inflammation post-MI is a challenge because of the fine-tuned coordination of inflammatory components that, when imbalanced, is more likely to damage tissue than heal. Likewise, the inflammatory response is first a reflection of the initial injury and not a direct cause of the subsequent clinical events arising from the damaged tissue [21].

Because of the lack of success in targeting inflammation, most pharmacologics administered post-MI aim to limit the spread of fibrotic tissue in order to preserve cardiac structure and function and prevent the progression to heart failure. Current drugs are incapable of reducing the degree of tissue remodeling, but they have been successful in limiting the expansion of fibrotic tissue. Angiotensin II receptor type 1 (**AT_1R**) blockers (also known as **ARBs**) and angiotensin converting enzyme inhibitors (**ACEi**) prevent the creation of the pro-fibrotic hormone angiotensin II (**AngII**) from its precursor angiotensin I. Both of these classes of drugs have been effective in limiting fibrosis and attenuating LV dilation and are used as the first choice drugs following MI [23]–[26]. β-blockers are another ubiquitous class of drug prescribed following MI. Targeting β-adrenergic receptors is effective for inhibiting CF activation and ECM deposition; however; a 2018 study revealed that β-blockers cease to be beneficial three years after MI [27]. Statins are also frequently prescribed to MI patients. Used in many cardiovascular pathologies, studies have shown statins are capable of lowering cholesterol. While potentially able to prevent subsequent ischemic events, statins have been shown to be ineffective for blocking the progression of fibrosis post-MI [16]. Identification of an effective drug target to specifically control the fibrotic response to MI in a manner that prevents the progressive deterioration of cardiac tissue would massively benefit a significant portion of the population suffering from this disease.

1.4 5-HT$_{2B}$ influences fibrotic cardiopulmonary disease

Cardiopulmonary disease is driven by a plethora of factors, some well characterized and others still undiscovered. Serotonin 2B receptor (**5-HT$_{2B}$**) is one such factor that has gained attention and contributed to the understanding of disease development. 5-HT$_{2B}$ is present throughout the cardiopulmonary system, most notably in cardiac valves, lung tissue, and the myocardium. Persistent activation of the receptor contributes to disease onset, initially reported following administration of anti-obesity compounds whose metabolites were potent 5-HT$_{2B}$ agonists [28], [29]. These patients had increased incidences of valve disease as well as pulmonary arterial hypertension (**PAH**). Diseased valves of patients taking medications with off-target 5-HT$_{2B}$ activation appear hyperplastic with plaque-like lesions and are incapable of providing optimal function [30]. Improper activation of this receptor is believed to impair the function of fibroblast-like interstitial cells which are responsible for maintaining valve matrix homeostasis [31]. In the case of PAH, blocking 5-HT$_{2B}$ activation can prevent small artery muscularization and increased right ventricular pressures that lead to right heart failure and death. This effect is understood to act on a bone marrow-derived cell population disrupting small artery homeostasis [32], [33]. 5-HT$_{2B}$ is integral to normal cardiac development, and there is evidence describing the impact of 5-HT$_{2B}$ activation inducing cardiac hypertrophy through CF-mediated cytokine release [34], [35]. These reports intersect at a pro-fibrotic role of 5-HT$_{2B}$ following injurious stimuli.

1.5 Dissertation overview

My doctoral work has sought to investigate the cell-specific contribution of 5-HT$_{2B}$ to scar formation after MI and how controlling tissue mechanics can impart long-term benefits. The first major focus of this research was to explore the effect of global 5-HT$_{2B}$ antagonism on cardiac structure and function post-MI. The second aim of my work sought to identify which cell

population expressed 5-HT_{2B} to influence fibrotic remodeling post-MI. Multiple experimental and genetic models systematically explored the contribution of 5-HT_{2B} from various cell lineages. Lastly, my work focused on the 5-HT_{2B}-driven cellular processes in CFs which regulate tissue remodeling.

In this dissertation, I present a thorough background of the known roles of 5-HT_{2B} in cardiopulmonary disease initiation and progression. Subsequently, I present a summary of my doctoral research into the benefits of global 5-HT_{2B} antagonism using an experimental model of MI. Histological and microstructural analyses describe tissue-level alterations of 5-HT_{2B} inhibition. Following this, I describe the generation and implementation of novel genetic models to explore cell-specific 5-HT_{2B} contribution to fibrotic remodeling post-MI. Next, I present my exploration into cell phenotype and cell signaling in 5-HT_{2B}-knockout CFs. RNA sequencing and *in vitro* assays are implemented to characterize molecular and phenotypic alterations downstream of 5-HT_{2B} ablation. Finally, I discuss the impact of this work and potential future directions the research could be taken.

Chapter 2

5-HT_{2B} in Cardiopulmonary Disease

Text for Chapter 2 was adapted from **Snider JC** and Merryman WD. *5-HT_{2B}R in Cardiopulmonary Disease*, in 5-HT2B Receptors, Giuseppe Di Giovanni, Editor. Springer Science, NY.

2.1 Introduction

Cardiopulmonary disease is widely appreciated to be the leading cause of death worldwide. Such diseases have a vast range of etiologies, and extensive research efforts have been focused on understanding disease initiation and progression. Serotonergic dysfunction has long been understood to contribute to cardiopulmonary pathology, and recent discoveries have elucidated unique roles for serotonin — or 5-hydroxytryptamine (**5-HT**) — receptors, such as 5-HT_{2B}, in the pathophysiology of various cardiopulmonary diseases. This chapter focuses on three main areas of research involving 5-HT_{2B}: 1) heart valve disease, 2) pulmonary hypertension, and 3) cardiac hypertrophy. The following studies have motivated the investigation of 5-HT_{2B} as a chief mediator of cardiopulmonary disease.

2.2 Heart valve disease

The discovery that 5-HT plays a causal role in cardiopulmonary disease can be traced back to 1931 when the Dutch pathologist A. J. Scholte documented thickened tricuspid valves in a deceased carcinoid syndrome patient [36]. Carcinoid syndrome occurs following oncogenic transformation of enterochromaffin cells, which are the primary synthesizers of 5-HT in the gastrointestinal tract. If a carcinoid tumor metastasizes to the liver, tumor cells will release vasoactive 5-HT into the systemic circulation via the hepatic vein. Increased plasma 5-HT level

leads to carcinoid heart disease, indicated by the characteristic development of a plaque-like, fibrous thickening of the heart valves found in over 65% of carcinoid syndrome patients [29], [37], [38]. Further, several classes of drugs that target 5-HT signaling were found to contribute to the onset of heart valve disease and ultimately led to the investigation of the specific 5-HT receptor subtype responsible for the development of heart valve disease.

Discovery of the role of 5-HT_{2B} in heart valve disease can be attributed to the observation of diseased valves in patients taking medications for non-valve related conditions. Several classes of medications have metabolites now known to activate 5-HT_{2B}, resulting in compromised cardiac valves, which are summarized in **Table 2-1**.

Table 2-1 5-HT_{2B}-mediated, drug-induced valvulopathy

Drug Class	Intended Use	Mechanism of 5-HT_{2B} Activation	Valve Pathology	References
Anorexigen	Appetite control and weight loss	Derivative norfenfluramine is a high affinity 5-HT_{2B} agonist. Inhibition of 5-HT reuptake transporters.	Valve hypertrophy and scarring lesions. Plaque deposition in glycosaminoglycan matrix.	[39]–[42]
Ergot derivatives	Migraine suppression	High affinity for 5-HT_{2B} due to the structural similarity of ergot agents and 5-HT.	Moderate-to-severe regurgitation. Fibrotic lesions.	[43]–[47]
Amphetamines	Anti-obesity and recreational use	Reverses 5-HT reuptake transporter to concentrate bioavailable 5-HT. Derivatives bind to 5-HT_{2B} with high affinity.	Induce prolonged mitogenic signaling *in vitro* in valve interstitial cells.	[48], [49]

2.2.1 Anorexigens as initiators of heart valve disease

Imbalance between energy intake and expenditure can result in eating disorders and obesity, which are important health concerns in developed countries. Medication for excessive eating disorders inadvertently aided in the discovery of 5-HT_{2B} as a key mediator of heart valve

disease. The anorexigen combination regimen of *fen*fluramine and *phen*termine ('Fen-Phen') became widely prescribed starting in 1984. While both drugs had been previously prescribed with minimal success, the combination of the two drugs resulted in sustained weight loss with fewer adverse side effects and improved appetite control [50]. Phentermine primarily functions through the release of norepinephrine to reduce perception of hunger [51]. However, fenfluramine is an amphetamine derivative that stimulates serotonin release while simultaneously inhibiting the function of 5-HT uptake transporters, increasing available 5-HT which signals through the hypothalamus to suppress appetite [39]. Fen-Phen was highly popular until 1997 when it was found that it increased both left- and right-sided heart valve defects after 12 months of use [40]. The incidence of heart valve disease was later reported to be as high as 25% in patients treated on average for 20 months [41]. These studies were followed by a seminal report which comprehensively tested 15 molecules at 11 distinct 5-HT receptor subtypes and systematically determined that the fenfluramine metabolite, norfenfluramine, exhibited high potency and high affinity for 5-HT_{2B}. All other 5-HT receptor subtypes were ruled out based on pharmacological differences from heart valve disease-associated molecules and negative control molecules. Interestingly, phentermine did not display agonism at 5-HT_{2B}, providing an explanation as to why the use of phentermine for decades prior to Fen-Phen did not result in the emergence of heart valve disease and further connected serotonin signaling through 5-HT_{2B} to disease [28].

Prescribed to patients with hypertriglyceridemia or diabetes, benfluorex functioned as an appetite suppressant due to its close structural relationship with amphetamines. This drug, like Fen-Phen, metabolizes into norflenfluramine, now known to be a high affinity 5-HT_{2B} agonist. A 2012 study documented that a 40-year-old woman on benfluorex therapy underwent a mitral valve replacement and resumed the therapy after the operation. Upon examination 4 years after valve replacement, the woman presented with mitral valve bioprosthesis hypertrophic scarring

and similar histopathological lesions on the aortic valve. These lesions were formed by smooth muscle α-actin- and vimentin-positive cells which deposited plaques in the glycosaminoglycan matrix [42]. This case further validates the hypothesis that norfenfluramine activation of 5-HT_{2B} causes valve disease.

2.2.2 Ergot derivatives as initiators of heart valve disease

Migraine headaches are believed to be transmitted through blood vessels in the brain associated with the meninges. Several human meningeal tissues express *HTR2B* – the gene encoding 5-HT_{2B} – and circulating 5-HT levels fluctuate during the phases of a migraine. In an animal model exposed to a known migraine-inducing agent, 5-HT_{2B} activation is required for the release of neuroinflammatory peptides which mediate trigeminal nerve activation and the sensation of pain. It is known that 5-HT_{2B} activation can induce the release of nitric oxide as well as induce the relaxation of cerebral vessels, suggesting a causative role of 5-HT_{2B} activation in neuroinflammation, endothelium-dependent relaxation, and activation of sensory trigeminovascular afferents [52], [53].

Ergot-derived therapeutics were the standard treatment for migraines until the mid-1960s when a strong link was discovered between the ergot agents – methysergide and ergotamine – and heart valve disease. A later study determined that these compounds possessed a high affinity for 5-HT_{2B} in heart valve tissue [43]. It is even suggested that the similar structure of 5-HT and ergot agents could point to a common pathology with carcinoid valve disease [44].

The non-specific dopamine agonists pergolide and cabergoline were popular therapeutics prescribed to patients with Parkinson's disease and are also ergot-derived compounds. Unsurprisingly, the interference of these compounds with the dopamine/5-HT

signaling axis resulted in decidedly similar echocardiographic and histopathological findings as observed in patients with carcinoid heart disease [45]. Patients receiving either pergolide or cabergoline were reported to have moderate-to-severe regurgitation in at least one heart valve more frequently compared to patients who received non-ergot therapeutics or controls. Furthermore, the incidence of heart valve disease has been found to be as high as 28% in patients receiving ergot-derived dopamine agonists where no increase in prevalence is associated with other dopamine agonists [47], [54].

Pergolide and cabergoline induced fibrotic changes in cardiac valves due to their high affinity for 5-HT_{2B}. The association of ergot-derived compounds with fibrotic pathologies as well as the structural and functional similarity to 5-HT acting upon 5-HT_{2B} reveal yet another pathological function of 5-HT_{2B} signaling.

2.2.3 Amphetamines as initiators of heart valve disease

While amphetamine derivatives have been prescribed as anti-obesity drugs, the amphetamine 3,4-methylenedioxymethamphetmaine — MDMA ("ecstasy") — is a psychostimulant drug of abuse used recreationally throughout Europe and North America. This drug reverses the function of the 5-HT reuptake transporter, resulting in a concentrated release of 5-HT and psychostimulatory effects [48]. MDMA and its metabolite 3,4-methylenedioxyamphetamine — MDA — preferentially bind and activate human recombinant 5-HT_{2B}. Similarly to fenfluramine, these drugs induce and prolong mitogenic signaling through 5-HT_{2B} *in vitro* which suggests that MDMA would induce valvular heart disease with continued use [49].

2.2.4 Heart valve disease mechanisms

HTR2B and *HTR2A* mRNAs are highly expressed in human heart valves with no *HTR2C* mRNA detectable. 5-HT_{2B} signaling is of particular interest since the above-mentioned prescribed drugs and their active metabolites activate this receptor and result in valve disease whereas chemically similar drugs which do not bind 5-HT_{2B} (e.g., lisuride and terguride) do not result in valve pathology. This highlights the public health implications of therapeutics aimed at 5-HT signaling. In order to avoid mistakes of the past, 5-HT_{2B} screening is a necessity to identify potential drug-induced valvular heart disease.

Despite the litany of disease-causing agents described, mechanistic characterization of 5-HT_{2B}-induced valve disease is lacking. It is known that medications acting through serotonergic mechanisms, specifically 5-HT_{2B}, are likely to result in valvulopathy. While it appears that the valve interstitial cells are responsible for valve fibroplasia, it is unclear if they are the direct target of 5-HT_{2B} agonists. Valvular regurgitation and insufficiency can result from subtle, non-destructive thickening and the associated hemodynamic overload can lead to myocardial dysfunction and heart failure, highlighting the need to understand 5-HT_{2B} signaling mechanisms and limit erroneous receptor activation.

Several reports have described valvular lesions arising after treatment with anorexigens, ergot alkaloids, or carcinoid syndrome as “glistening, superficial plaque-like thickenings” that present on the surface of the leaflets and cusps [30]. This valve phenotype is recapitulated in Sprague-Dawley rats by continuous 5-HT administration over a three-month period. Morphological and echocardiographic alterations of the rat aortic valve mimic those observed in carcinoid heart disease. Aortic valve leaflets are thickened and retracted with evident carcinoid-like plaques made of collagen rich tissue in rats treated with 5-HT. These changes are thought to be due to increased proliferation of cardiac valvular subendocardial cells which concomitantly increased expression of the 5-HT_{2B} (**Figure 2.1**) [55]. Another study observed similar changes

as early as seven days following 5-HT administration. Modified Movat's pentachrome staining revealed significantly thicker mitral and aortic valves due to an expansion of glycosaminoglycan content resulting in loss of valve compliance and function. The glycosaminoglycan network was also more vascularized following 5-HT administration indicating a loss of quiescence and increased remodeling. These changes faithfully mimic anorexigen-associated valvulopathy. 5-HT treated rats had transcription of the gene encoding the 5-HT transporter (**SERT**) down regulated, indicating a decrease in 5-HT receptor recycling; 5-HT_{2B} gene transcription was also increased [30]. SERT is critical to protect against the adverse effects of 5-HT overactivity, so valve remodeling is thought to be a combined effect of its downregulation combined with increased mitogenic 5-HT_{2B} signaling.

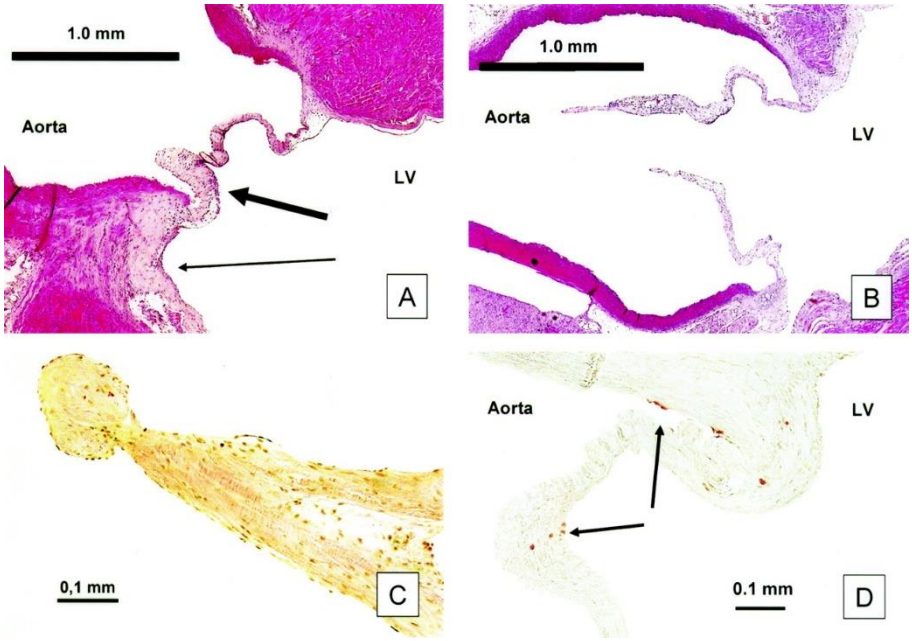

Figure 2.1. Diseased aortic valves due to serotonin overexposure.
A, Bold arrow indicates a thickened and retracted aortic valve with collagen deposits at the valve cusp (thin arrow) after 3 months of 5-HT administration in a rat model. **B**, Healthy aortic valve in untreated rat. **C**, Higher magnification image of a 5-HT-treated rat with aortic valve insufficiency, seen in a shortened, thickened, and collagen-rich cusp. **D**, Ki-67 positive nuclei reveal proliferation in the valve after only 5 days of 5-HT administration. (Reprinted with permission from Gustfasson et al. [55])

Similar to six other classes of 5-HT receptors, 5-HT_{2B} is a G protein-coupled receptors (**GPCR**) that follows a well characterized signaling cascade. The Gαq subunit is released upon receptor activation which proceeds to activate the downstream effectors phospholipase C-β and protein kinase C through release of intracellular calcium and diacylglycerol liberation. 5-HT_{2C} receptors are absent in the cardiovascular system while 5-HT_{2A} and 5-HT_{2B} are presumed to have similar cardiovascular functions due to the significant sequence homology. In the context of valve disease, specific activation of the 5-HT_{2B} GPCR also activates second messenger signals identified by the phosphorylation and activation of both the tyrosine kinase Src and extracellular regulated kinases (**ERK**) pathways. These pathways may synergize with signaling of transforming growth factor β (**TGFβ**) leading to enhanced mitogenesis [29].

Valve interstitial cells are thought to be the drivers of valve remodeling. In the context of calcific aortic valve disease, quiescent cells are activated into a myofibroblast-like phenotype, leading to increased ECM deposition and eventual formation of bone-like calcific nodules. Nodule formation can be modeled *in vitro* by treating valve interstitial cells with TGFβ1 resulting in simultaneous phosphorylation of the tyrosine kinase Src and expression of the contractile marker SM22α. Interestingly, treatment with the specific 5-HT_{2B} antagonist SB204741 mitigates the formation of nodules by preventing SM22α upregulation, but Src phosphorylation is still increased. Time-lapse microscopy revealed Src is sequestered upon administration of the 5-HT_{2B} antagonist, arresting its motility to restrict the phosphorylation and activation of the type II TGFβ receptor [31].

5-HT_{2B} may also play a role in the progression of mitral valve disease. In a canine model of myxomatous mitral valve disease, a significant increase in the expression of 5-HT_{2B} was observed in symptomatic valves compared to control animals while there was no change in 5-HT_{2A} expression in either group. Staining of this receptor co-localized with α-smooth muscle actin expression, indicating a potential role for the 5-HT_{2B} in valve remodeling by contractile

interstitial cells [56]. A subsequent study investigated 5-HT_{2B} in the context of mitral valve prolapse in human, canine, and murine tissue and observed an association between mitral valve prolapse and leaflet 5-HT_{2B} expression in humans. The same was observed in canine tissue along with an increase in ERK phosphorylation, which is known to increase interstitial cell activation and remodeling. This effect was prevented with the 5-HT_{2B} antagonist LY272015. Finally, in mice given chronic AngII infusion, valve leaflet area was significantly increased in response to AngII but was mitigated in the presence of a 5-HT_{2B} antagonist; neither 5-HT_{2A} antagonist terguride or ketansarin had an effect on leaflet area [57]. These studies sufficiently describe a role for 5-HT_{2B}, but not 5-HT_{2A}, in the remodeling of mitral valves.

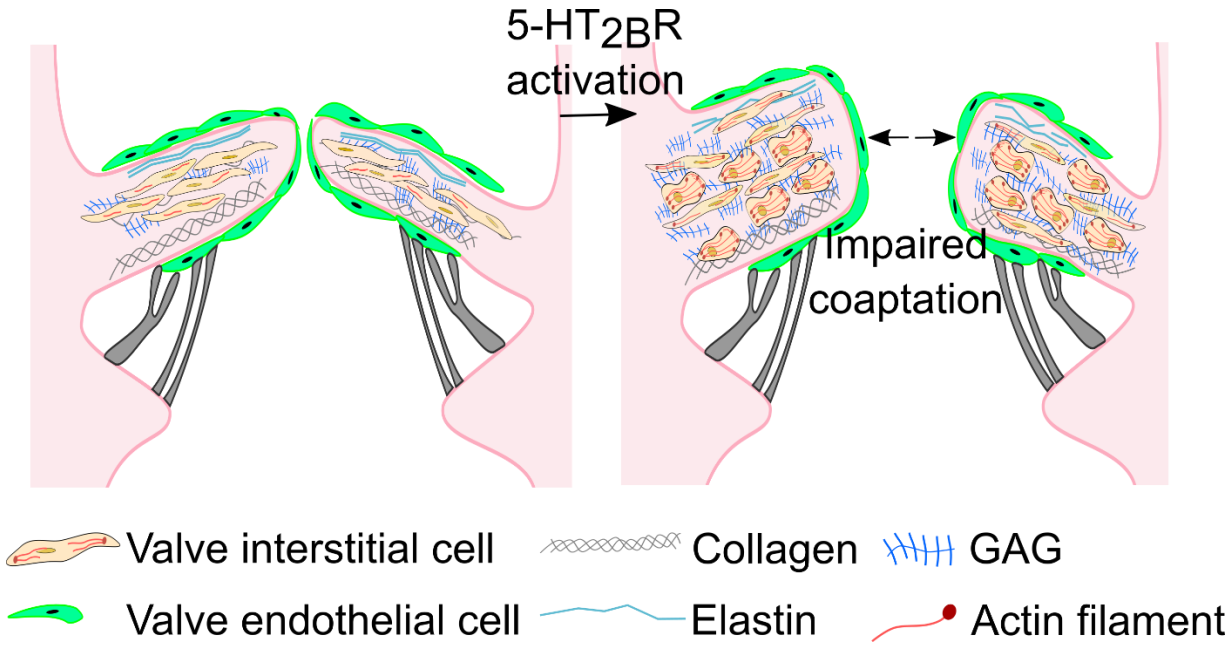

Figure 2.2. Impact of 5-HT_{2B} activation on valve structure and function.
Interstitial cell expansion and glycosaminoglycan (GAG) deposition decreases valve compliance and coaptation

Due to the lengthy nature of valve disease onset, the scarcity of available tissue, and a variety of disease triggers, animal models of valve disease are lacking and have limited studies focused on perturbations and probing of specific molecular mechanisms behind valvulopathies. However, observational studies have made it clear that 5-HT_{2B} signaling plays an extensive role

in disease development — most likely through the activation of normally quiescent valve cells — resulting in valve remodeling, loss of compliance, and ultimately, loss of valve function (**Figure 2.2**).

2.3 Pulmonary arterial hypertension

PAH is a deadly disease of the pulmonary vasculature that is incompletely understood in terms of its cellular and molecular mechanism. Over 200,000 people are hospitalized annually in the United States with some form of pulmonary hypertension (**PH**) with a mortality rate approaching 10% [58]. PH is clinically defined as a mean pulmonary arterial pressure exceeding 25 mmHg, measured by right ventricle catheterization [59]. Group 1 PH encompasses PAH which can be idiopathic, heritable, or acquired. Idiopathic PAH has no known cause with 2-3 new cases per million annually, whereas over 75% of heritable PAH is due to a mutation in the bone morphogenetic protein receptor II (**BMPRII**) gene and is about 10 times less prevalent than idiopathic PAH. Acquired PAH is commonly associated with exposure to other risk factors such as human immunodeficiency virus, scleroderma, or anorexigen use [60]. While incidence is rare, the mortality rate is striking, with merely 67% of patients surviving three years after diagnosis. However, this number may even be artificially high due to a strong influence of survival bias introduced from the method of data collection [61], [62].

2.3.1 Models of PAH

Increased pulmonic blood pressure, the hallmark of PAH, is due to a progressive increase in pulmonary vascular resistance and remodeling associated with vasoconstriction. It is histologically characterized by neomuscularization of small pulmonary arteries, intimal thickening, medial hypertrophy, adventitial proliferation, and abnormal ECM deposition. The

culmination of these remodeling events is irreversible lumen narrowing, increased pulmonary artery resistance, hypoxia, right heart hypertrophy, and eventually, right heart failure and death [32]. Multiple experimental models of PH in rodents have been utilized to capture different aspects of the disease, and interpretation of results should consider the method used to induce disease. Small rodents do not develop disease that completely recapitulates human PAH. While many experimental models are characterized as PH models and do not further designate a PH group, for the sake of simplicity in this chapter, the discussed experiments will be referred to as models of PAH.

The classical model of PAH is chronic hypoxia exposure. This model has led to understanding of hypoxia-induced vascular remodeling, however, the obliterative lesions observed in human patients with severe PAH are not replicated with chronic hypoxia. The monocrotaline lung injury model attempts to address this limitation of chronic hypoxia by causing pulmonary arterial endothelial cell dysfunction and inflammatory cell infiltration. Pulmonary vasoconstriction and right heart hypertrophy are faithfully modeled with monocrotaline administration; however, this model is restricted to rats as mice do not develop disease in response to monocrotaline, which is yet to be understood. While monocrotaline injury is simple and reproducible, it is an acute injury that fails to fully capture the evolving nature of human PAH [63]. In order to recapitulate heritable PAH, mouse models harboring BMPRII mutations have been developed to study the disease. Smooth muscle- and vascular endothelial cell-specific knockouts of BMPRII have independently been shown to generate pulmonary vascular remodeling and increases in right ventricular systolic pressure (**RVSP**). However, this model is highly variable, incompletely penetrant, and complex vascular lesions do not form [64]. Toward this end, the vascular endothelial growth factor receptor 1 and 2 blocker, SU5416 (“Sugen”), combined with chronic hypoxia has served as a preclinical drug model. Sugen-hypoxia results in angioobliterative pulmonary lesions and increased RVSP which is not

reversible upon returning to normal air. This model has been useful for studying the reversibility of PAH and uncovering the immunological mechanisms behind the pathobiology of PAH [64]. While no one method completely emulates human PAH, these models have increased the understanding of disease progression and characteristics.

The cellular mechanism behind PAH hinges upon an interplay between the vascular endothelium, pulmonary artery smooth muscle cells (**PASMCs**), and bone marrow-derived cell populations. Nitric oxide is a key mediator of vasodilation, as well as downregulation of leukocyte adhesion and vascular proliferation. Reduced nitric oxide bioavailability has been reported in PAH and contributes to increased PASMC migration and proliferation in the distal arteries of the lungs [65]. Disruption of vascular homeostasis in the context of PAH is commonly due to an imbalance of prostacyclin and endothelin. Prostacyclin is produced by endothelial cells and induces PASMC relaxation and vasodilation. Endothelin is produced by vascular endothelium, PASMCs, and lung fibroblasts and induces calcium release by the sarcoplasmic reticulum as well as PASMC proliferation and vasoconstriction. As these factors become imbalanced, vascular resistance and remodeling occurs, leading to right ventricle hypertrophy [66]. On a molecular level, receptor tyrosine kinases play a critical role in modulating cell proliferation, migration, and differentiation. In humans and experimental models of PAH, platelet-derived growth factor (**PDGF**), epidermal growth factor, fibroblast growth factor, and c-kit receptors have all been investigated for their pathogenic role in contributing to excessive vascular remodeling. Ample evidence exists for the tyrosine kinase Src being abnormally activated in PAH and mediating the effect of receptor tyrosine kinases [67]. Evidence for inflammatory infiltrate in the onset and progression of PAH pathology is growing. Known increases in cytokines such as IL-6, IL-1β, and tumor necrosis factor-α are elevated in patients with PAH. Elevated circulating cytokine levels are associated with inflammatory cell recruitment and accumulation, and they have been correlated with worse clinical outcomes [68].

Therapies aimed at treating PAH are lacking and often focus on mitigating symptoms of the disease but are yet unable to address the underlying pathophysiology due to the limited understanding of disease mechanisms. Three classes of medications currently used include: prostacyclin analogues to restore deficient endogenous prostacyclin levels, phosphodiesterase type 5 inhibitors to compensate for down-regulated nitric oxide signaling, and endothelin antagonists to inhibit the up-regulated endothelin pathway [69]. These medications were adopted from treatments for other illnesses and are not ideal for managing PAH. They modestly improve disease symptoms through transitory vessel dilation without addressing the underlying pathophysiological hypertensive agents of vessel stiffening and remodeling [70], [71]. This highlights the need for a more specific class of therapies aimed at directly targeting molecular pathways relevant to PAH.

2.3.2 Serotonin in PAH

Identification of the role of 5-HT in PAH pathogenesis goes back to the 1960's when an epidemic of PAH arose in a Swiss population taking the anorexigen aminorex fumarate; a second serotonergic aneroxigen-induced outbreak of PAH accompanied the use of Fen-Phen in the 1990s [72]. These drugs are SERT substrates responsible for modulating bioavailable plasma 5-HT levels. SERT inhibitors abrogate 5-HT-induced mitogenesis, and mice deficient for SERT have partially reduced pulmonary vascular remodeling under hypoxic conditions [73]. A correlation between high plasma 5-HT levels and total pulmonary resistance was established in the 1980s when a patient was diagnosed with PH while carrying a familial platelet storage deficiency [74]. 5-HT is released by pulmonary neuroendocrine cells and neuroepithelial bodies in response to hypoxia and is sustained in PH patients. 5-HT mediates a myriad of functions in the vasculature, most notably smooth muscle cell hypertrophy and hyperplasia [75]. PASMCs and endothelial cells both express mRNA encoding 5-HT_{1B}, 5-HT_{2A}, 5-HT_{7}, and 5-HT_{2B}. Being a

potent pulmonary vasoconstrictor and capable of inducing vascular remodeling, 5-HT has a dual role in response to hypoxia and acting through its cognate receptors [76].

2.3.3 5-HT$_{2B}$ mechanism in PAH

The anorexigens fenfluramine and dexfenfluramine increase the risk of developing PH by a factor of 3.7- to 23-fold depending on the study referenced [77], [78]. The primary dexfenfluramine metabolite, nordexfenfluramine, is a high affinity 5-HT$_{2B}$ agonist. Furthermore, 5-HT$_{2B}$ overexpression (but not 5-HT$_{2A}$) is observed in PAH [76]. This led to the discovery of 5-HT$_{2B}$ activation being necessary for the development of hypoxia-induced increases in RVSP and vascular muscularization. In mice, five weeks of exposure to 10% O_2 causes a pathologic increase in RVSP that is completely nullified in the presence of the 5-HT$_{2B}$ antagonist RS127445. Compared to normoxic mice, hypoxia significantly increases the number of fully muscularized arteries, an effect prevented with RS127445 administration. These results were reproduced in 5-HT$_{2B}$ knockout mice, and the utility of 5-HT$_{2B}$ ablation was further strengthened when the dual insult of hypoxia and dexfenfluramine was unable to increase RVSP. Hallmarks of lung-remodeling associated with PAH progression are cell proliferation and increased serine elastase, which activates stores of growth factors such as TGFβ. Cell proliferation, elastase activity and TGFβ levels are all normalized in hypoxic animals treated with RS127445 and in 5-HT$_{2B}$ knockout animals. Interestingly, repeated acute exposure to hypoxic conditions increases RVSP independent of 5-HT$_{2B}$ activity, but 5-HT$_{2B}$ knockout mice do not have increase elastase activity compared to wild-type (**WT**) mice after repeated acute hypoxia [76]. This indicates the function of 5-HT$_{2B}$ is not at the level of acute vasoconstriction but rather at the level of downstream signaling mechanisms that govern vascular remodeling.

Following the discovery that 5-HT$_{2B}$ is necessary for hypoxia-induced PAH, the experimental inflammatory model of PAH using monocrotaline administration was investigated

in rats in order to parse out the individual contributions of SERT and 5-HT receptors. It was demonstrated that SERT inhibitors were able to prevent an increase in RVSP and pulmonary artery muscularization but 5-HT_{2B} antagonism was not. SERT inhibitors abrogate the production of inflammatory cytokines characteristic of monocrotaline-induced injury as well as reverse right ventricle hypertrophy with no effect of 5-HT_{2B} antagonism reported [79]. These findings point back to the original serotonin hypothesis of PAH that peripheral 5-HT availability is the key driver of disease. However, the monocrotaline model of PAH has received fair amounts of criticism for the acute, destructive nature of disease, and since it has been shown that 5-HT_{2B} inhibition does not confer protection over acute disease onset [76], these data should be considered carefully. In contrast, subsequent studies in the monocrotaline experimental model of disease have shown the utility of 5-HT_{2B} antagonism in treating PAH in rats. Multiple 5-HT_{2B}-specific antagonists have been shown to reduce RVSP, vascular remodeling, and right ventricle hypertrophy in monocrotaline-injected rats [80], [81]. The discordant results in the discussed monocrotaline experiments demonstrate a need for a better experimental model of PAH that captures disease progression more faithfully.

Mice expressing the patient-derived R899X BMPRII mutation develop PAH within a few weeks with about 50% disease penetrance. These mice have been a useful model for exploring the cellular mechanism behind the heritable form of PAH for patients harboring a BMPRII mutation. 5-HT_{2B} antagonism with SB204741 normalizes RVSP to control levels and decreased the stiffness of distal pulmonary vessels, consistent with other models of PAH. In this model, 5-HT_{2B} antagonism was observed to work through the tyrosine kinase Src. Antagonism simultaneously decreased Src phosphorylation and trafficking. Abrogation of Src activity lead to decreased activation of downstream effectors and eventual transcription of genes encoding contractile proteins such as RhoA, gamma actin, and myosin light chain 12a. Isolated mutant BMPRII smooth muscle cells displayed significantly enhanced contractile behavior which was

abrogated with 5-HT$_{2B}$ antagonism (**Figure 2.3**). Interestingly, administration of a 5-HT$_{2B}$ antagonist to WT animals increased immune cell infiltrate and slightly increased vessel stiffening, findings opposite from the treated BMPRII mutants [67]. These data indicate a protective role of 5-HT$_{2B}$ in heritable PAH most likely through direct control of signaling downstream of BMPRII through Src. Notably, this model does not require exposure to hypoxic conditions or endovascular injury, and as such is able to directly isolate signaling mechanisms that could influence disease.

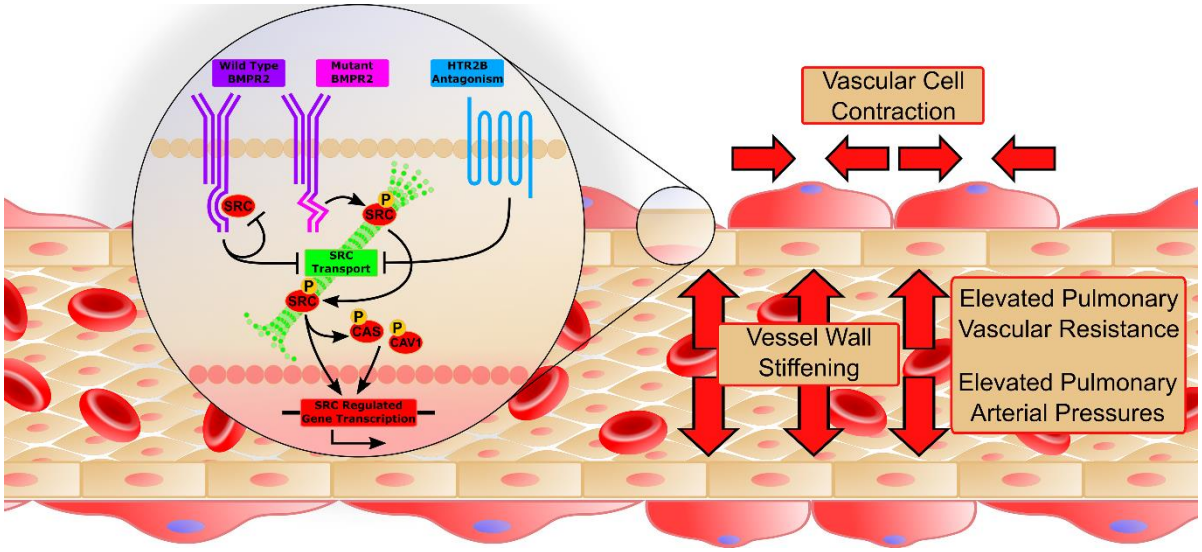

Figure 2.3. Proposed 5-HT$_{2B}$ mechanism in heritable PAH.
BMPRII mutations increase Src transport and signaling. 5-HT$_{2B}$ antagonism arrests Src trafficking and decreases Src signaling. This functionally causes increased small vessel compliance, reduced inflammatory infiltrate, and decreased vascular smooth muscle contractility to restore mean pulmonary arterial pressure. (Reprinted from Bloodworth et al. [67])

Platelets are a primary source of peripheral 5-HT, but do not express 5-HT$_{2B}$. Therefore, a link between 5-HT levels and 5-HT$_{2B}$ must be established to understand the mechanism behind 5-HT$_{2B}$'s control over the development of PAH. Hypoxia-induced increase in plasma 5-HT can be prevented in 5-HT$_{2B}$ knockout mice or with 5-HT$_{2B}$ antagonism. Plasma 5-HT strongly correlates with RVSP, lung 5-HT$_{2B}$ expression, and the plasma 5-HT metabolite 5-HIAA, but not blood 5-HT, indicating a platelet-independent mechanism [82]. While SERT expression levels

are not altered by treatment of dexfenfluramine or RS127445, SERT uptake of plasma 5-HT is significantly increased with 5-HT_{2B} ablation. 5-HT_{2B} agonism causes the reverse effect, and pretreatment with the SERT inhibitor paroxetine prevents 5-HT_{2B} mediated increase in plasma 5-HT [82]. These findings indicate that the hypoxia-induced increase in plasma 5-HT is completely dependent on both 5-HT_{2B} and SERT and is carried out in a platelet-independent manner. The molecular regulators guiding this effect are uncertain, however 5-HT_{2B}-dependent SERT phosphorylation has been observed in a mouse stem cell line providing a potential molecular link between the two [83].

2.3.4 5-HT_{2B} controls bone-marrow contribution to PAH

While early studies have focused on the form and function of 5-HT and its availability, a shift in focus to bone marrow-derived cell contributions to differentiating/proliferating smooth muscle cells has gained significant attention recently. Striking evidence using bone marrow transplantation combined with chronic hypoxia showed that bone marrow 5-HT_{2B} expression is required to develop pathologic RVSP measurements. WT mice receiving *Htr2b*$^{-/-}$ bone marrow were immune to RVSP increases following 3 weeks of exposure to hypoxic conditions. Prior to hypoxia exposure, *Htr2b*$^{-/-}$ mice have altered bone marrow composition. Most notably, there are fewer CD45+CD11b-CD31+ proangiogenic precursor cells, and this composition is preserved following exposure to hypoxia and may constitute the endothelial/PASMCs responsible for PAH [32].

Bone marrow-derived proangiogenic cells (**PACs**) are a subset of myeloid lineage cells thought to directly contribute to small-vessel remodeling. While they are poorly characterized, they are commonly identified by a combination of endothelial and hematopoietic or stem cell markers, and their presence in peripheral blood has been correlated with PAH through indirect mechanisms of promoting pathologic vascular remodeling in neighboring cells. In the Sugen-

hypoxia model of PAH, ablation of PACs prevents any RVSP increase and vessel stiffening, indicating the direct contribution of PACs to experimental PAH with enhanced endovascular injury. Administration of the 5-HT_{2B} antagonist SB204741 decreases the number of PACs (CD45+CD11b-CD31+) in peripheral blood as well as the number of PACs that have taken residence in lung tissue, leading to normalized RVSP values and vessel wall stiffness. PAC ablation following three weeks of Sugen-hypoxia is also sufficient to reverse disease. This phenomenon is potentially conserved in humans as the presence of at least one bone marrow-derived CD31+ cell in pulmonary vessels from PAH patients enhances vessel wall stiffness [33]. This study relied upon enhanced endovascular injury, indicating endothelial injury response is integral for PAC function. This cell population is also broadly defined and translation beyond mouse models will be aided by further characterization of the cell type. While the mechanism driving PAC-induced vessel stiffening and RVSP elevation has yet to be investigated, the discovery that 5-HT_{2B}-driven PAC recruitment promotes the development of PAH provides further impetus to pursue 5-HT_{2B} as a driver and potential therapeutic target for PAH.

The data presented above clearly shows that 5-HT_{2B} contributes to the development and progression of disease in experimental models of PH mimicking human PAH. The myriad of experimental procedures model different contributors to disease, with strengths and weaknesses evident for each. Convincing evidence has been put forth regarding 5-HT_{2B} affecting unique aspects of PAH in various disease models (**Figure 2.4**). While the exact mechanism is not fully understood and current understanding must be viewed in a context-dependent manner, encouragement can be taken from the successful application of 5-HT_{2B} ablation in mitigating pulmonary hypertensive disease across the board.

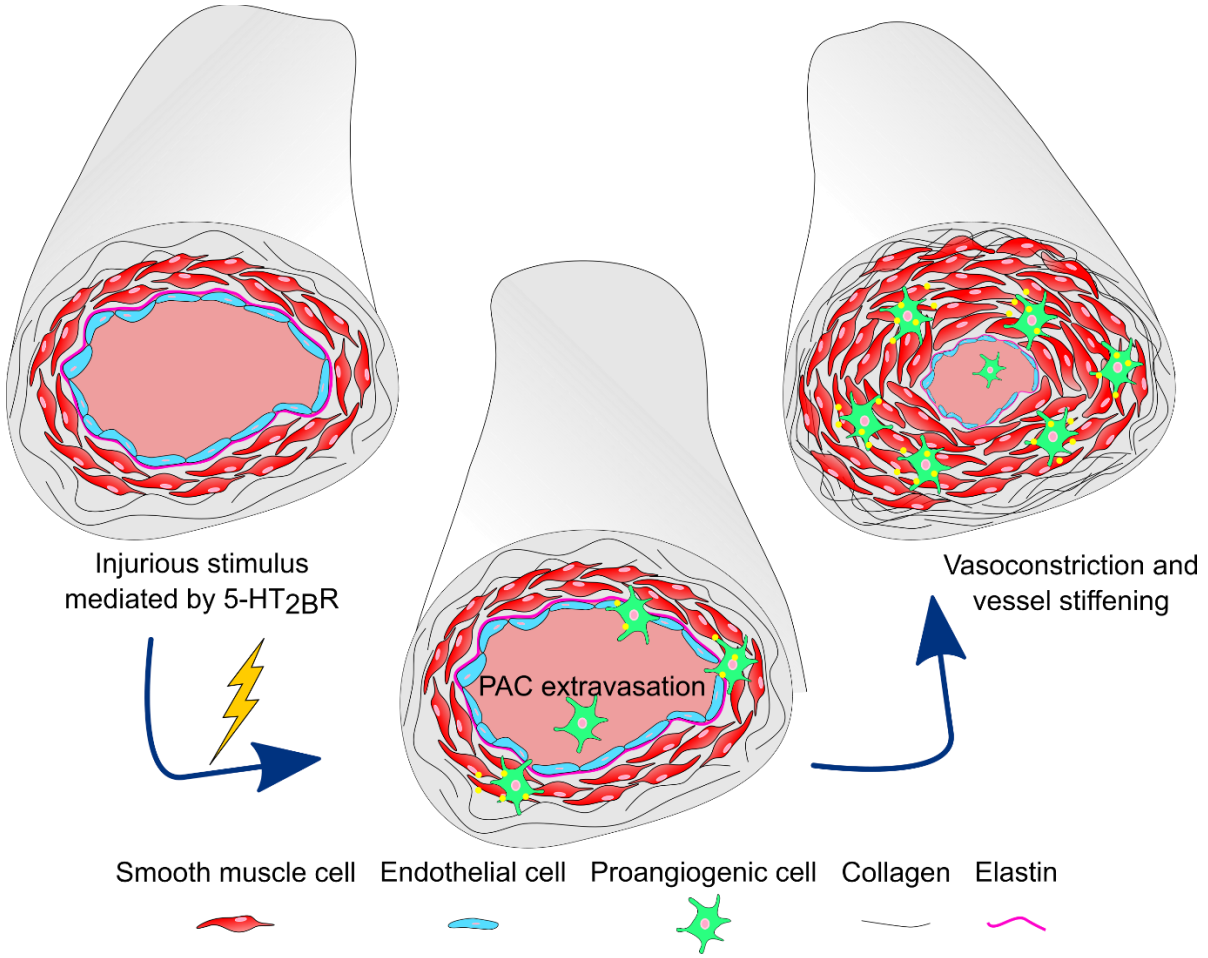

Figure 2.4. 5-HT$_{2B}$ dependent PAH initiation.
PAH is mediated by 5-HT$_{2B}$ via recruitment of PACs which drive arterial muscularization and stiffening

2.4 5-HT$_{2B}$ in cardiac development, vascular injury, and hypertrophy

5-HT is an active signaling molecule throughout early embryogenesis. 5-HT signaling can be impaired even before neurogenesis, indicating an even wider role beyond neurotransmission. 5-HT's suspected role in cardiovascular morphogenesis was confirmed when embryos grown in high concentrations of 5-HT or SERT inhibitors were observed to decrease the proliferation of myocardium, cardiac mesenchyme, and cardiac endothelium [84]. Prior to the generation of 5-HT$_{2B}$ knockout mice, no obvious developmental defects (other than

behavioral) had been attributed to 5-HT receptors. The generation of mice harboring a specific genetic mutation deleting *Htr2b* uncovered the contribution of 5-HT_{2B} to cardiac development.

2.4.1 5-HT_{2B} is required for normal cardiac development

In the year 2000, the existence of cardiovascular abnormalities associated with 5-HT_{2B} mutation were first documented. The observed frequency of pups from 5-HT_{2B}-mutant parents was lower than the expected frequency, indicating a non-negligible rate of midgestational lethality. At 10.5 days postcoitum, fewer trabecular cells and decreased myocardial thickness are observed. Thinner myocardial walls lead to myocardial rupture as the cause of death, explaining the observed accumulation of blood in the pericardium [34].

Neuregulin, a protein playing a significant role in neural and cardiac development, functions through binding its receptor ErbB-2. ErbB-2 is localized to the ventricular wall of the myocardium, and interestingly, mice lacking neuregulin exhibit a similar embryonic cardiac phenotype as mice lacking 5-HT_{2B}. There is a significant reduction of ErbB-2 expression in 5-HT_{2B} mutant mice, providing a potential mechanism for abnormalities in cardiac development. The signaling cascade of ErbB-2 is transactivated by GPCRs, suggesting Gq-coupled 5-HT_{2B} transactivates the ErbB-2 pathway to regulate cardiac morphogenesis. This hypothesis is further supported by data showing that cardiomyocytes in newborn mice will proliferate in response to 5-HT or neuregulin, but 5-HT_{2B} mutant cardiomyocytes do not display a mitogenic response to these signals [34].

The developmental defects of 5-HT_{2B} mutant mice manifest themselves in impaired cardiac structure and function in adult hearts. Adults exhibit noticeable LV dilatation with increased LV end-diastolic and end-systolic diameter, consistent with persistent tissue-level remodeling in response to impaired cardiac morphogenesis. Functionally, 5-HT_{2B} mutant hearts

have a 20% decrease in fractional shortening compared to WT mice. These changes coincide with a 15% decrease in the number of cardiomyocytes, and the existing cardiomyocytes are 12% shorter, resulting in decreased ventricular mass (**Figure 2.5**). Upon ultrastructural analysis, myofilaments are misaligned, I bands are not observed, and Z bands are wider than expected, resulting in decreased sarcomere length. Despite increased preload condition (indicated by increased LV end-diastolic diameter), mutant hearts treated with the adrenergic stimulant isoproterenol generate significantly less force upon contraction than WT hearts [85]. Decreased force generation resulting from fewer cardiomyocytes formed into shorter sarcomeres is the ultimate functional consequence of the developmental deficiency of 5-HT_{2B} and is typical of what is observed in dilated cardiomyopathy. Of note, myocardial apoptosis or immune cell infiltrate is not observed in response to 5-HT_{2B} deletion. Additionally, this appears to be a partially sex-dependent phenomenon as male mice had more pronounced biological changes than age-matched females [85]. While cardiomyocyte defects are the most pronounced and easily observable, fibroblasts have been specifically shown to transduce mitogenic signals in a 5-HT_{2B}-dependent manner [86]. Note that these developmental studies were all performed in the context of global 5-HT_{2B} deletion.

Cardiomyocyte-specific overexpression of 5-HT_{2B} was shown to have the inverse effect of global 5-HT_{2B} deletion. Mice exhibiting cardiomyocyte-restricted 5-HT_{2B} overexpression displayed an increase in LV free wall thickness as well as approximately 11% more cardiomyocytes, resulting in an overall increase in cardiac mass. The effect is not accompanied by a concomitant decrease in systolic performance indicative of compensated LV hypertrophy. Similar to 5-HT_{2B} knockout animals, 5-HT_{2B} overexpression does not lead to myocardial apoptosis, fibrosis, or notable inflammatory cell infiltration. Contrary to the knockout model,

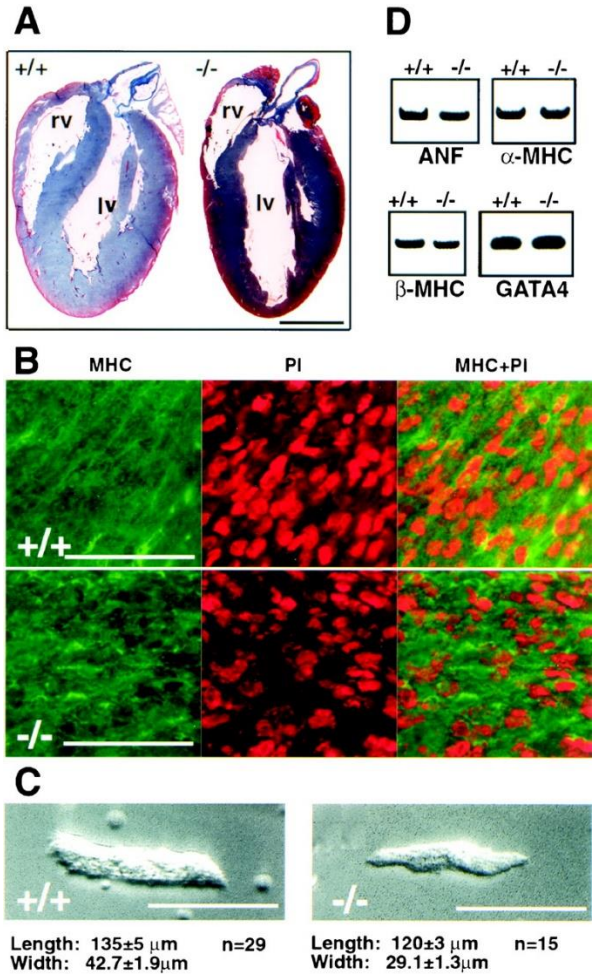

Figure 2.5. Developmental deficiencies in 5-HT$_{2B}$ mutant mice.
A, Mice lacking 5-HT$_{2B}$ exhibit decreased ventricular mass due to decreased cardiomyocyte number and size. **B**, Decreased staining of the cardiomyocyte marker (MHC) normalized to total cell population (PI-stained). **C**, Ventricular myocytes from newborn mice are narrower and shorter. **D**, No compensatory increase in hypertrophic markers (ANF, MHC, and GATA4) were observed in adult mice. (Reprinted with permission from Nebigil et al. [85])

sarcomeric structure is normal, but differences in mitochondria can be observed. They appear rounded, irregular, and more abundant. Functionally, the mitochondria are significantly more enzymatically active with decreased expression of the mitochondrial defect marker adenine nucleotide translocator. These data suggest 5-HT$_{2B}$ signaling increases metabolic activity and oxidative phosphorylation in mitochondria [87]. 5-HT signaling through 5-HT$_{2B}$ acts as a survival signal to cardiomyocytes by inhibiting serum withdrawal-induced apoptosis. [88].

This effect could potentially transition from a hypertrophic to cardiomyopathic phenotype, controlled by the signaling of 5-HT_{2B}.

2.4.2 5-HT_{2B} mediates vascular function and remodeling

Due to the peripheral storage of 5-HT in platelets and its vasoactive function, 5-HT likely plays a pathologic role in low-flow conditions such as thrombosis, ischemic injury, and hypertension. In autoperfused rat hindquarters, 5-HT results in conflicting vasoactive functions, causing vasodilation at low concentrations and vasoconstriction at high concentrations. In this investigation of healthy vessels, the contractile response was mimicked with the non-selective 5-HT_2 agonist α-methyl-5-HT, but not the selective 5-HT_{2B} agonist BW723C86 indicating a 5-HT_{2B} independent mechanism [89]. However, 5-HT_{2B} expression does increase in the context of injury. In the small arteries of deoxycorticosterone acetate (**DOCA**)-salt-hypertensive rats, 5-HT causes contraction, exacerbating the hypertensive phenotype. mRNA levels of *Htr2b* are increased in the mesenteric arteries suggesting this receptor begins to contribute to the disease phenotype. Endothelium-denuded isolated superior mesenteric arteries of DOCA-salt rats have a substantial increase in maximum contraction in response to the 5-HT_{2B} agonist BW723C86 compared to normotensive rats, indicating a smooth muscle cell-mediated effect. The 5-HT_{2B} antagonist LY-272015 effectively reduced mean blood pressure in DOCA-salt rats with no effect on normotensive rats [90]. These results indicate that in the context of injury, 5-HT_{2B} influences vessel contraction contributing to hypertension.

The use of percutaneous interventions such as balloon angioplasty and stenting has widened for the treatment of occluded vasculature. A concern accompanying these types of interventions is the restenosis of the vessel through infiltration of smooth muscle cells. 5-HT_{2B} influences vascular restenosis modeled through wire injury of the femoral artery. Administration of BW723C86 intensifies restenosis by increasing the degree of neointima formation. Wire injury

denudes the vascular endothelium, inducing a strong smooth muscle cell response. Smooth muscle cells respond to 5-HT_{2B} agonism by increasing their proliferation and migration. This adverse response contributes to neointima formation and is blocked in 5-HT_{2B} knockout mice. The intracellular signaling of 5-HT_{2B} in this context is not through the canonical Gαq protein but through β-arrestin2 mediated activation of mammalian target of rapamycin/p10S6K signaling [91].

These findings reveal a smooth muscle cell-mediated role of 5-HT_{2B} in exacerbating arterial contraction in hypertensive patients and vascular restenosis following percutaneous intervention which could potentially be leveraged to therapeutically reduce injurious vascular remodeling.

2.4.3 Hypertrophic response to 5-HT_{2B} stimulation

Cardiac hypertrophy is a physiological adaptation in response to increased workload, whether it is through increased chronotropic or ionotropic effects. While this can be an advantageous adaptation, as seen following exercise by an athlete, prolonged and extensive hypertrophic remodeling can lead to cardiomyocyte death and cardiac fibrosis. 5-HT_{2B} functions in cardiac hypertrophy in a context-dependent manner wherein different experimental models yield results contingent upon the method of hypertrophy induction and cell populations influenced.

Chronic adrenergic stimulation of cardiomyocytes through β-adrenergic activation is a strong predictor of morbidity and mortality in cases of congestive heart failure. Models using prolonged dosing with norepinephrine and the specific β1/β2 adrenergic agonist isoproterenol have been instrumental in elucidating the mechanisms underlying cardiac hypertrophy in response to sympathetic stimulation. 5-HT levels are also associated with sympathetic

overstimulation providing a potential mechanism for 5-HT_{2B} overexpression-induced myocardial hypertrophy [92]. Isoproterenol administration causes an increase in heart mass, heart rate, and cardiomyocyte size. Despite cardiomyocytes expressing 5-HT_{2B}, activation of the receptor does not elicit a contractile response [48]. One reported function of 5-HT_{2B} antagonism in norepinephrine induced cardiac hypertrophy is through the downregulation of Bax, decreasing cardiomyocyte apoptosis and partially reversing established cardiac hypertrophy [93].

An important hallmark of cardiac hypertrophy is an increase in the inflammatory milieu within the myocardium. In response to *in vitro* isoproterenol induction, CFs will secrete the inflammatory cytokines IL-6, IL-1β, and tumor necrosis factor-α. This increase is prevented in 5-HT_{2B} knockout CFs or when treated with a 5-HT_{2B} antagonist. This same cytokine response is observed *in vivo*, and the 5-HT_{2B} antagonist SB206553 prevents increases in plasma levels of these inflammatory cytokine and subsequent cardiac hypertrophy, indicating a deleterious role of CF 5-HT_{2B} signaling [92]. The contribution of CFs was further magnified in a model of cardiomyocyte-driven overexpression of 5-HT_{2B} in mice on a *Htr2b*$^{-/-}$ background, thus relegating 5-HT_{2B} expression strictly to cardiomyocytes. In response to chronic isoproterenol infusion, these transgenic animals do not develop cardiac hypertrophy or exhibit a decrease in cardiac function. The transgenic animals also do not exhibit an increase in IL-6, IL-1β, or TGFβ1, indicating a cardiomyocyte-independent mechanism. It was reported in human LV tissue that 5-HT_{2B} co-localizes and co-precipitates with another GPCR, AT_1R. These two receptors work in concert to initiate cytokine release that drives ventricle dilatation, wall thinning, and hypertrophy (**Figure 2.6**). Activation of both receptors by their respective ligands is required to achieve cytokine release. An investigation of 16 patients diagnosed with congestive heart failure revealed that 5-HT_{2B} expression is significantly elevated irrespective of cardiomyopathy etiology, disease severity, or treatment. 5-HT_{2B} expression significantly correlated with

expression of the cytokines IL-6, tumor necrosis factor-α, and TGFβ1, further highlighting its contribution in cardiac hypertrophy [35].

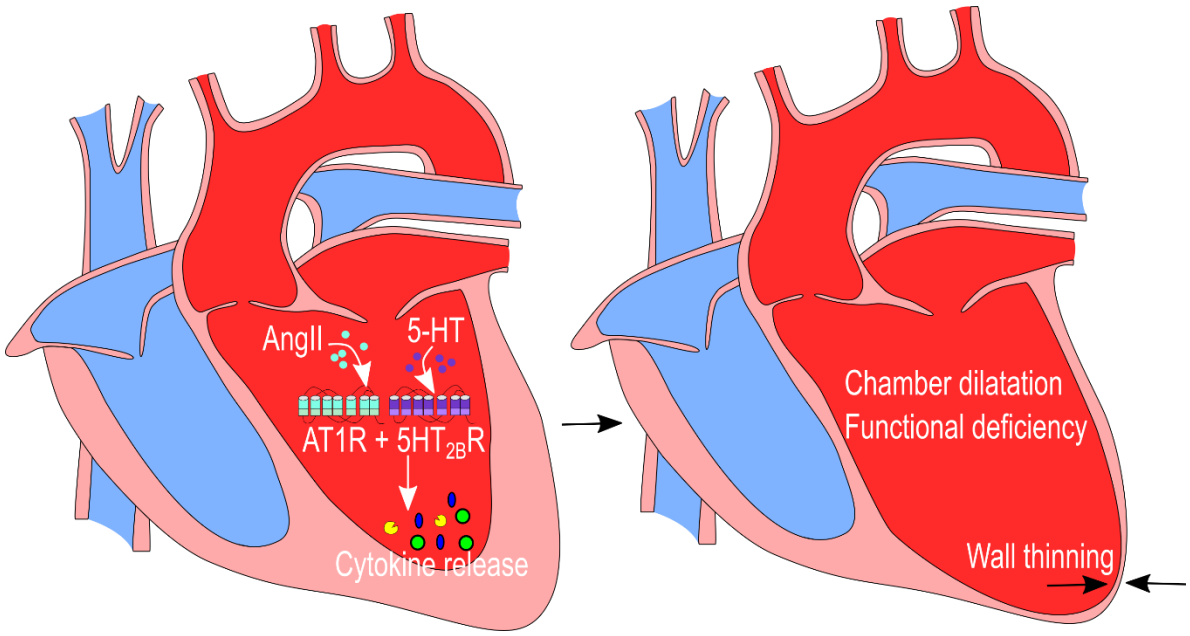

Figure 2.6. Cardiac hypertrophy driven by concomitant activation of AT_1R and 5-HT_{2B}. Inflammatory and fibrotic cytokines released following AT_1R and/or 5-HT_{2B} activation lead to LV remodeling as seen by wall thinning and chamber dilatation.

Left ventricular hypertrophy has been linked with excessive formation of reactive oxygen species (**ROS**). Cardiac ROS is triggered by AngII as well as isoproterenol, both of which elicit a hypertrophic cardiac response. Administration of the 5-HT_{2B} antagonist SB215505 is sufficient to prevent cardiac dilatation and increased mass in a load-independent manner as it acts without cardiodepression or lowering blood pressure. The effect of treatment can be attributed to a normalization of the superoxide anion of oxygen by abolishing NAD(P)H oxidase over-activation. The *in vivo* findings were replicated in LV fibroblasts, further supporting the idea that 5-HT_{2B} acts through CFs [94]. In addition, ROS generation could potentially be linked to a functional role of 5-HT_{2B} in mitochondria. This study highlights the interplay between 5-HT_{2B} and AT_1R to regulate cardiac hypertrophy through production of hypertrophic cytokines and ROS.

Arterial banding is another methodology to induce cardiac hypertrophy by artificially increasing loading immediately distal to the ventricles. The tissue responds through cardiomyocyte hypertrophy, fibrosis, and cardiomyocyte apoptosis. Banding of the pulmonary artery causes a decrease in cardiac output due to TGFβ1-induced collagen deposition which can be mitigated through 5-HT_{2B} antagonism [95]. Wistar rats that have undergone an aortic banding procedure increase the expression of *Htr2b* in cardiomyocytes. Administration of a 5-HT_{2B} antagonist prevents the hypertrophic characteristics of increased heart mass and decreased wall thickness. Cardiomyocyte hypertrophy in response to mechanical stress was found to be mediated by nuclear factor-κB and blocked through 5-HT_{2B} antagonism [96]. These data point to 5-HT_{2B} directly influencing cardiomyocyte hypertrophy in response to mechanical load.

Spontaneously hypertensive rats (**SHR**) progressively develop diastolic dysfunction with preserved ejection fraction without any exogenous stimuli. After a few weeks of hypertension, diastolic dysfunction develops without a deterioration of systolic function, similar to essential hypertension in humans. Administration of the highly selective 5-HT_{2B} antagonist RS127445 during the natural course of hypertensive cardiomyopathy in SHRs did not reduce left ventricular dilatation despite increased *Htr2b* mRNA but instead exacerbated LV dilatation and thinning of the septal and posterior walls, resulting in a severe eccentric hypertrophic phenotype. Brain natriuretic peptide levels, a cardiac hormone correlated with hypertension and hypertrophy, are decreased by RS127445 despite worsened cardiac hypertrophy, pointing to an intracellular mechanism independent of the pathological state. Interestingly, 5-HT_{2B} antagonism causes an increase in subendocardial interstitial fibrosis in SHRs. In the same study, aortic rings isolated from WT and 5-HT_{2B} knockout mice demonstrated different vasoactive responses when stimulated with the general 5-HT_2 agonist α-methyl-5-HT. WT samples respond in a dose dependent manner, where 5-HT_{2B} mutants vasoconstrict with increased tension, indicating a

potential vasodilating role of 5-HT_{2B} [97]. These confounding results to aforementioned studies highlight the context-dependent action of 5-HT_{2B} signaling in the realm of cardiac hypertrophy, and its actions must be understood in a variety of environments to characterize its pathologic or therapeutic mechanisms.

Cardiac hypertrophy is a complex condition associated with a wide variety of initiating factors. 5-HT_{2B} plays a dual function in both CFs and cardiomyocytes regulating the *in vivo* response to these factors.

2.5 Future considerations

Findings throughout the literature show that multiple cardiopulmonary diseases can potentially be addressed through therapeutic manipulation of 5-HT_{2B} signaling (**Figure 2.7**). The tissue distribution and function of 5-HT_{2B} in rodents and humans are similar, emphasizing the translational importance of the findings described in rodent models [98]. Importantly, drugs (and their metabolites) targeting serotonergic signaling should be screened for activation of 5-HT_{2B}, as it has been well documented in cases of valve disease and PAH that 5-HT_{2B} activation significantly increases risk of disease. Multiple conditions mediated by vascular and interstitial cell dysfunction have been reported to be facilitated through signaling of 5-HT_{2B}. In particular, valve hyperplasia, arterial remodeling leading to pathologic RVSP and subsequently PAH, and inflammatory cytokine secretion upstream of cardiac hypertrophy all have contributions from 5-HT_{2B}. Evidence has been presented for the influence of 5-HT_{2B} signaling over both resident and recruited cells, indicating a utility in both early and chronic stages of disease. Further investigation into disease- and tissue-specific 5-HT_{2B}-targeted treatment paradigms is warranted based on the therapeutic potential supported by strong evidence put forth throughout years of research and current lack of effective therapies for cardiopulmonary disease.

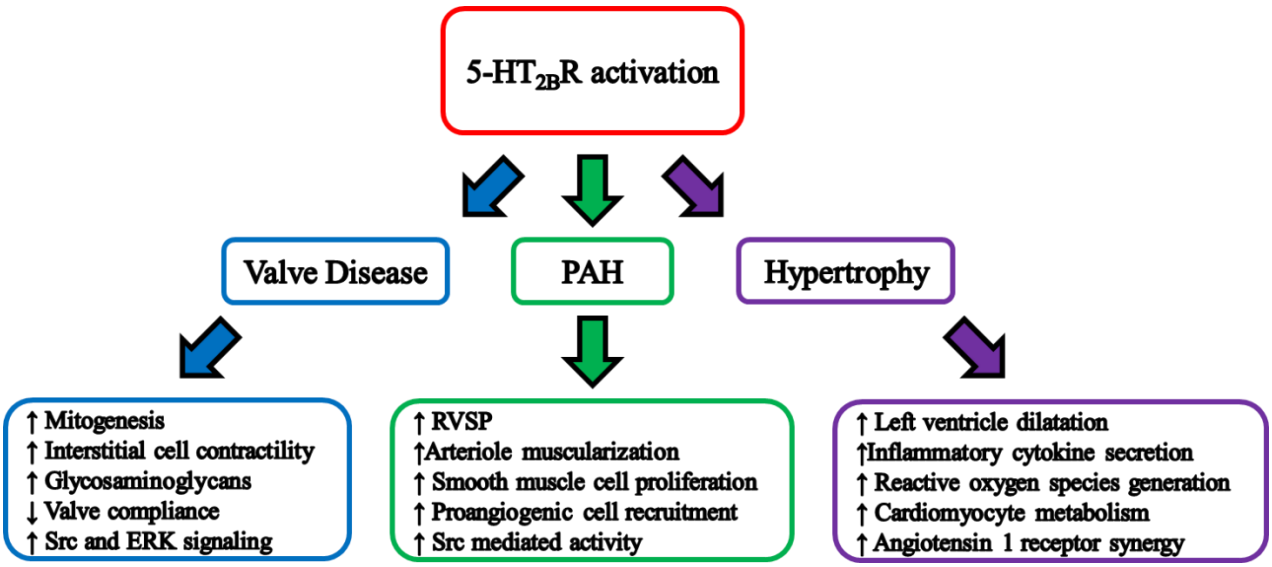

Figure 2.7. Cardiopulmonary diseases facilitated by 5-HT$_{2B}$ activity.

Chapter 3

Global 5-HT$_{2B}$ Antagonism Preserves Cardiac Structure and Function Following MI

Text for Chapter 3 was adapted from **Snider JC**, Riley LA, Mallory NT, Bersi MR, Gautam R, Zhang Q, Mahadevan-Jansen A, Maroteaux L, Lal H, and Merryman WD. Targeting 5-HT$_{2B}$ Receptor Signaling Prevents Border Zone Expansion and Improves Microstructural Remodeling after Myocardial Infarction. *Submitted*

3.1 Abstract

Introduction: Serotonin signaling, specifically from the 5-HT$_{2B}$ receptor, has been shown to control fibrotic remodeling in the setting of various cardiopulmonary pathologies. One pathology that has not been associated with 5-HT$_{2B}$ signaling is MI. The tissue response to MI is drastic, with infiltration of various cells types which coordinate to remove cellular debris and form a permanent scar. The scar formation process has been shown to directly influence future cardiac outcomes. Since 5-HT$_{2B}$ signaling plays a role in fibrotic remodeling in cardiopulmonary disease, we investigated the therapeutic potential of 5-HT$_{2B}$ antagonism following MI in mice.

Methods: Two independent 5-HT$_{2B}$ antagonists were administered following experimental MI in adult mice. Echocardiography was used to assess cardiac structure and function throughout the duration of the experiment after which we investigated histological and microstructural changes. The scar and BZ were characterized, and collagen content was analyzed using PSR stain, PSR staining imaged under polarized light, SHG imaging, and AFM. Lastly, we investigated changes to uninjured myocardium through quantifying cardiomyocyte area distant to the infarct.

Results: Systolic structure and cardiac function were both improved with administration of a 5-HT_{2B} antagonist following MI. The fibrotic injury response was hampered, as seen by a decrease in scar thickness and prevention of BZ expansion. Thinner collagen fibers were also more highly aligned, contributing to an increase in contractility. Tissue stiffness was decreased with 5-HT_{2B} antagonism measured by AFM. These changes to scar formation prevented cardiomyocyte hypertrophy in the viable, remote tissue.

Conclusions: 5-HT_{2B} signaling plays a detrimental role in the healing process following MI. Pharmacological inhibition of 5-HT_{2B} improves the quality of scar formation, preventing scar expansion and adverse myocardial remodeling.

3.2 Introduction

Serotonergic dysfunction has long been understood to contribute to a myriad of cardiopulmonary pathologies. Specifically, signaling through 5-HT_{2B} controls the fibrotic remodeling involved in valvular heart disease and pulmonary hypertension [43], [76], [78], [99]. In response to TGFβ, fibroblast-like valve interstitial cells undergo myofibroblast transformation and remodel the valve, which can be prevented with the administration of a 5-HT_{2B} antagonist [31]. In a murine model of experimental PAH, it has been shown that 5-HT_{2B} is necessary in the myeloid compartment to develop disease and instigate the contraction and stiffening of arterioles [32], [33]. 5-HT_{2B} has also been shown to play an integral role in mediating isoproterenol-induced cardiac hypertrophy through modulating the inflammatory milieu in a CF-dependent manner [35]. Downstream mediators of 5-HT_{2B} signaling are the mitogen-activated protein kinase effector p38 and the tyrosine kinase Src; both of which are known regulators of cell contractility, ECM deposition, and ECM stiffness [67], [100]–[102].

MI initiates a drastic and coordinated wound healing response to address myocardial necrosis. An initial inflammatory response begins with neutrophil influx to degrade damaged ECM and facilitate macrophage polarization [103]. Monocytes infiltrate the injury to digest damaged and degraded tissue to debride the wound. These cells then shift their function to attenuate inflammation and promote CF infiltration, angiogenesis, and collagen deposition [104]. CFs are best characterized by their role in matrix production and deposition following injury or insult. The resolution of inflammation is not merely a cessation of pro-inflammatory signals, but the activation of inhibitory pathways, driven by mediators such as TGFβ1 and IL-10, to aid in the resolution of inflammation. While CFs have not been directly established as an anti-inflammatory cell type, their drastic phenotypic changes in response to anti-inflammatory signals suggest a potential role [11]. The start of the remodeling phase of healing is marked by the infiltration of the infarct BZ with myofibroblasts. Myofibroblasts are an activated fibroblast phenotype that is hyper-secretory and hyper-contractile, extensively secreting matrix proteins and contracting newly deposited matrix.

Several strategies for improving healing and controlling cardiac fibrosis have been proposed and implemented in the clinic, but there is less success in human patients than studies suggest from *in vitro* and *in vivo* animal models. This discrepancy in part is due to the complex, multi-cellular system that controls chemical and mechanical cues during healing. The diverse population of cells that express and are controlled by 5-HT_{2B} has resulted in many interesting findings, all of which could affect the healing process following MI. 5-HT_{2B} has been shown to stimulate detrimental behaviors in major cell types that are also involved in healing following MI. Despite the diverse processes that are initiated following an MI, the ultimate outcome is the formation of a permanent scar. The degree, duration, and successful resolution of the inflammatory phase as well as the emergence of CFs as the main effector cell type all influence the quantity and quality of fibrotic tissue deposited to repair the wound. Therefore, we

hypothesized that global 5-HT_{2B} antagonism could preferentially alter the wound healing response in a manner that improves cardiac performance. We utilized a permanent occlusion model of experimental MI along with administration of 5-HT_{2B} antagonists and performed serial echocardiography to track the changes in cardiac structure and function. We then explored the histological and microstructural changes induced by 5-HT_{2B} antagonism to establish 5-HT_{2B} as a target for improving outcomes following experimental MI.

3.3 Methods

Mice

All mouse experiments were approved by the Vanderbilt Institutional Animal Care and Use Committee before their commencement. Mice used in this study were WT C57BL/6 (Jackson Laboratory, Stock No. 000664).

Animal Studies

MI was induced in 12-week-old mice by permanent coronary artery ligation, as previously described [105]–[107]. Briefly, mice were anesthetized with 2% isoflurane inhalation. A small incision was made over the left chest and dissection and retraction of the pectoral major and minor muscles was performed. A small hole was punctured in the fourth intercostal space and gently held open with a mosquito clamp. Using gentle pressure superior and inferior to the heart, the heart was popped out of the chest. A 6-0 silk suture was used to ligate the left main descending coronary artery approximately 3 mm from its origin. The heart was immediately placed back into the chest cavity, air was manually evacuated, the muscle was replaced, and the skin sutured.

For antagonist studies, mice were administered 1 mg/kg/day of either the 5-HT_{2B} antagonist SB204741 (**SB**; Tocris, Cat. No. 1372) or RS127445 hydrochloride (**RS**; Tocris, Cat. No. 2993) – both dissolved in a 50:50 mixture of dimethyl sulfoxide (**DMSO**; Sigma D8418) and polyethylene glycol 400 (**PEG400**; Fisher Scientific, P167-1) to dilute the organic solvent. Control mice were administered 50:50 PEG400:DMSO. SB was administered subcutaneously via microosmotic pumps (**Figure 3.1**; Alzet Corp, 1004). RS was administered through twice-daily intraperitoneal injections of 0.5 mg/kg separated by 6-8 hours due to the limited half-life of the compound *in vivo* (**Figure 3.2**) [108].

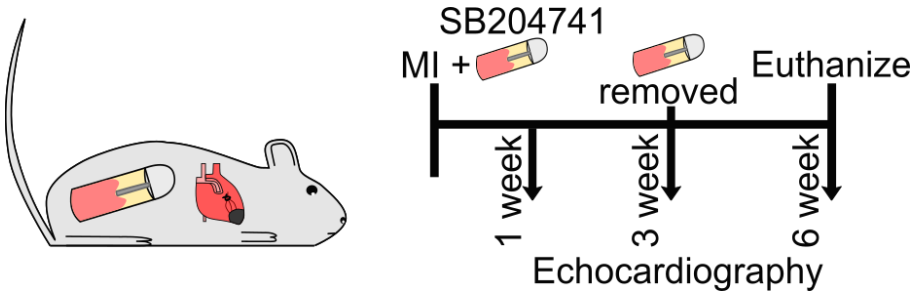

Figure 3.1. Experimental approach for MI with SB treatment.
12-week-old mice were subjected to MI surgery and coincidentally administered either vehicle control or the 5-HT_{2B} antagonist SB. Treatments were administered subcutaneous via microosmotic pump. Treatment began day of injury and continued for three weeks. Microosmotic pumps were removed at 3 weeks, and mice were dissected six weeks after injury. Echocardiography was performed at indicated times.

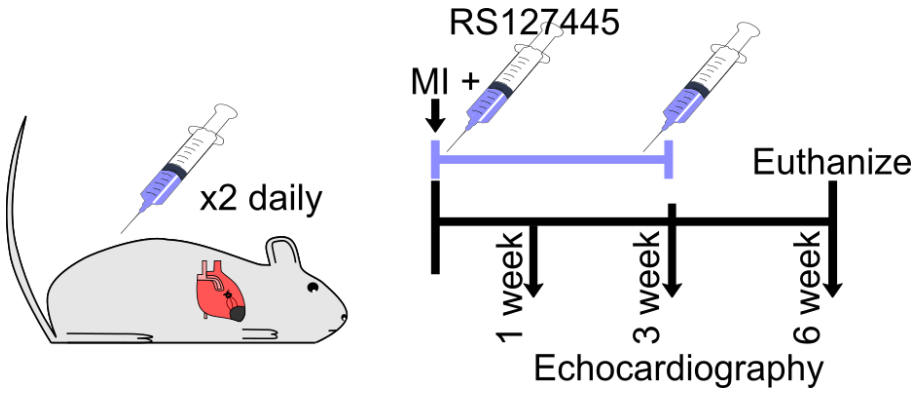

Figure 3.2. Experimental approach for MI with RS treatment.
12-week-old mice were subjected to MI surgery and coincidentally administered either vehicle control or the 5-HT_{2B} antagonist RS. Treatments were administered intraperitoneal via twice-daily injections. Treatment began day of injury and continued for three weeks. Injections ceased at 3 weeks, and mice were dissected six weeks after injury. Echocardiography was performed at indicated times.

At the end of each study, mice were euthanized through CO_2 inhalation in accordance with Vanderbilt University Medical Center's Division of Animal Care guidelines.

Echocardiography

Blinded echocardiographic measurements were taken from short-axis cardiac M-mode images captured on a Vevo2100 small-animal ultrasound system (VisualSonics). A minimum of 9 independent measurements of ventricle dimensions were used to calculate metrics of cardiac structure and function for each mouse at each time point. Global longitudinal strain (**GLS**) measurements were acquired using the VevoStrain software package to measure long-axis B-mode images (VisualSonics) at the initiation of contraction. Two independent images were analyzed for each mouse at each time point. Measurements were taken prior to surgery (Day 0), as well as 1, 3, and 6 weeks post-surgery. Exclusion criteria were employed for animals without at least a 15% decrease or more than an 85% decrease in ejection fraction at day seven compared to day zero to ensure that surgery was successful.

Histology

Upon euthanasia, hearts were perfused with PBS-/-, excised, and submerged in 3M potassium chloride to arrest hearts in diastole. Hearts were then bisected along the transverse plane just above where the suture was tied to induce MI, embedded in OCT media (Fisher Scientific, 23-730-571), and snap frozen. Frozen tissue was cryosectioned at 7µm, mounted onto glass slides, then stored at -20°C. Picrosirius red (**PSR**) staining was employed to identify fibrosis (red) and cell bodies (yellow). Prior to staining, slides were brought to room temperature, OCT was removed via PBS-/- wash, and sections were fixed for one hour in Bouin's solution (Sigma-Aldrich, HT10132) at 55°C. Slides were stained in PSR (Electron

Microscopy Sciences, 26357) for one hour at room temperature, dehydrated in ethanol, and cleared in xylenes. Images were analyzed using a semiautomated image-processing pipeline that was developed based on local ventricular thickness measurements and color segmentation [109], [110]. This process extracted regional area fractions of myocardium and fibrosis as well as local thickness values used to quantify tissue properties. The BZ was defined by the change in collagen area fraction per circumferential degree in the transition region lying between tissues comprised of 85% collagen (scar) to 15% collagen (uninjured myocardium). PSR-stained sections were imaged under polarized light to study collagen fiber thickness distributions and analyzed using a color segmentation algorithm as previously described [110].

Second Harmonic Generation

Second harmonic generation (**SHG**) produces images with a diffraction-limited resolution (<300 nm), is intrinsic to specific structures allowing for quantification of collagen without staining or background noise, and can be used to classify the anisotropic properties of collagen fibers [111], [112]. SHG images were acquired using home built multimodal imaging platform equipped with a photomultiplier tube (GaAsP Amplified PMT, Thorlabs, USA) on the epi-detection port [113]. Each image was integrated for 7 microseconds/pixel and recorded using a 20x water immersion objective (Olympus XLUMPLFLN, 1.0NA) with a high spatial sampling density (401 nm/pixel) covering 1024x1024 pixels per image. SHG signals were generated using 798 nm picosecond laser operates with a pulse repetition rate of 80MHz (power ~30mW on the sample) and collected at using 400/±40nm filter (Semrock, Brattleboro, VT, USA). Scanning and detection for imaging is controlled through ThorImageLS version 2.1 (Thorlabs Imaging Research, Sterling, VA, USA).

The OrientationJ plugin was used in ImageJ (NIH) to obtain the distribution of fiber angles from each image [114], [115]. Each distribution was smoothed using a centered moving average with a five degree window, followed by calculation of the cumulative distribution function (**CDF**),

$$F(\Phi) = \sum_{\Phi_i=-89.5°}^{x} I(\Phi_i)$$

where I(Φ) is the amplitude of the distribution at angle Φ. The CDF of an isotropic distribution is a straight line. Therefore, we a fit a first-degree polynomial to the distribution and calculated the correlation coefficient (R^2) as a goodness of fit. If the R^2 was above a threshold of 0.98 (below which dominant orientations in the fiber orientation distributions started to peak), the distribution was considered isotropic, otherwise, the distribution was considered anisotropic. **Figure 3.3** shows a range of obtained R^2 value from accompanying SHG images and fiber angle distributions. [116].

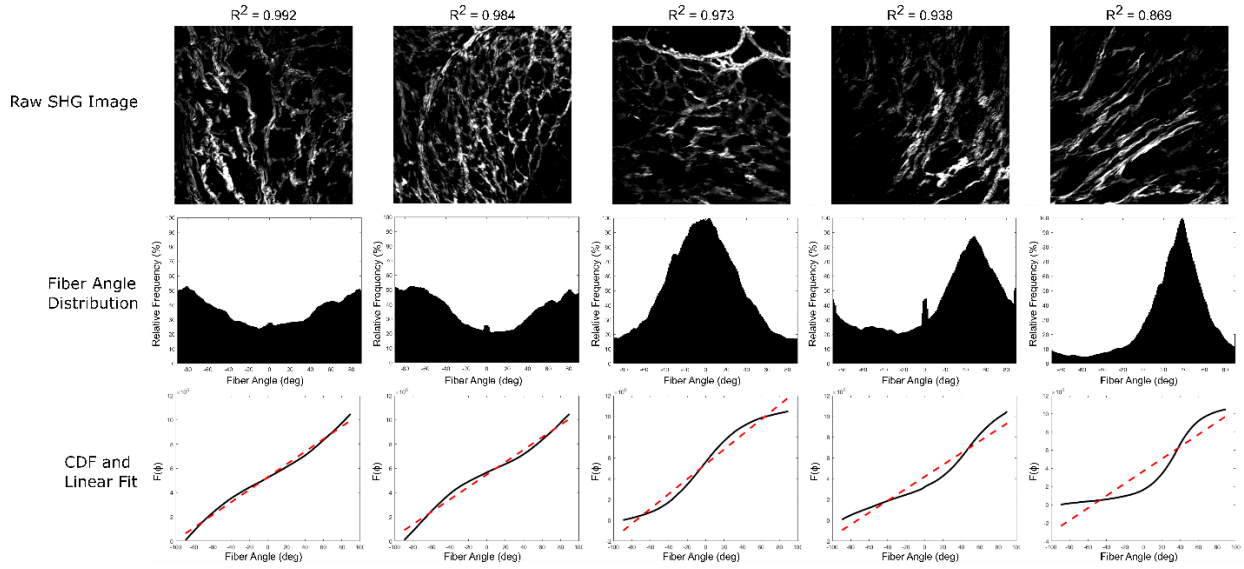

Figure 3.3. SHG analysis and curve fitting to determine anisotropy.
Top Row, Raw SHG images throughout the BZ organized from best (left) to worst (right) fit of a first-order polynomial. Middle Row, Distribution of fiber angles. As you move from left to right, peaks start to emerge which would result in anisotropic distribution. These peaks start to emerge at $R^2 < 0.98$ and the width of the peak thins and amplitude increases as R^2 decreases. Bottom Row, First-order polynomial fitting (red dashed line) to the CDF obtained from the distributions in the middle row.

Atomic Force Microscopy

Tissue sections which had been arrested in diastole using 3M potassium chloride upon dissection were brought to room temperature and cleared of OCT in PBS-/-. A Biocatalyst atomic force microscope (**AFM**; Bruker, CA) was used to measure tissue topology and stiffness. The AFM was operated in peak force quantitative nanomechanical mapping scanning mode (Peak Force QNM) using probes constituted of blunted pyramidal tips designed for biological samples (MLCT-Bio, Bruker, CA). The system was calibrated to obtain the spring constant and deflection sensitivity of each probe then confirmed on standard polyacrylamide gels of known stiffness (2, 20, and 40 kPa). Measurements were made in PBS for the scar, BZ, and remote myocardium by scanning 3-6 regions of 36 – 100 μm^2 each. Mean elastic modulus was calculated for each scan, then averaged for each mouse.

Wheat Germ Agglutinin Staining

For cardiomyocyte cross-sectional area analysis, tissue sections which had been arrested in diastole upon dissection were brought to room temperature and OCT was removed via Hank's balanced salt solution wash. The tissue was fixed in 4% paraformaldehyde for 15 min at 37°C then stained in 50 µg/mL wheat germ agglutinin (**WGA**; Invitrogen, Cat# W11262) for 30 minutes at room temperature to label cardiomyocyte cell walls. Three, 20x images of short-axis cardiomyocytes were taken in the uninjured myocardium. Cardiomyocyte area was calculated using a custom pipeline in CellProfiler [117]. A minimum of 580 cells were quantified per animal.

Quantitative Polymerase Chain Reaction

A cohort of animals was set aside exclusively for quantitative polymerase chain reaction (**qPCR**) and dissected under RNase-free conditions and immediately snap frozen. Samples were subsequently thawed, and scar tissue was isolated via microdissection by transversely bisecting the tissue at the suture and homogenized using a bead beater and lysis matrix tubes (MP Biomedicals, 116923050). RNA was isolated using the RNeasy Mini Kit (Qiagen, 74104) and cDNA was synthesized using the Superscript IV system (Invitrogen, 18091050). Real time qPCR was performed using SYBR Green PCR Supermix (Bio-Rad, 1708882), the primers listed in **Table 3-1**, and a Bio-Rad CFX96 C100 thermocycler. *Gapdh* and *Hprt1* were used as housekeeping genes. Data presented was calculated using the delta delta Ct method and statistical analysis was run on delta Ct values.

Table 3-1 qPCR primer sequences

Gene Target	Forward Primer (5' to 3')	Reverse Primer (5' to 3')
Gapdh	ATGACAATGAATACGGCTACAG	TCTCTTGCTCAGTGTCCTTG
Hprt1	CCCCAAAATGGTTAAGGTTGC	AACAAAGTCTGGCCTGTATCC
Nppb	GCACAAGATAGACCGGATCG	CCCAGGCAGAGTCAGAAAC
Htr2b	TCAATAGGCATCGCCATCCCAG	CCATGATGGTGAGAGGTGCGAA
Htr2a	AACCCCATTCACCATAGCC	TGCCACAAAAGAGCCTATGAG

Statistical Analysis

Statistical analysis was performed using SigmaPlot version 11. Shapiro-Wilk test was used to test for data normality. Subsequent statistical analyses used either a 2-way ANOVA with Holm-Sidak post hoc or a Kruskal-Wallis rank-sum test with Conover-Iman post hoc test for nonparametric data. A 2-tailed Student *t* test was used for comparisons of two normally distributed groups. Applicable tests and significance are labeled in figure captions with $P<0.05$ as the cutoff for data to be considered significantly different.

3.4 Results

3.4.1 5-HT$_{2B}$ antagonism improves echocardiographic metrics after MI

To test our hypothesis that 5-HT$_{2B}$ regulates scar formation following MI, we first confirmed the induction of *Htr2b* gene expression after experimental MI. We observe a marked increase in *Htr2b* expression in the early stages of wound healing at three days after injury which was sustained into the fibrotic healing phase seven days after infarction. *Htr2a*, which encodes the only other member of the 5-HT$_2$ receptor subfamily expressed in the cardiovascular system [48], is not upregulated until seven days post-MI, and it is still only induced to a fraction of *Htr2b* levels (**Figure 3.4**).

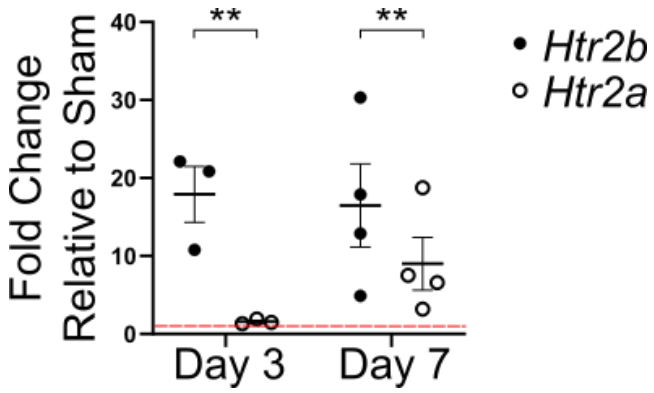

Figure 3.4. *Htr2b* expression increases early and is sustained following MI.
The gene encoding 5-HT$_{2B}$, but not 5-HT$_{2A}$ is significantly upregulated compared to sham operation 3 days after MI surgery and remains significantly upregulated 7 days after MI (N=3-4). Mean ± SEM, **P<0.01, via 2-tailed Student *t* test.

3.4.2 5-HT$_{2B}$ antagonism improves functional outputs and LV dimensions after MI

These findings motivated our exploration into 5-HT$_{2B}$ signaling. To determine if 5-HT$_{2B}$ signaling influences LV remodeling after MI, WT adult mice underwent permanent coronary artery ligation and were administered either vehicle control (DMSO) or the 5-HT$_{2B}$ antagonist SB at the time of injury.

We observed a preservation of cardiac function as determined by increased LV ejection fraction (**EF**) and fractional shortening (**FS**) one week after injury in mice treated with 5-HT_{2B} antagonist; this effect was maintained for the six-week period after injury, even with the removal of the antagonist three weeks post-MI (**Figure 3.5A-B**). There were no observed differences in LV inner dimension (**LVID**) and LV volume (**LV Vol**) at end-diastole (**Figure 3.5C,E**). LVID and LV Vol at end-systole were significantly lower with SB treatment, indicating a contractile capability closer to resembling uninjured levels (**Figure 3.5D,F**).

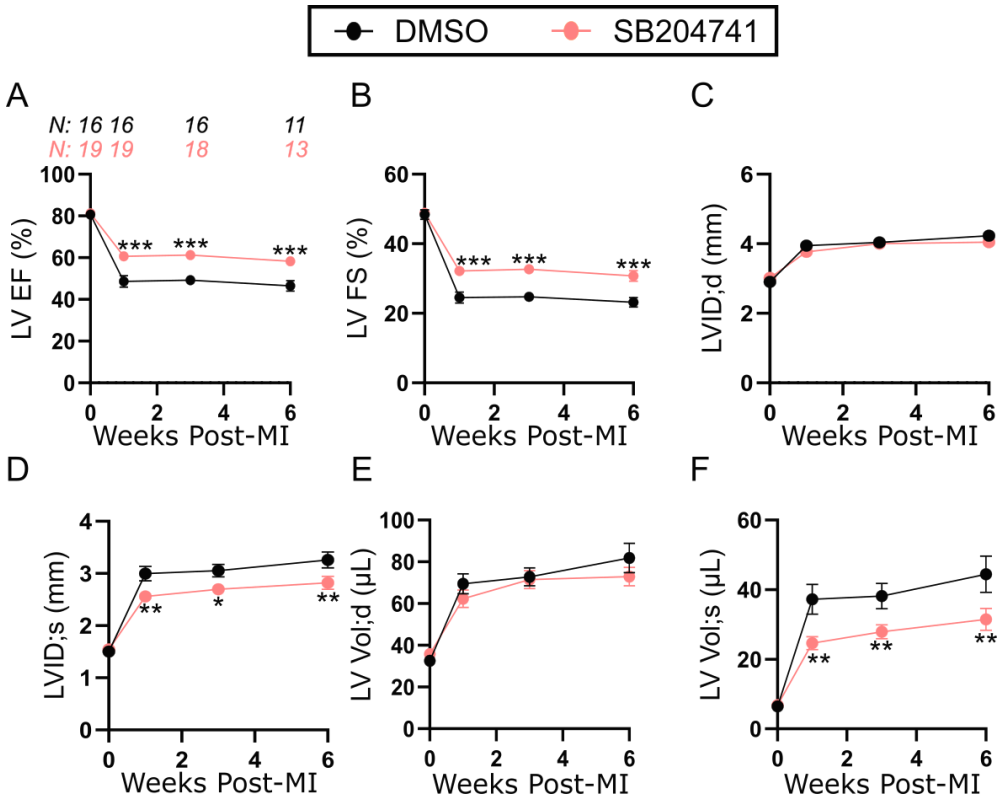

Figure 3.5. SB treatment post-MI preserves cardiac function and systolic structure. **A**, LV EF is improved one week after injury and maintained for the duration of the experiment. **B**, LV FS is improved one week after injury and maintained for the duration of the experiment. **C**,**D**, LVID at end-systole but not at end-diastole was improved with SB treatment. **E**,**F**, LV Vol at end-systole but not at end-diastole was improved with SB treatment. Mean ± SEM, *P<0.05, **P<0.01, ***P<0.001 between DMSO and SB treatments following 2-way ANOVA and Holm-Sidak post hoc test. Number of mice denoted in A applies to subsequent groups.

In order to confirm these results, we repeated this experiment with another selective, high affinity 5-HT_{2B} antagonist, RS. Despite being administered through a different route, we

observed comparable functional effects. LV EF and LF FS were both preserved one week after injury which was maintained for the duration of experiment (**Figure 3.6A-B**). However, we did not observe significant differences in either of the measures of cardiac structure (LVID or LV Vol) during diastole or systole (**Figure 3.6C-F**).

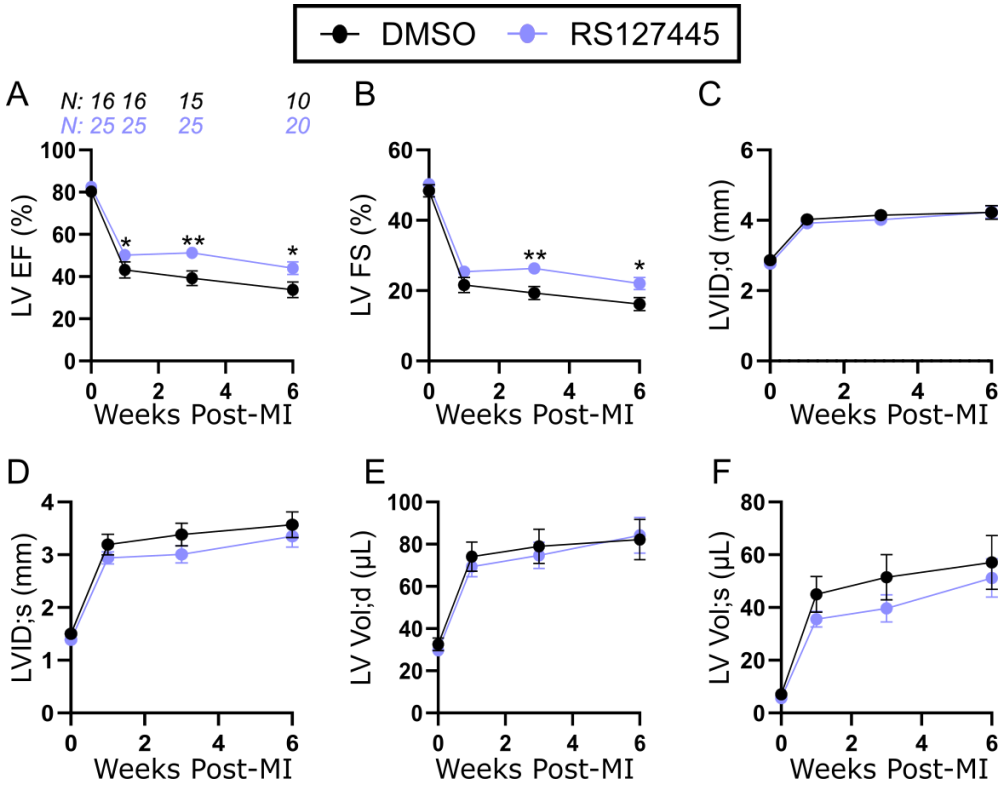

Figure 3.6. Antagonism of 5-HT$_{2B}$ with RS preserves cardiac function post-MI. **A**, LV EF is improved one week after injury and maintained for the duration of the experiment. **B**, LV FS is improved one week after injury and maintained for the duration of the experiment. **C-F**, There were no observed differences with RS treatment in the structural measurements of LVID and LV Vol at both end-diastole and end-systole. Mean ± SEM, *P<0.05, **P<0.01, between DMSO and RS treatments following 2-way ANOVA and Holm-Sidak post hoc test. Number of mice denoted in A applies to subsequent groups.

Interestingly, female mice showed no response to SB treatment (**Figure 3.7A-C**). Therefore, all antagonist studies shown are conducted exclusively in male mice.

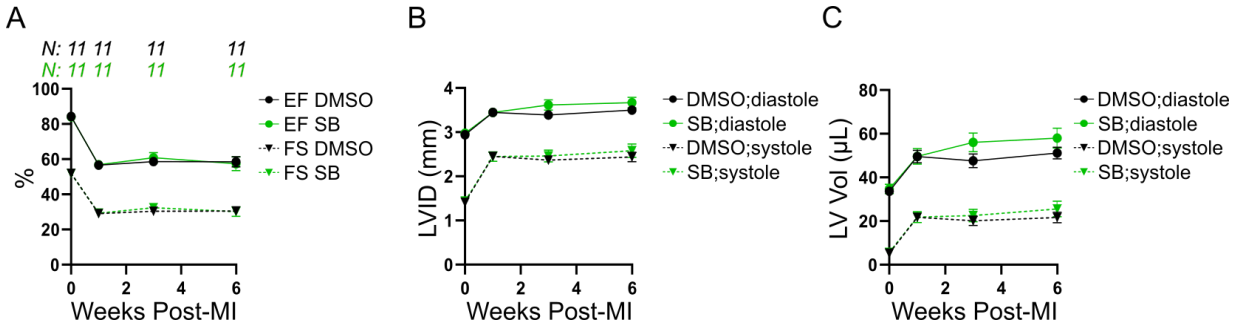

Figure 3.7. 5-HT$_{2B}$ antagonism is ineffective following MI in females.
12-week-old female mice underwent MI surgery. **A**, No difference in EF or FS was observed between DMSO control and SB-treated female mice. **B**, LVID at both end-diastole and end-systole were similar between the two treatments. **C**, LV Vol at both end-diastole and end-systole were similar between the two treatments.

3.4.3 Improved LV deformation observed in the 5-HT$_{2B}$ antagonist-treated cohort

We employed a speckle-tracking algorithm to obtain the GLS of the LV as another sensitive measure of LV function. Uniform elements are formed across the LV wall and the strain is calculated based on the deformation across the elements during a contraction cycle. GLS is a metric that measures the maximum shortening during systole normalized to diastolic length.

While GLS was identically reduced in the control and antagonist-treated groups the first week after injury, cardiac contractility in SB-treated animals was stabilized, while function in DMSO-treated animals continued to deteriorate over the duration of the experiment (**Figure 3.8A-B**). The same trends were observed in the RS-treated cohort. GLS was similarly decreased between the two groups at one week, but the GLS of the control group significantly deteriorated over time while the treated group exhibited a stabilized metric of cardiac contractility (**Figure 3.8C**).

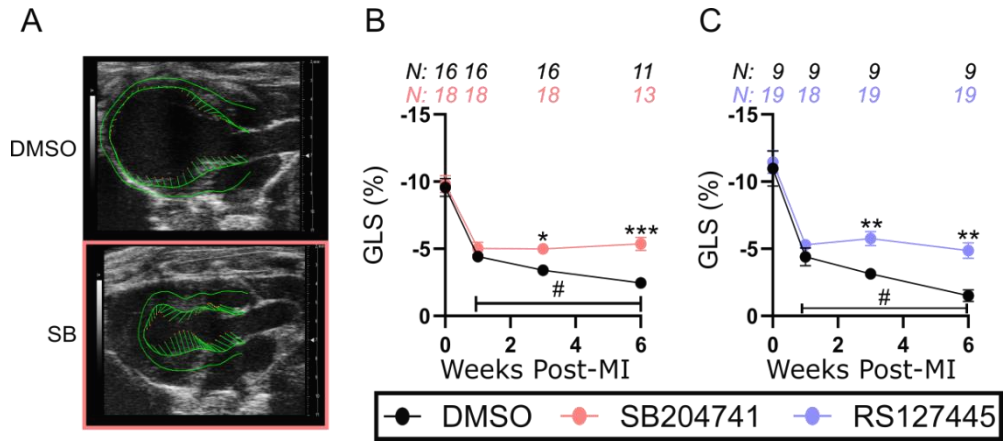

Figure 3.8. Antagonism of 5-HT$_{2B}$ stabilizes LV contractility after MI.
A, Vector diagram showing magnitude and direction of myocardial deformation in systole. **B**, Quantified GLS in DMSO vs. SB treated animals. **C**, Quantified GLS in DMSO vs. RS treated animals. Mean ± SEM, *P<0.05, **P<0.01, ***P<0.001 between DMSO and SB treatments, #P<0.05 between previous timepoint within treatment group following 2-way ANOVA and Holm-Sidak post hoc test.

3.4.4 Scar formation after MI is altered by 5-HT$_{2B}$ antagonism

To understand how changes in tissue architecture contributed to the observed alterations in echocardiographic outputs, we used a custom-built image processing pipeline to analyze short-axis tissue sections six weeks (unless explicitly noted) following MI and explored differences between groups receiving 5-HT$_{2B}$ antagonist or DMSO [12]. PSR staining demarcated viable myocardium (cell bodies stained yellow) from collagenous scar tissue (stained red) and was used to calculate regional tissue thickness as well as identify the BZ (**Figure 3.9A-B**). In SB-treated mice, the deposition of fibrotic tissue was diminished as indicated by the formation of a thinner scar than control mice (**Figure 3.9D**). Scars in the SB-treated group appear to form thinner one week after injury and retain this thinness throughout the course of the experiment.

The BZ (green dots; **Figure 3.9B-C**) was defined as the transition region between collagen-dominated scar tissue (stained >85% red) and myocardium dominated tissue (stained >85% yellow). We calculated the BZ transition rate to quantify the area of material mismatch

between contractile myocardium and stiff, collagenous scar. We observed an increased rate of change from collagen to myocardium (i.e. a shorter BZ region) with 5-HT_{2B} antagonism revealing decreased BZ infiltration and scar disruption of viable myocardium (**Figure 3.9E**). There were no changes detected in the amount of interstitial fibrosis calculated as the area fraction of collagen in the remote, uninjured myocardium (**Figure 3.9F**). Scar thickness and interstitial fibrosis outcomes were similar in RS-treated animals (**Figure 3.9G-H**).

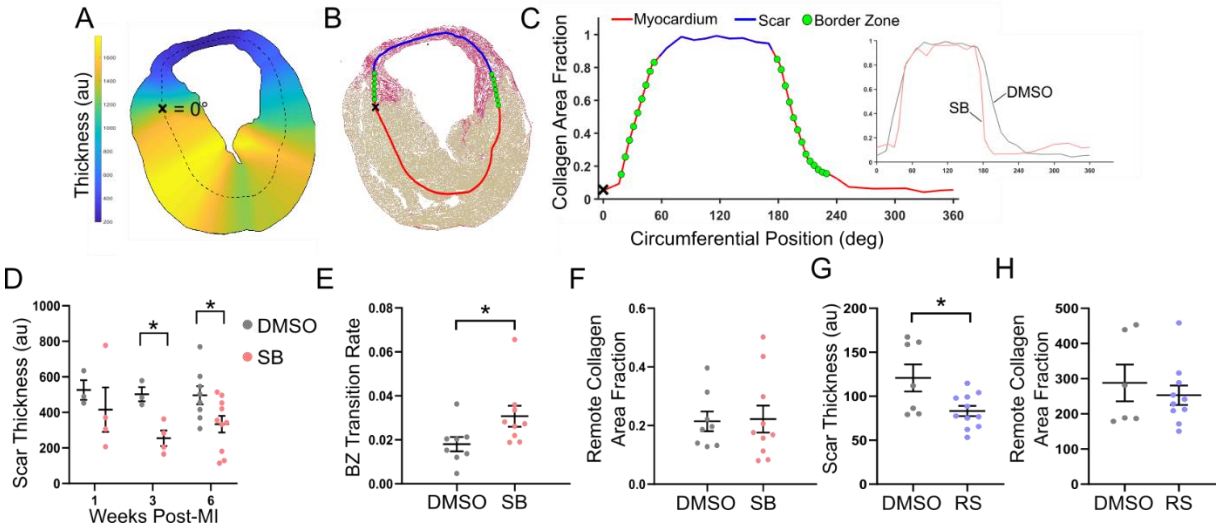

Figure 3.9. Scar morphology and ECM deposition is altered by 5-HT_{2B} antagonism. **A-C**, Analytical approach of calculating tissue thickness (A), demarcation of scar vs. healthy myocardium (B) and (C) identification and mathematical definition of BZ as the transition region between scar dominated (>85% collagen stained red with PSR) and myocardium dominated (>85% myocardium stained yellow) with inset illustrating a representative curve from each treatment. **D**, Thickness of the formed scar is decreased with SB treatment but does not thin over time (N=3-10). **E**, Decreased BZ infiltration with 5-HT_{2B} antagonism as indicated by the rapid transition from scar to myocardium (N=8-10). **F**, No difference in interstitial fibrosis was observed with SB treatment (N=8-10). **G**, Thickness of the formed scar is decreased with RS treatment (N=7-11). **H**, No difference in interstitial fibrosis was observed with RS treatment (N=6-9). All data 6 weeks post-MI except where noted in D. Mean ± SEM, *P<0.05 following (D) 2-way ANOVA and Holm-Sidak post hoc test or (E-H) 2-tailed Student *t* test.

After observing alterations in collagen deposition, we used two separate imaging techniques to gain a better understanding of collagen composition. First, we imaged PSR-stained collagen under polarized light to observe collagen fiber thickness. While there was no

shift in the distribution of collagen fiber thickness in the scar, a higher percentage of thin collagen fibers was present in the BZ with SB treatment and a decreased percentage of thick fibers in the BZ with RS treatment (**Figure 3.10A-C**). Second, SHG imaging was used to analyze collagen fiber orientation. SB-treated mice had a higher fraction of fields of view (**FOV**) dominated by strongly aligned, anisotropic collagen fibers in the BZ, which would impart an improved contractility (**Figure 3.10D**).

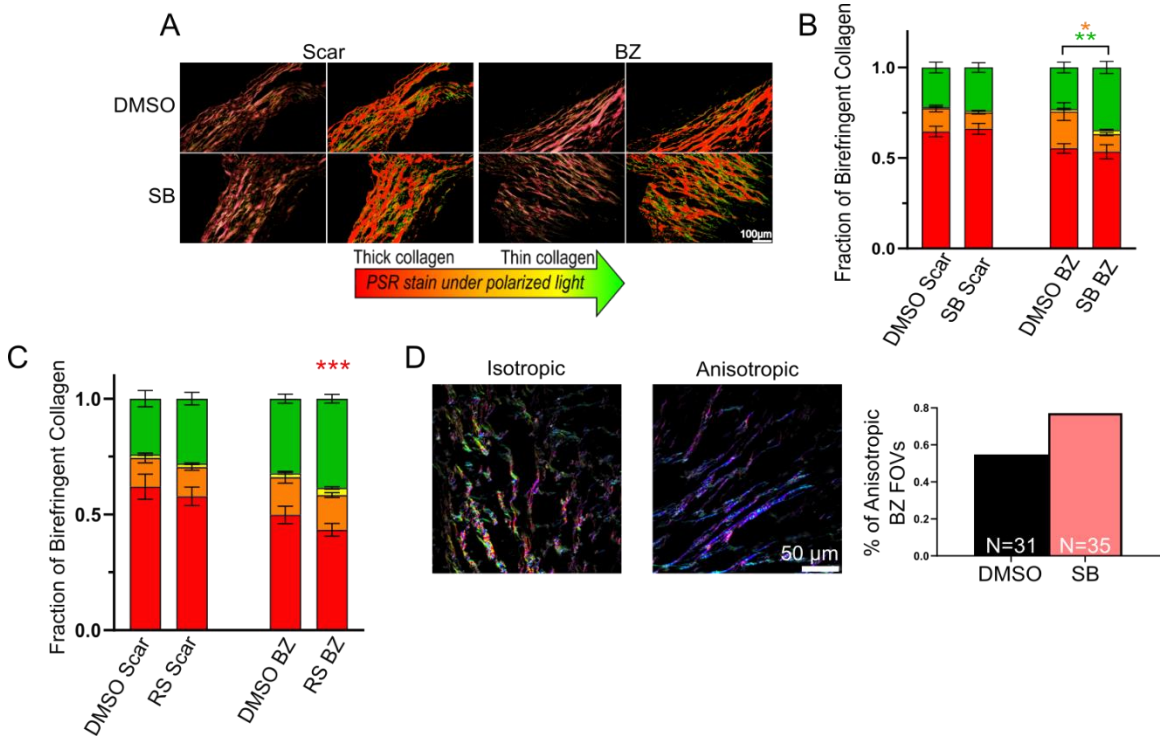

Figure 3.10. Collagen composition is altered by 5-HT$_{2B}$ antagonism.
A-B, PSR stain imaged under polarized light in the BZ and scar revealed an increased proportion of thinner, less mature collagen fibers in the BZ of SB-treated mice (N=9-10). **C**, RS treatment resulted in fewer thick collagen fibers which was redistributed throughout the thinner fiber compartments (N=8-15). **D**, Analysis of collagen fiber orientation in the BZs of DMSO- (31 FOVs across 4 mice) and SB- (35 FOVs across 5 mice) treated animals to quantify the distribution of orientations to classify as isotropic or anisotropic. All data 6 weeks post-MI. B,C, Mean ± SEM, *P<0.05, **P<0.01, ***P<0.001 (color denotes difference between corresponding color proportion following 2-way ANOVA and Holm-Sidak post hoc test.

Despite alterations in the deposition of fibrotic scar tissue and composition of the scar with 5-HT_{2B} antagonism, we did not observe any changes in survival, indicating the preservation of scar integrity (**Figure 3.11A-B**).

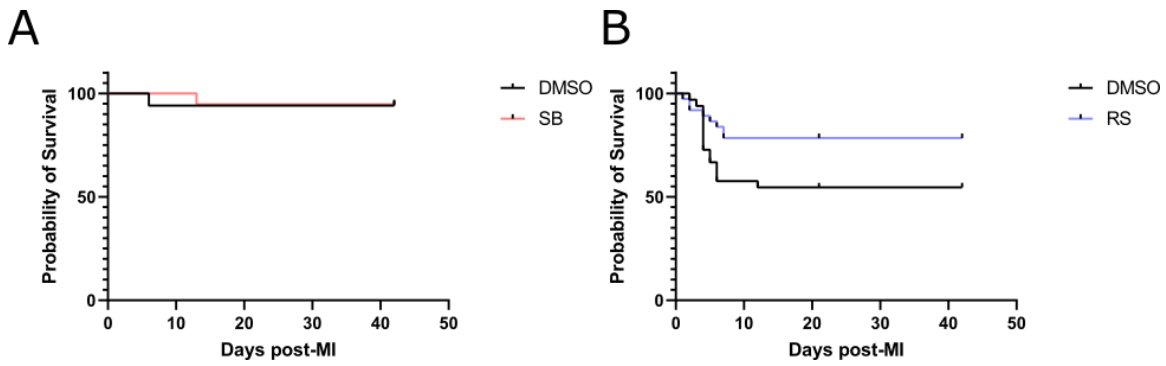

Figure 3.11. Survival post-MI.
No difference in proportion of mice that survived post-MI. **A,** DMSO (N=16) and SB (N=19) and **B**, DMSO (N=33) and RS (N=37)

Histological analyses indicate that treatment with a 5-HT_{2B} antagonist is capable of controlling scar formation after MI and limiting BZ expansion through alterations in collagen fiber formation.

3.4.5 Microstructural changes in response to impaired 5-HT_{2B} signaling

We next explored how the alterations in collagen deposition and composition affected tissue mechanics. AFM was used to investigate the mechanical changes of the fibrotic area to determine if tissue compliance could play a role in preserving cardiac function in response to 5-HT_{2B} antagonism. While there was not an initial difference in tissue stiffness in the early stages of scar formation, antagonist-treated groups showed a decrease in tissue stiffness in both the scar and BZ six weeks following injury (**Figure 3.12A-D**) While the stiffness of tissue in SB-treated groups remains steady, it appears there is a slight but steady increase in scar and BZ stiffness of control animals over the six-week time course (**Figure 3.12B-C**).

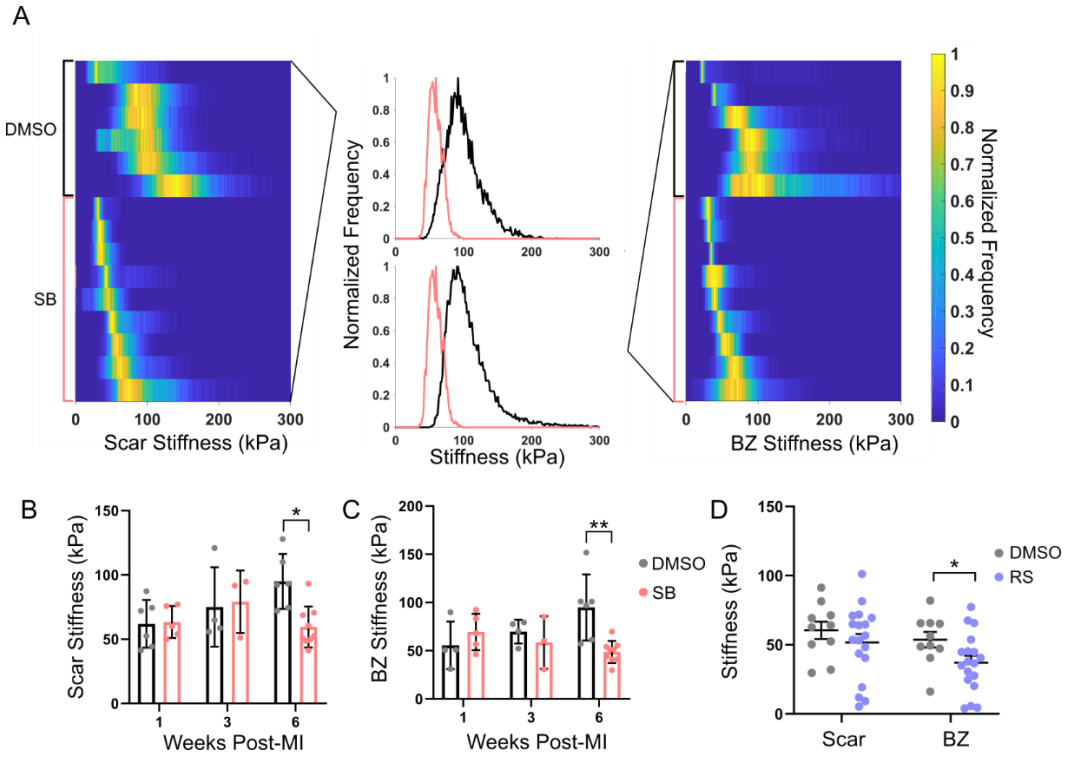

Figure 3.12. Tissue stiffening is prevented with 5-HT$_{2B}$ blockade.
AFM analysis revealed scar and BZ stiffness after MI. Each heart was arrested in diastole via submersion in 3M potassium chloride upon dissection. **A**, Each row illustrates the distribution of stiffness values within an individual mouse with representative histogram in the middle. **B-C**, Mean tissue stiffness of scar (B) and BZ (C) (N=3-9) at multiple timepoints with SB treatment. **D**, Scar and BZ stiffness in RS treated mice 6 weeks after MI (N=10-18). Mean ± SEM, *P<0.05, **P<0.01, following (B-C) 2-way ANOVA and Holm-Sidak post hoc test or (D) 2-tailed Student *t* test.

Since increased tissue stiffening can lead to a hypertrophic response in cardiomyocytes, we quantified the expression of the gene encoding the cardiomyocyte injury marker natriuretic peptide B (***Nppb***) [118], [119]. Six weeks after MI, there was a significant reduction in *Nppb* expression in the SB group (**Figure 3.13A**). As this finding indicated that cardiomyocytes were undergoing an injury response and potentially remodeling, we assessed the short-axis cross-sectional area of cardiomyocytes distant to the infarcted tissue. We observed a significant increase in cardiomyocyte area six weeks after MI in vehicle-treated animals compared to both SB- and RS-treated animals (**Figure 3.13B-D**). There was also a significant increase in cardiomyocyte area of vehicle-treated animals over their sham counterparts which was

prevented with SB treatment (**Figure 3.13C**). These results indicate a biophysical alteration in cardiac composition downstream of the scar formation process influences remote cardiomyocyte hypertrophy after MI.

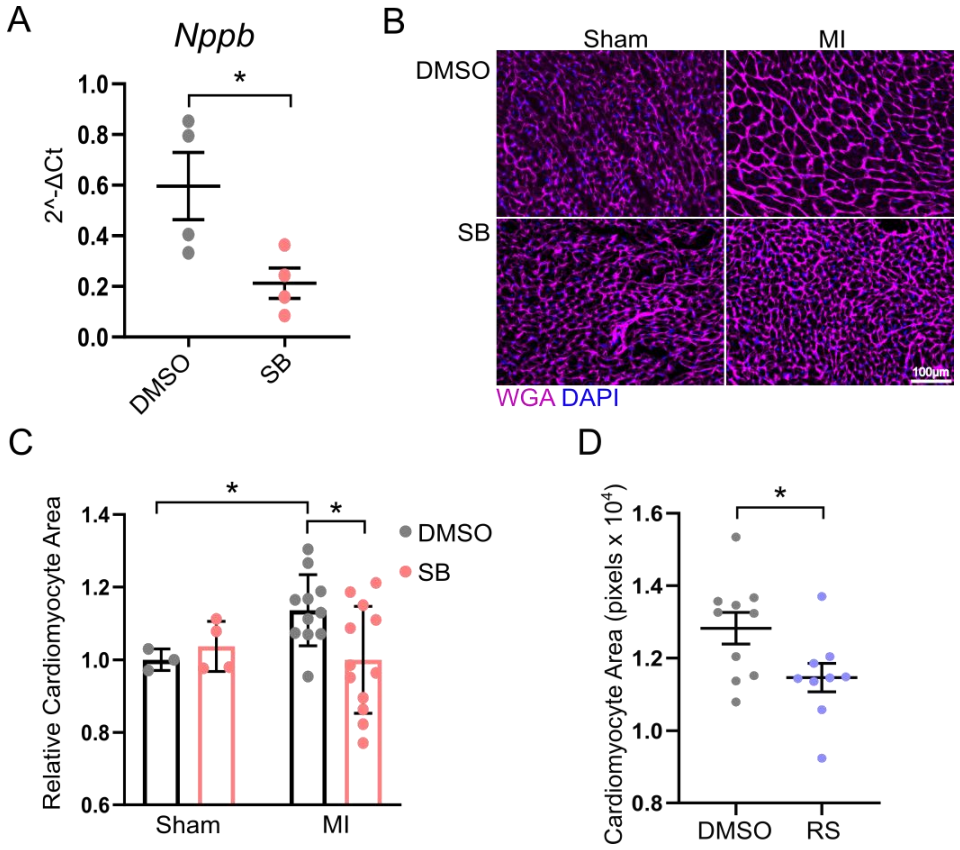

Figure 3.13. Cardiomyocyte remodeling is prevented by 5-HT$_{2B}$ antagonism. **A**, qPCR analysis of *Nppb* (N=4). **B-C**, WGA staining of short-axis cardiomyocytes reveals increased cross-sectional area in control-treated animals after MI compared to sham operation is prevented with SB treatment (N=3-12). **D**, RS treatment results in decreased cardiomyocyte area compared to control. Mean ± SEM, *P<0.05, following (A,D) 2-tailed Student *t* test or (C) 2-way ANOVA and Holm-Sidak post hoc test.

3.5 Discussion

Experimental MI induced by coronary artery occlusion results in the formation of a permanent, collagenous scar. Since cardiomyocytes are unable to regenerate and replace the necrotic cells in the injury site, scar formation has the integral function of patching the ventricular wall. The quality of initial scar formation has lasting effects on cardiac outcomes. A structurally

sufficient scar is necessary to reinforce the LV wall, but persistent fibrotic activity leads to chronic cardiac deterioration [14], [15]. Fibrotic lesions are associated with poor prognoses and attributed to excessive ECM deposition which limits diastolic and systolic function [120]. Therefore, it is desirable to properly tune the fibrotic response following MI such that a functional scar is able to form but is dampened before the fibrotic activity becomes deleterious.

Prior studies have shown anti-fibrotic effects of 5-HT_{2B} disruption in various cardiopulmonary pathologies [31]–[33], [35], [57], [94], [95]. To our knowledge, this study is the first investigation into the direct contribution of 5-HT_{2B} signaling in wound healing after MI. Through the implementation of two pharmacological inhibitors, we have shown that the 5-HT_{2B} receptor is an effective target to limit fibrosis following MI in mice.

In the present study, echocardiographic analysis revealed global 5-HT_{2B} antagonism improves cardiac structure and function one week after MI, evidenced by preserved EF, FS, and systolic LV volume and internal dimension. While there were not significant changes in these metrics between one and six weeks after injury, GLS deteriorated from week one to six in the control groups whereas 5-HT_{2B} inhibition stabilized this measure of cardiac contractility. GLS has been shown to be an independent predictor of adverse remodeling after ST-elevated MI in humans and can be a more sensitive functional output than the traditionally used EF [121], [122]. Systolic function is preserved, seen more strongly in the SB-treated cohort, which is supported by the increased strain generated by the LV measured by GLS. These echocardiographic results support the hypothesis that 5-HT_{2B} signaling is involved in determining cardiac outcomes after MI.

Global knockout of 5-HT_{2B} results in more severe histopathological lesions and a stronger systolic dysfunction in adult male mice compared to females [85]. No differences were seen in female mice administered 5-HT_{2B} antagonist which could be attributed to a decreased

influence of 5-HT_{2B} signaling in females which was unaffected by administration of a pharmacological agent.

We further explored the changes to tissue architecture that contributed to an improvement in cardiac contractility and alterations in scar formation. A heavier collagen burden increases passive tissue stiffness, heightening afterload and hindering systolic function [123], [124]. 5-HT_{2B} antagonism successfully decreased fibrosis, indicated by decreased scar thickness, without negatively affecting survival rate. There were no temporal changes of scar thickness, indicating that the first week of ECM deposition was deterministic of the future scar thickness. While scar thinning can result in the loss of cardiac function and potential LV rupture [125], [126], our results show a stabilized scar made up of less fibrotic tissue. There were no changes in survival in the SB-treated cohort, and the RS-treated cohort had a slightly higher survival probability, further supporting the formation of a less expansive, yet fully functional scar.

The BZ is a vulnerable region of tissue where scar expansion occurs, further damaging cardiomyocytes that were not directly affected by the initial ischemic event [17], [127]. We demonstrated an increased transition rate from scar tissue to surviving myocardium (i.e. shorter BZ region length), revealing decreased BZ area and decreased intrusion of collagen fibers from the scar into uninjured myocardium. Limiting scar expansion can minimize the disruption of the cardiac syncytium, providing a more coordinated systolic cycle [23]. Similar to reports linking 5-HT_{2B} to collagen content and composition through activation of lung and valve fibroblasts [57], [128], our results show a redistribution of collagen fiber thickness in the BZ, favoring less mature, more compliant collagen fibers. This difference was not seen in the scar, further suggesting the formation of a mechanically sound scar with limited capacity to expand beyond the BZ. The collagen fibers in BZs of SB-treated animals exhibited more frequent regions of anisotropic collagen fiber distributions determined by quantifying fiber orientation from SHG images. Anisotropy of collagen fibrils will confer corresponding anisotropy to the mechanical

properties of the tissue in which they reside [129], and more highly aligned collagen fibers have been shown to increase LV contraction [130], [131]. Regions of anisotropic collagen fibers are able to undergo elastic deformation along the length of the fiber in response to the strain generated by cardiomyocyte contraction. The increased anisotropy in SB-treated BZs allows for coordination of collagen deformation with cardiomyocyte deformation, increasing contractility and cardiac output. These findings point to a muted initial fibrotic response that provided adequate scar formation without hindering the systolic capabilities of the heart.

We then proceeded to investigate how changes in collagen architecture altered tissue mechanics. In control animals, AFM analysis revealed a significant increase in both scar and BZ stiffness six weeks after injury compared to 5-HT_{2B} antagonist-treated animals, indicating sustained tissue remodeling. While not statistically significant, there appears to be a continual increase in tissue stiffness in the scar and BZ of control animals throughout the experimental timeline. The lack of temporal changes in tissue stiffness with 5-HT_{2B} inhibition mirror the results seen in the GLS data. Both of these data sets reveal similar initial results between treatment groups, but as the tissue undergoes chronic remodeling, control animals worsen while 5-HT_{2B} antagonist-treated animals maintain their tissue properties. These findings further support the achievement of optimized scar formation.

Following MI, the heart undergoes a hypertrophic response to the increased workload. Cardiac hypertrophy was once believed to be a necessary response to injury in order to maintain normal function, but this view has been challenged by recent data showing sustained hypertrophy causes maladaptive remodeling that leads to HF secondary to cardiomyocyte death [35]. The remodeling observed in vehicle-treated animals culminated in early signs of cardiac hypertrophy, indicated by increased expression of *Nppb* and increased cardiomyocyte area of remote cardiomyocytes, while 5-HT_{2B} antagonism prevented cardiomyocyte hypertrophy compared to cardiomyocytes in sham-operated hearts. Improved cardiac structure and function

are supported by these microstructural analyses demonstrating desirable mechanical and biophysical outcomes following MI.

The differences between echocardiographic and survival outcomes with RS and SB treatment should be noted. While we assume the muted differences observed in cardiac structure with RS treatment are due to rapid clearance of the drug, it is worth confirming identical mechanisms of action. With regards to survival, overall survival appears to be decreased in the RS-treated cohorts compared to SB. This can likely be attributed to slight alterations in technique and experience with regards to the surgical technique or the added stress of twice-daily injections and the associated handling of the mice for the three weeks of treatment.

This study shows that cardiac structure and function following MI can be preserved with the administration of a 5-HT_{2B} antagonist. The quantity and quality of collagen deposition have an integral role in mediating these changes and determining lasting tissue properties. A pharmacological approach for improving tissue mechanics and pump function would be an exciting breakthrough in the therapeutic approach to post-MI healing.

Chapter 4

Genetic Ablation of 5-HT$_{2B}$ from Cardiac Fibroblasts and Myofibroblasts Improves Cardiac Outcomes Following Myocardial Infarction

Text for Chapter 4 was adapted from **Snider JC**, Riley LA, Mallory NT, Bersi MR, Gautam R, Zhang Q, Mahadevan-Jansen A, Maroteaux L, Lal H, and Merryman WD. Targeting 5-HT$_{2B}$ Receptor Signaling Prevents Border Zone Expansion and Improves Microstructural Remodeling after Myocardial Infarction. *Submitted*

4.1 Abstract

Introduction: CFs are the effector cells responsible for deposition and remodeling of ECM following MI. CFs respond to stimuli such as hypoxia, altered tissue mechanics, and inflammatory and fibrotic cytokines by transdifferentiating into myofibroblasts and potentiating a wound healing response. Resident CFs are marked by *Tcf21* and give rise to the vast majority of myofibroblasts, which can be marked by periostin. 5-HT$_{2B}$ signaling has been shown to mediate fibrotic disease through both fibroblast and bone-marrow derived populations. Therefore, we set out to isolate different cell populations and determine their relative contributions to 5-HT$_{2B}$-mediated wound healing after MI.

Methods: Sham operation and bone marrow transplantation were used to test effect of 5-HT$_{2B}$ signaling in cardiomyocytes and hematopoietic cells, respectively. Two novel models of cell-specific 5-HT$_{2B}$ ablation were generated. Resident CFs were targeted using the *Tcf21* promotor as a driver of inducible Cre expression, and myofibroblasts were targeted by *Postn* expression after injury. Experimental MI was performed and echocardiographic analysis was

used to investigate the effects of 5-HT_{2B} in each cell compartment on cardiac structure and function.

Results: 5-HT_{2B} antagonism in sham-operated animals did not induce any changes in cardiomyocyte behavior. Bone marrow transplantation of *Htr2b*$^{-/-}$ bone marrow into WT recipients did not result in any alterations of echocardiographic outputs following MI. 5-HT_{2B} ablation in *Tcf21* lineage-traced CFs improved cardiac function and both diastolic and systolic LV structure after MI. These animals also presented with a decreased hypertrophic cardiac phenotype. Ablation of 5-HT_{2B} in myofibroblasts (driven by *Postn* expression) after injury effectively replicated the results from *Tcf21*-expressing CFs.

Conclusions: 5-HT_{2B} signaling works through CFs to negatively influence wound healing post-MI. CF- and myofibroblast-specific ablation of 5-HT_{2B} effectively improves cardiac outcomes after MI.

4.2 Introduction

CFs comprise approximately 20% of non-cardiomyocytes in the adult heart [132]. Quiescent CFs reside in healthy ventricles and maintain homeostasis through low-level ECM turnover and organization [133], [134]. CFs arise from epicardial and endothelial origins as progenitor cells invade the developing heart. Most CFs are derived from transcription factor 21 (***Tcf21***), Wilms tumour 1, or T-box 18 lineages, however, *Tcf21* is the only marker that continues to be expressed into adulthood [135]–[137]. Environmental stimuli, such as hypoxia, altered tissue mechanics, and cytokines like TGFβ, signal the phenotypic switch of CFs to a more proliferative, hypercontractile, and hypersecretory state [12], [13]. This phenotypic switch gives rise to myofibroblasts; myofibroblast infiltration is a major player in all published experimental models of MI (rat, mouse, rabbit, canine, and zebrafish) [11]. While several studies have shown

contributions from various lineages to the myofibroblast pool, Kanisicak et al. convincingly showed that myofibroblasts primarily and overwhelmingly originate from tissue-resident, *Tcf21*-lineage CFs. These myofibroblasts can then be traced through their expression of the marker periostin – a secreted matricellular protein produced in adults exclusively following injury [135], [138], [139]. Resident CFs rapidly proliferate following MI to create a pool of cells primed to respond to chemical and mechanical signals to transdifferentiate into myofibroblasts and potentiate scar formation.

Following MI, myofibroblasts play the indispensable role of stabilizing and reinforcing the LV via formation of a collagen-dominated scar [10], [12]. Myofibroblasts localize to both infarcted tissue and surrounding BZ to potentiate the reparative fibrotic injury response due to the lack of intrinsic regenerative capacity of myocardium [9], [140], [141]. Insufficient ECM deposition can lead to LV rupture or aneurysm, while excessive ECM deposition leads to tissue stiffening, scar expansion, and arrhythmias [14], [15]. Furthermore, replacement of contractile myocardium with a collagenous scar creates a local increase in mechanical strain at the BZ of surviving myocardium and scar tissue. To compensate for biomechanical alterations, connective tissue often expands beyond the original injury, creating a subsequent decline in tissue compliance and cardiac output [16], [17]. Most chronic myocardial conditions are associated with excessive deposition of fibrotic tissue, making the myofibroblast a desirable therapeutic target to limit fibrotic overactivity [120], [142].

In the context of cardiopulmonary pathologies, 5-HT_{2B} has been best described in regulating cellular activity in lung and valve tissue. Platelets are the main source of peripheral serotonin which functions to regulate cardiovascular homeostasis and blood pressure [34]. Interestingly, in *Htr2b* $^{-/-}$ mice, hematopoiesis is altered as seen by a decrease in platelet number and an increase in CD11b+ circulating granulocyte/macrophage populations. These mice also have decreased production of CD11b-CD31+ cells which are a population of endothelial

progenitors [32]. 5-HT_{2B}-mediated alteration of hematopoietic cells has been shown to be effective in preventing small vessel remodeling in the context of an experimental model of PAH. Pharmacologic inhibition of 5-HT_{2B} prevents an increase in RVSP and remodeling of the distal vasculature in the lungs. There is a decrease in the muscularization and stiffness of small vessels in the lungs following 5-HT_{2B} antagonism. Bloodworth et al. showed that the benefits of 5-HT_{2B} inhibition can be recapitulated through genetic ablation of bone marrow-derived PACs, indicating a causative role of 5-HT_{2B} in PAH mediated through PACs [33].

5-HT_{2B} has also been implicated to drive disease through activation of resident cardiac cell populations. Valve interstitial cells, a fibroblast-like cell population which undergoes transdifferentiation into myofibroblasts under disease conditions, mediate aortic valve disease through contraction and remodeling valve ECM. Myofibroblast activation of valve interstitial cells has been shown to be prevented by 5-HT_{2B} antagonism. Impaired TGFβ1 signaling, diminished activation of the mitogen-activated protein kinase p38, and physically restricted tyrosine kinase Src all culminated in the decreased expression of the myofibroblast markers α-smooth muscle actin and smooth muscle protein 22-α [31]. In a model of cardiac hypertrophy, 5-HT_{2B} has been shown to colocalize with AT_1R and mediate ventricular remodeling. This study restricted 5-HT_{2B} expression to cardiomyocytes, implicating a non-cardiomyocyte cell population responsible for alterations in ventricular structure. Inhibition of either AT_1R or 5-HT_{2B} mitigated the hypertrophic injury response to chronic isoproterenol administration [35].

Based on the available literature, we sought out to identify the cell population responsible for the beneficial effects of global 5-HT_{2B} antagonism following MI. We utilized a bone marrow transplant model and novel genetic models to determine how 5-HT_{2B} facilitated adverse remodeling in a cell-specific manner.

4.3 Methods

Bone Marrow Transplants

6- to 8-week-old mice carrying the CD45.1 hematopoietic marker (Jackson Laboratory, Stock No. 002014) were given a split 12 Gy dose of radiation from a Cs^{137} source. Twenty-four hours later, 1 – 2.5x10^6 bone marrow cells isolated from age- and sex-matched cogenic WT or *Htr2b*$^{-/-}$ donors (carrying the CD45.2 allele) were transplanted via retro-orbital injection [33]. Six weeks were given for reconstitution, then permanent occlusion MI was performed. Transplant efficiency was confirmed by flow cytometry of isolated bone marrow by observing the engraftment of donor cells expressing the CD45.2 allele with concomitant absence of the native CD45.1 allele.

Generation of cell-specific 5-HT$_{2B}$ knockout animals

Two novel, inducible 5-HT_{2B} knockout animals were generated. *Htr2b* floxed (*Htr2b*$^{fl/fl}$) animals were generated and provided by Dr. Luc Maroteaux [143]. Briefly, genomic contigs were generated and a LoxP site were inserted within the 5'-untranslated region of the second exon of the *Htr2b* genetic locus. A neomycin-resistant selection cassette flanked by two LoxP sites was also inserted in the second intron. Active Cre recombinase will recombine the allele harboring these mutations, deleting the second exon and rendering 5-HT_{2B} ineffective.

Mice with *Tcf21* locus harboring the tamoxifen-inducible MerCreMer (**MCM**) cDNA, provided by Dr. Michelle Tallquist [144], were bred with *Htr2b*$^{fl/fl}$ animals to produce *Htr2b*$^{fl/fl}$*Tcf21*$^{MCM/+}$ animals. *Htr2b*$^{fl/fl}$ mice were bred with *Rosa26*-stop-tdTomato reporter mice (Jackson Laboratory, Stock No. 007914) to allow for identification of recombination events through detection of the fluorescent reporter which is activated upon Cre-mediated removal of the stop codon preceding the tdTomato encoded sequence. Experimental animals were

obtained through mating *Htr2b*$^{fl/fl}$*R26tdTomato*$^{+/+}$ females with *Htr2b*$^{fl/fl}$*Tcf21*$^{MCM/+}$ males to ensure progeny had either zero (littermate control) or one (*Htr2b* knockout) copy of MCM cDNA, 1 copy of the tdTomato reporter, and were homozygous for *Htr2b*$^{fl/fl}$ (**Figure 4.1**). Resident CFs (marked by *Tcf21* expression) in the presence of Cre recombinase and tamoxifen will have truncated *Htr2b* preventing activation of the 5-HT$_{2B}$ receptor.

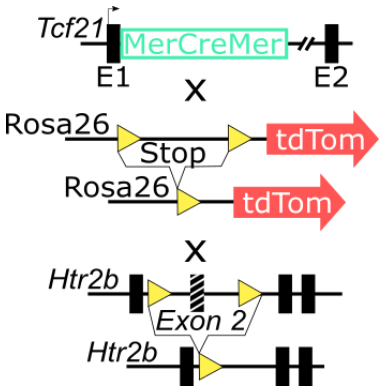

Figure 4.1. *Htr2b* deletion in resident CFs.
Schematic illustrating the *Tcf21* locus harboring a tamoxifen-inducible MCM cDNA, tdTomato reporter in the *Rosa26* locus preceded by a loxP-flanked stop codon, and a loxP-flanked *Htr2b* target allele.

We utilized a mouse model which expressed the MCM cDNA driven by the periostin promoter (***Postn***, *Postn*^{MCM}), provided by Dr. Jeffery Molkentin [139], to breed with *Htr2b*$^{fl/fl}$ animals to produce *Htr2b*$^{fl/fl}$*Postn*$^{MCM/+}$ animals. *Htr2b*$^{fl/fl}$ mice were bred with *Rosa26*-stop-tdTomato reporter mice (Jackson Laboratory, Stock No. 007914) to allow for identification of recombination events through detection of the fluorescent reporter which is activated upon Cre-mediated removal of the stop codon preceding the tdTomato encoded sequence. Experimental animals were obtained through mating *Htr2b*$^{fl/fl}$*R26tdTomato*$^{+/+}$ females with *Htr2b*$^{fl/fl}$*Postn*$^{MCM/+}$ males to ensure progeny had either zero (littermate control) or one (*Htr2b* knockout) copy of MCM cDNA, 1 copy of the tdTomato reporter, and were homozygous for *Htr2b*$^{fl/fl}$ (**Figure 4.2**). Myofibroblasts (marked by *Postn* expression) in the presence of Cre recombinase and tamoxifen will have truncated *Htr2b* preventing activation of the 5-HT$_{2B}$ receptor.

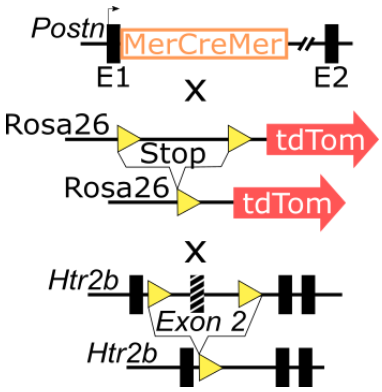

Figure 4.2. *Htr2b* deletion in myofibroblasts.
Schematic illustrating the *Postn* locus harboring a tamoxifen-inducible MCM cDNA, tdTomato reporter in the *Rosa26* locus preceded by a loxP-flanked stop codon, and a loxP-flanked *Htr2b* target allele.

Experimental MI

MI was induced in 11-17-week-old mice by permanent coronary artery ligation, as previously described in Chapter 3. $Htr2b^{fl/fl}Tcf21^{MCM/+}$, $Htr2b^{fl/fl}Postn^{MCM/+}$, and $Htr2b^{fl/fl}$ control mice were administered tamoxifen chow (Envigo, TD. 130860) exclusively one week prior to surgery and maintained throughout the remainder of the study. Sham-operation was performed similar to MI operation with SB treatment conducted as described in Chapter 3, however, a suture was not placed within the wall of the LV. Echocardiography was performed as described in Chapter 3.

At the end of each study, mice were euthanized through CO_2 inhalation in accordance with Vanderbilt University Medical Center's Division of Animal Care guidelines.

Flow Cytometry and Fluorescence-activated Cell Sorting (FACS)

Engraftment of bone marrow transplantation was tested using flow cytometry. Peripheral blood was obtained via cardiac puncture into a K-EDTA-loaded syringe. Red blood cells were immediately lysed (BioLegend, 420301), and the solution was centrifuged, resuspended in

FACS buffer (PBS + 3% FBS), and filtered. Cells were labeled with DAPI (1:100,000; Thermo-Fisher Scientific) to identify dead cells then stained with conjugated antibodies: Ter-119 (1:100; violetFluor™ 450 clone; Tonbo Biosciences), CD45.1 (1:100; PE clone A20; BD Biosciences), and CD45.2 (1:100; PErCP-Cy5.5 clone 104; Tonbo Biosciences). Cells were analyzed using a BD LSRFortessa. The percentage of CD45.2+ donor cells was used as the metric of engraftment.

Isolation of CFs for testing recombination efficiency was performed via FACS. Hearts were excised, and the atria and greater vessels were removed. Hearts were placed in > 175 units/mL collagenase type 2 (Worthington Biochemical, LS004202) at 37°C for 30 minutes, triturated, and replaced at 37°C for 15 minutes. Tissue was filtered through a 70 µm cell strainer, centrifuged at 350g at 4°C, and resuspended in 1x red blood cell lysis buffer for 10 minutes at room temperature. Tissue was filtered through a 40 µm cell strainer, centrifuged, and resuspended in FACS buffer with Fc block (1 µl/ 1 x 10^6 cells; BD Biosciences 553141) for 10 minutes on ice. Cells were then stained at 4°C for 30 minutes with DAPI (1:500,000) and Ter-119 (1:400; violetFluor™ 450 clone; Tonbo Biosciences). Cells were analyzed using a BD LSRFortessa and DAPI-Ter119-tdTomato+ cells were collected.

Recombination Confirmation

To test recombination efficiency, *Tcf21*$^{MCM/+}$*Htr2b*$^{fl/fl}$ animals harboring the Rosa26-stop-tdTomato reporter were fed tamoxifen chow for two weeks. Hearts were digested as previously described for flow cytometry, and viable, single, tdTomato-expressing cells were collected. Genetic DNA was isolated using the DNeasy Blood and Tissue Kit (Qiagen, 69504). PCR was conducted to identify three targets: 1) floxed allele before recombination with reverse primer sitting within DNA that is excised upon recombination, 2) recombined allele with primers outside

the targeted exon which will only amplify under our cycling conditions if recombination has occurred, and 3) the WT, non-floxed allele as a positive control (**Figure 4.3, Table 4-1, Table 4-2**).

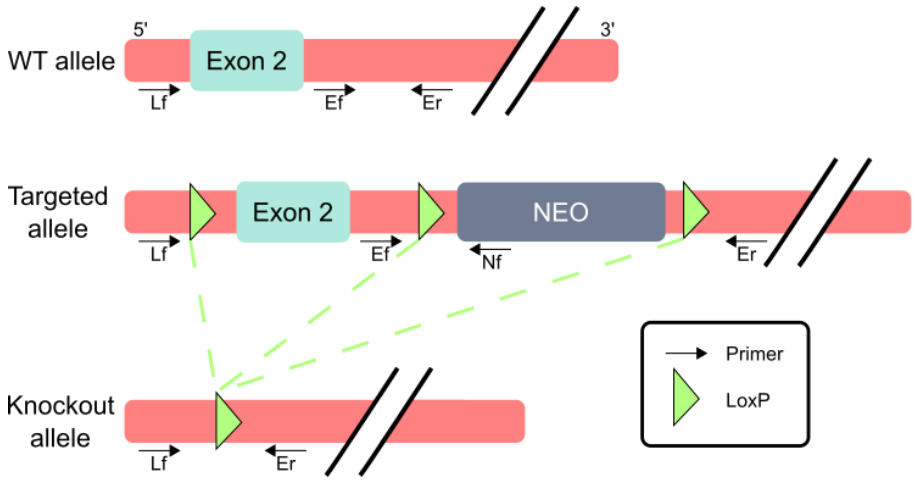

Figure 4.3. *Htr2b*^{floxed} gene map.
Schematic illustrating recombination of *Htr2b* exon 2 and the primers used to achieve 5-HT$_{2B}$ ablation.

Table 4-1 PCR primer sequences for genotyping

Primer	Sequence (5' to 3')
Lf	TACATACCGTCCTATCAAAACG
Ef	TTTCTTAGGAGCATGTTTACCC
Er	TGCCTAACTTTAATTGGGACTC
Nf	CAGCTCATTCCTCCCACTCATGATC

Table 4-2PCR products to identify WT, targeted, or knockout alleles

Primer pairs	WT allele product size	Targeted allele	Knockout allele
Lf/Er	940 b.p.	n.d.	393 b.p.
Ef/Nf	n.d.	489 b.p.	n.d.

- b.p. = base pairs, n.d. = not detected under cycling conditions used

Statistical Analysis

Statistical analysis was performed using SigmaPlot version 11. Shapiro-Wilk test was used to test for data normality. Subsequent statistical analyses used either a 2-way ANOVA with Holm-Sidak post hoc or a Kruskal-Wallis rank-sum test with Conover-Iman post hoc test for nonparametric data. A 2-tailed Student *t* test was used for comparisons of two normally distributed groups. Applicable tests and significance are labeled in figure captions with $P<0.05$ as the cutoff for data to be considered significantly different.

4.4 Results

4.4.1 5-HT$_{2B}$ antagonism does not alter cardiac structure or function in the absence of injury

We examined potential cell populations responsible for the effects seen following systemic administration of a 5-HT$_{2B}$ antagonist. It is known 5-HT$_{2B}$ influences cardiomyocyte development and mitogenesis but does not induce contraction [34], [48], [85], [86]. We did not observe alterations cardiomyocyte behavior presenting as changes in cardiac structure or function in sham-operated animals given a 5-HT$_{2B}$ antagonist (**Figure 4.4**).

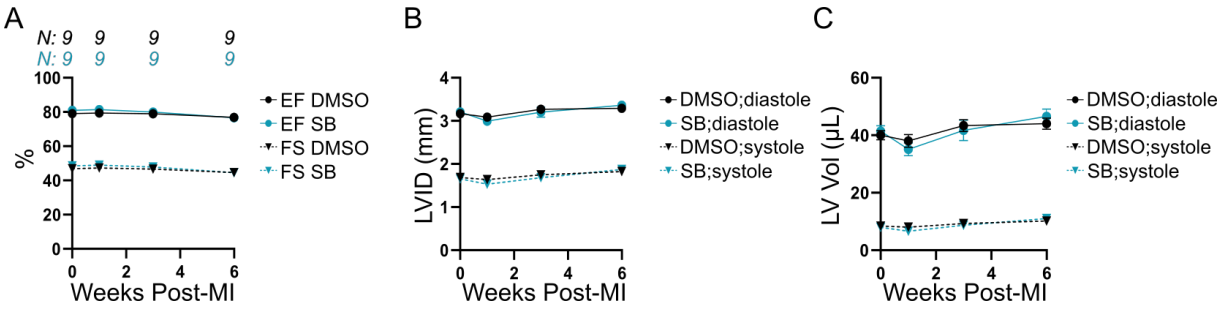

Figure 4.4. 5-HT$_{2B}$ antagonism does not alter cardiac phenotype after sham operation. 12-week-old mice underwent sham operation. **A**, No difference in EF or FS was observed between DMSO control and SB treated mice. **B**, LVID at both end-diastole and end-systole were similar between the two treatments. **C**, LV Vol at both end-diastole and end-systole were similar between the two treatments.

4.4.2 Expression of 5-HT$_{2B}$ in hematopoietic cells does not contribute to cardiac outcomes following MI

Based on previous findings showing that mice lacking 5-HT$_{2B}$ in the bone marrow compartment exhibit decreased tissue remodeling, we used a bone marrow transplant model to ablate 5-HT$_{2B}$ from hematopoietic cells to test their contribution to the wound healing process after MI. Age- and sex-matched donors (WT or *Htr2b*$^{-/-}$) were transplanted into WT mice with engraftment success of approximately 95% (**Figure 4.5**). After subjection to our MI protocol, we observed no statistical differences in either cardiac structure or function between the transplant groups, indicating a cell type of non-hematopoietic origin mediates the detrimental effects of 5-HT$_{2B}$ signaling after MI (**Figure 4.6**).

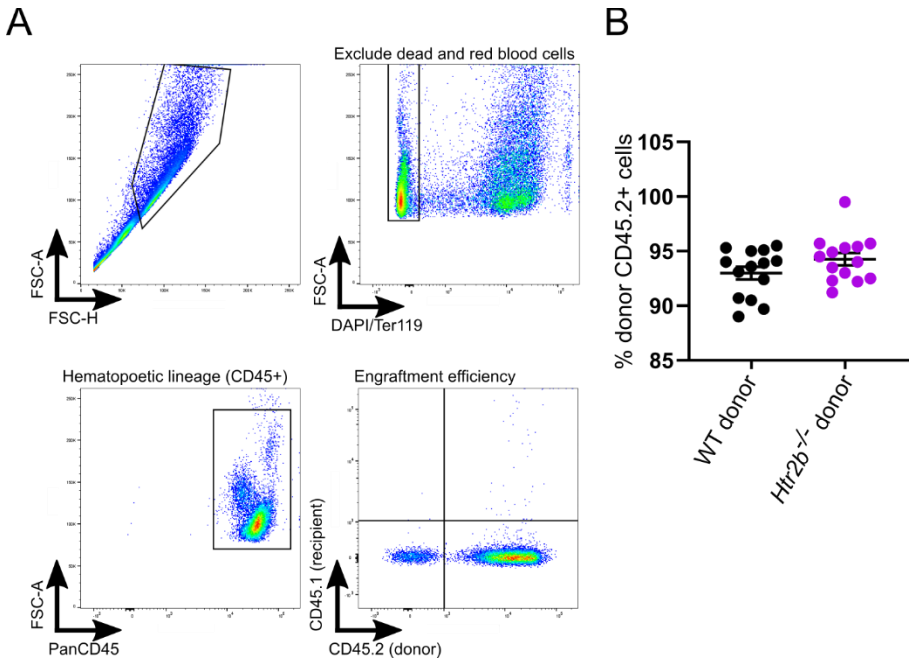

Figure 4.5. Determination of bone marrow engraftment efficiency.
A, Gating strategy to select for viable cells (excluding red blood cells), determine hematopoietic lineage (CD45+), and calculate engraftment efficiency (%CD45.2 donor cells of total CD45+ cells). **B**, Engraftment efficiencies for both WT recipients of both WT and *Htr2b*$^{-/-}$ donors.

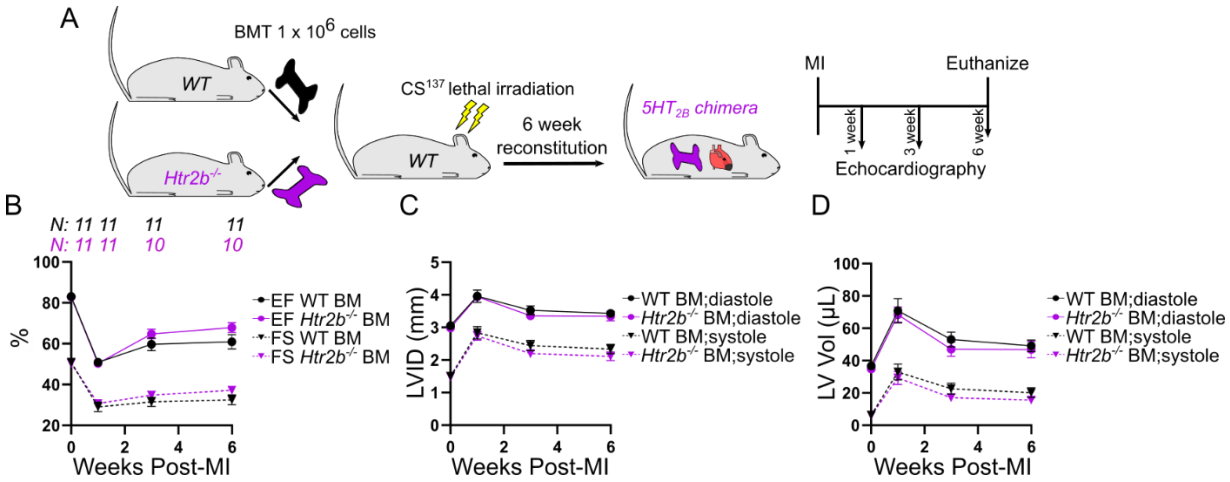

Figure 4.6. Mice lacking 5-HT$_{2B}$ in bone marrow-derived cells do not exhibit an improved phenotype after MI compared to mice with WT bone marrow.
A, Experimental approach. Age- and sex-matched donors (WT or *Htr2b*$^{-/-}$) were transplanted into lethally irradiated WT mice and upon reconstitution, were subject to MI surgery and serial echocardiography. **B**, No difference in EF or FS was observed **C**, LVID at both end-diastole and end-systole were similar between the two groups. **D**, LV Vol at both end-diastole and end-systole were similar regardless of bone marrow make-up.

4.4.3 Deletion of 5-HT$_{2B}$ in resident fibroblasts improves cardiac response to MI

To determine if 5-HT$_{2B}$ signaling in resident CFs impacts healing after MI, we deleted the gene encoding 5-HT$_{2B}$ in resident CFs using a tamoxifen-inducible, *Tcf21*^{MCM} transgene [135], [144]. The tdTomato fluorescent reporter was observed in all *Htr2b*$^{fl/fl}$*Tcf21*$^{MCM/+}$ mice indicating successful recombination in the CFs (**Figure 4.7A**). In tdTomato+ cells isolated from a healthy heart after administration of tamoxifen chow, we observed complete recombination of the *Htr2b* locus, suggesting all Cre-expressing cells have lost 5-HT$_{2B}$ signaling (**Figure 4.7B**).

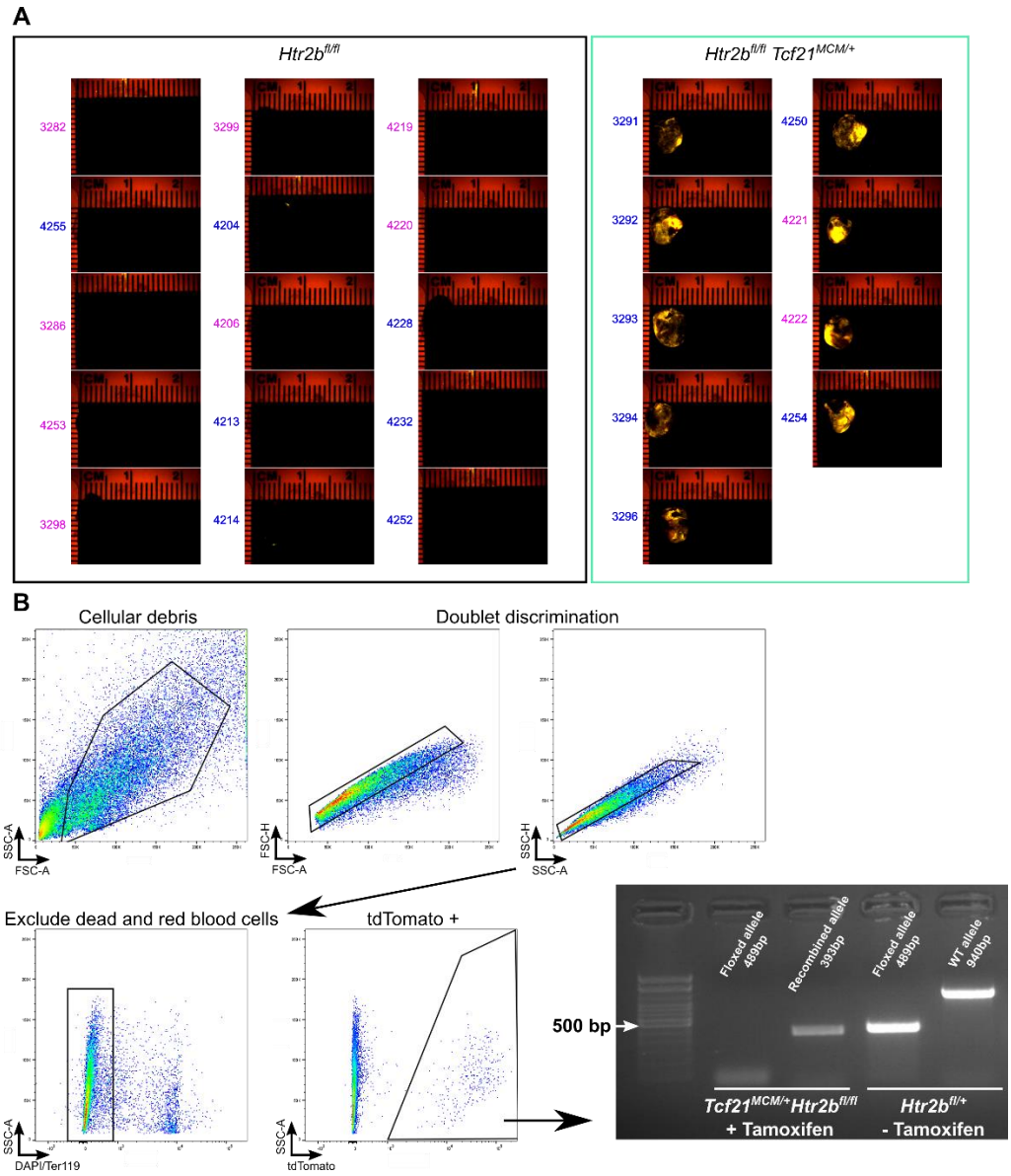

Figure 4.7. Verification of Cre activation in *Htr2b$^{fl/fl}$Tcf21$^{MCM/+}$* animals.
A, Control mice not harboring the MCM cDNA did not exhibit any fluorescent signal from the tdTomato reporter, whereas all mice harboring MCM cDNA under the control of the *Tcf21* promotor show fluorescent signal of the tdTomato reporter, indicating successful recombination. Mouse identifiers are color coded for male (blue) and female (pink). All images (control and experimental groups) acquired under the same imaging parameters with the same brightness/contrast adjustments made in ImageJ. **B**, PCR validating recombination efficiency. tdTomato+ cells were isolated and PCR was run to identify the recombined allele (second lane) compared with a control reaction which would amplify the non-recombined floxed allele (first lane) if present.

Following MI (**Figure 4.8A**), *Htr2b$^{fl/fl}$Tcf21$^{MCM/+}$* mice exhibited significantly improved EF and FS (**Figure 4.8B-C**). These mice also had preserved LV inner dimension and volume in both diastole and systole six weeks post-MI (**Figure 4.8D-G**). GLS steadily decreased over time

in *Htr2b*$^{fl/fl}$ mice lacking the *Tcf21*^{MCM} transgene and was significantly lower than the stabilized contractility of mice harboring the *Tcf21*^{MCM} transgene (**Figure 4.8H**). Six weeks after MI, morphometric analysis revealed increased heart weight to tibia length in *Htr2b*$^{fl/fl}$ mice indicative of cardiac hypertrophy (**Figure 4.8I**). These results show that ablation of the 5-HT$_{2B}$ receptor from resident CFs is effective in improving cardiac outcomes after MI.

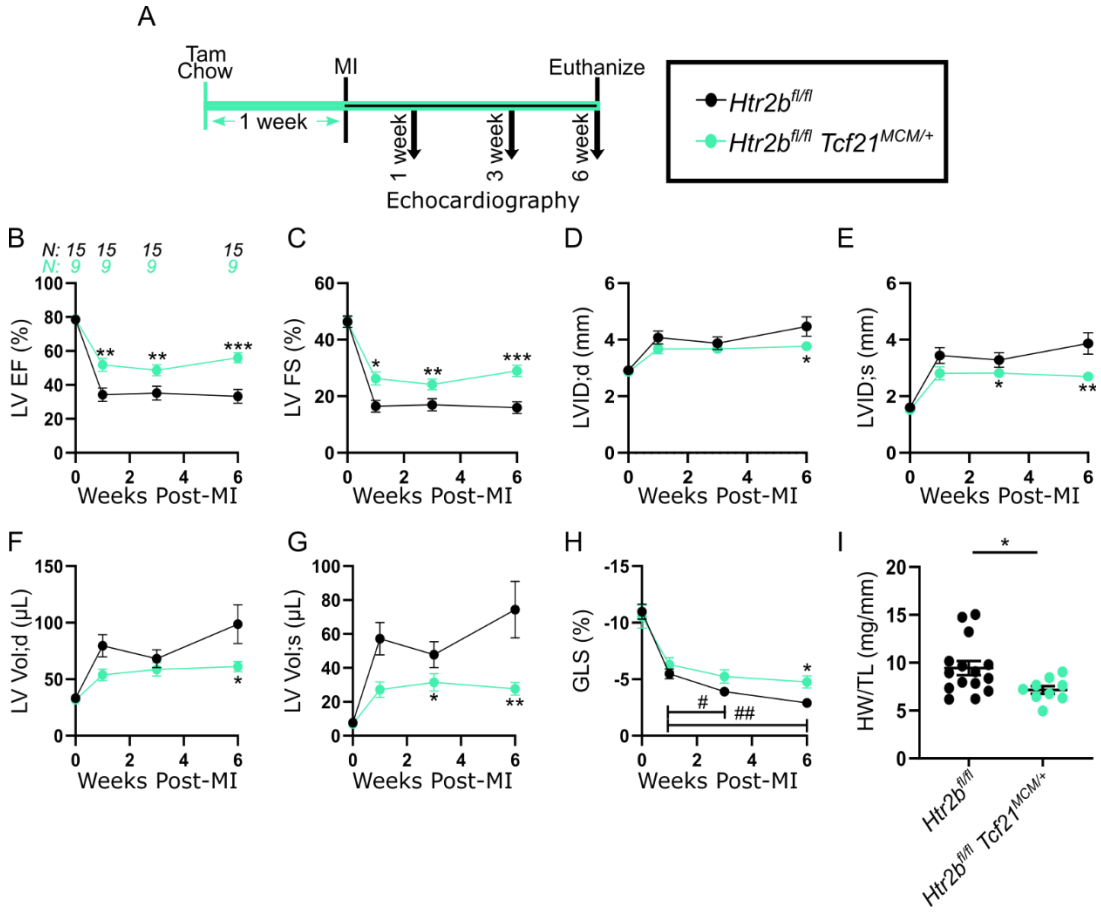

Figure 4.8. *Htr2b* deletion in resident CFs abates impact of MI
A, Experimental design for 16-17-week-old mice. **B**, LV EF. **C**, LV FS. **D,E**, LVID;d and LVID;s. **F,G**, LV Vol;d and LV Vol;s. **H**, GLS. **I**, Heart weight (HW) normalized to tibia length (TL). B-I, Mean ± SEM, *P<0.05, **P<0.01, ***P<0.001 between Htr2b$^{fl/fl}$ and Htr2b$^{fl/fl}$Tcf21$^{MCM/+}$ animals, #P<0.05, ##P<0.01 between timepoints within genotype following (B-H) 2-way ANOVA and Holm-Sidak post hoc test or (I) 2-tailed Student t test. Number of mice analyzed denoted in B applies to all subsequent data.

4.4.4 Myofibroblast-specific deletion of 5-HT$_{2B}$ improves cardiac response to MI

Tcf21^{MCM} driven ablation of 5-HT$_{2B}$ targets residential CFs present even in the absence of injury. We wanted to assess the functionality of ablating 5-HT$_{2B}$ after the induction of an MI. We utilized a mouse model which expressed the MCM cDNA driven by the periostin promoter. This mouse model has been well-characterized to demonstrate the marking of nearly all newly activated myofibroblasts following an injury, without induction prior to injury [102], [139], [145]. Following MI, all *Htr2b*$^{fl/fl}$*Postn*$^{MCM/+}$ hearts exhibited signal from the tdTomato reporter, indicating successful recombination (**Figure 4.9**).

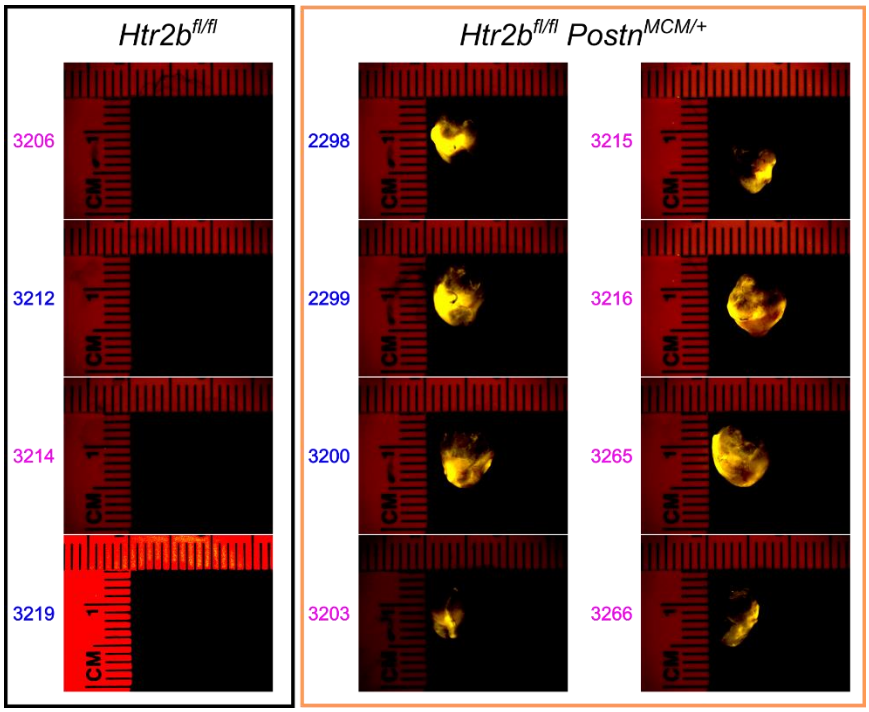

Figure 4.9. Verification of Cre activation in *Htr2b*$^{fl/fl}$*Postn*$^{MCM/+}$ animals.
Control mice not harboring the MCM cDNA did not exhibit any fluorescent signal from the tdTomato reporter, whereas all mice harboring MCM cDNA under the control of the Postn promotor show fluorescent signal of the tdTomato reporter, indicating successful recombination. Mouse identifiers are color coded for male (blue) and female (pink). All images (control and experimental groups, except 3219 overexposed for emphasis) acquired under the same imaging parameters with the same brightness/contrast adjustments made in ImageJ.

After MI (**Figure 4.10A**), *Htr2b*$^{fl/fl}$*Postn*$^{MCM/+}$ mice demonstrated a significant improvement in the functional metrics of EF and FS one week after MI compared to *Htr2b*$^{fl/fl}$ animals, which were maintained six weeks following the injury (**Figure 4.10B-C**). Myofibroblast-specific 5-HT_{2B} ablation resulted in improved LV inner dimension and volume in both diastole and systole six weeks after MI, indicating a preserved cardiac structure (**Figure 4.10D-G**). Ventricular deformation measured by GLS was preserved in the *Htr2b*$^{fl/fl}$*Postn*$^{MCM/+}$ group while the control group continued to deteriorate over the six-week experiment (**Figure 4.10H**). Finally, morphometric analyses revealed a decreased heart weight with 5-HT_{2B} ablation (**Figure 4.10I**). As it has been shown that tissue-resident fibroblasts of the *Tcf21* lineage are the primary source of subsequent injury-activated, periostin-expressing myofibroblasts [139], these results confirm 5-HT_{2B} expression in the CF population worsens the injury response to MI, and that blocking 5-HT_{2B} signaling after injury is sufficient to improve cardiac outcomes.

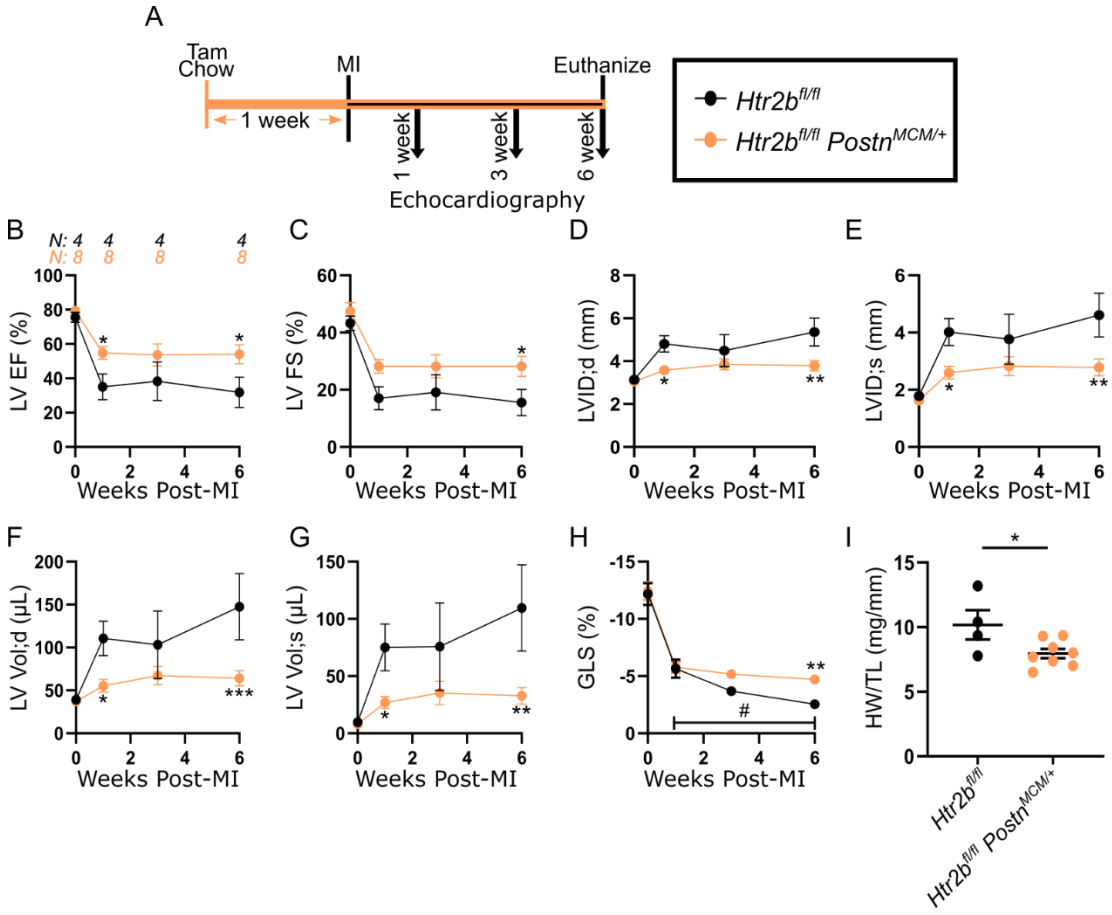

Figure 4.10. *Htr2b* deletion in activated myofibroblasts abates impact of MI.
A, Experimental design for 11-14-week-old mice. **B**, LV EF. **C**, LV FS. **D,E**, LVID;d and LVID;s. **F,G**, LV Vol;d and LV Vol;s. **H**, GLS. **I**, Heart weight (HW) normalized to tibia length (TL). B-I, Mean ± SEM, *P<0.05, **P<0.01, ***P<0.001 between Htr2b$^{fl/fl}$ and Htr2b$^{fl/fl}$Tcf21$^{MCM/+}$ animals, #P<0.05, ##P<0.01 between timepoints within genotype following (B-H) 2-way ANOVA and Holm-Sidak post hoc test or (I) 2-tailed Student t test. Number of mice analyzed denoted in B applies to all subsequent data.

4.5 Discussion

Experimental MI induced by permanent coronary artery occlusion triggers the expansion and activation of resident CFs from their quiescent, homeostatic state. CFs transdifferentiate into myofibroblasts in response to hypoxia, mechanical forces, and soluble factors such as chemokines, cytokines, and growth factors [133]. Myofibroblasts are highly active following injury, migrating and proliferating to the site of tissue damage to secrete ECM and contract scar tissue [146], [147]. Through the implementation of two models of genetically targeted ablation,

we have confirmed our antagonist studies demonstrating that the 5-HT_{2B} receptor is an effective target to improve cardiac outcomes following MI in mice. Due to advances in identification of genetic markers for CFs, we were able to isolate resident CFs and their subsequent activation into myofibroblasts as the cell population responsible for the improved recovery after MI seen in animals treated with a 5-HT_{2B} antagonist.

It is known that 5-HT_{2B} can be found expressed on cardiomyocytes and plays a role in the trabeculation and proliferation of cardiomyocytes during development [34]. However, adult mice with global 5-HT_{2B} deletion do not display differences in heart rate or developed force compared to WT mice [85]. We wanted to confirm that 5-HT_{2B} antagonism does not act directly on cardiomyocytes to alter their contractility. Sham-operated animals did not demonstrate any differences in cardiac structure in or function in the presence of 5-HT_{2B} antagonist. This suggests that 5-HT_{2B} antagonism does not alter cardiomyocyte activity in the uninjured environment. While this suggests that cardiomyocytes are not the primary cell population providing a protective role of 5-HT_{2B} antagonism after MI, this cannot be conclusively determined without the use of a cardiomyocyte-specific, inducible knockout, such as the α-myosin heavy chain driven $CreER^{T2}$ mouse [148], [149].

Previous reports exploring pulmonary and valve disease have shown a causative role in disease onset and progression of 5-HT_{2B} expression in bone marrow-derived cell populations [32], [33], [150]. However, using a bone marrow transplant model to eliminate 5-HT_{2B} from the bone marrow compartment, we did not observe a therapeutic effect after MI. We used WT, cogenic recipient mice to mimic the animals in which we performed the antagonist studies. Worth noting, it has been reported that bone marrow transplantation effects leukocyte recruitment in a model of aortic aneurysm, such that mice receiving a bone marrow transplant from a donor of identical genotype required nearly four times the dosage of AngII to induce aneurysm at the same rate as non-transplanted mice [151]. We observed a similar decrease in

cardiac function after MI in our transplant study compared to other models, indicating that the dramatic injury of MI should have overcome any protection that was provided through the bone marrow transplantation process. It has also been shown that CFs in the infarct are derived of epicardial origin with no contribution from bone marrow lineages, endothelial-to-mesenchymal transition, or blood [152]. Therefore, we are confident that 5-HT_{2B} antagonism in MI does not operate solely through a hematopoietic cell type to improve cardiac outcomes.

One major cell type not investigated in our study is endothelial cells. These cells are thought to be the most abundant non-cardiomyocyte cell population in the uninjured heart [132]. Following MI, endothelial cells are damaged which reduces barrier function and allows for the extravasation of inflammatory cell populations. They also upregulate expression of adhesion molecules, such as e-selectin and vascular cell adhesion molecule-1, to further mediate neutrophil and monocyte adhesion and rolling along the endothelium [153]. These cells also undergo endothelial-to-mesenchymal transition to contribute to the fibroblast pool [154], [155]. It is known that 5-HT_{2B} activation of human umbilical vein endothelial cells cause the production of ROS which exacerbate myocardial injury [156]. 5-HT_{2B} could potentially play a role in extent of injury or invasion of fibroblasts in an endothelial-specific manner, and this could be tested through the use of an inducible Cre driven by either the cadherin 5 or Tie2 promotor, both of which are commonly used.

Previous results led us to investigate CFs as a driver of 5-HT_{2B}-mediated fibrotic overactivity after MI. To target this cell type, we developed a novel murine model of CF-specific 5-HT_{2B} ablation. Using the *Tcf21* promotor to drive MCM expression, we were able to ablate 5-HT_{2B} from resident CFs prior to injury, the population giving rise to myofibroblasts after MI [139]. Myofibroblasts in the infarct do lose expression of *Tcf21*, but since they overwhelmingly derive from a *Tcf21* lineage, we are confident that these cells have ablated 5-HT_{2B}. Using this approach, we observed a vastly improved cardiac phenotype compared to control animals.

Htr2b$^{fl/fl}$*Tcf21*$^{MCM/+}$ animals exhibited similar improvements in functional outputs of EF and FS as the antagonist studies. These animals displayed an even more pronounced benefit in that both LV systolic and diastolic internal dimension and volume were improved six weeks after injury. The improvement in cardiac structure could be due to an increased penetrance of 5-HT_{2B} inhibition in the genetic modeled compared to the pharmacological approach. GLS was sustained over the course of the experiment whereas it deteriorated in mice over time. Importantly, heart weight normalized to tibia length was lower in the CF knockout group, indicating cardiac hypertrophy downstream of MI in the control group which is mitigated by 5-HT_{2B} ablation. These data further support the hypothesis that changes in fibroblast activity can prevent adverse remodeling after MI which leads to cardiac hypertrophy.

To directly assess the cells that would be therapeutically targeted after an MI and to control for the potential of the *Tcf21*-driven model imparting protective benefits before the onset of injury, we ablated myofibroblast expression of 5-HT_{2B}. Myofibroblasts are present during development but are not observed in the absence of injury in adults. We generated novel *Htr2b*$^{fl/fl}$*Postn*$^{MCM/+}$ mice to genetically ablate 5-HT_{2B} from myofibroblasts arising after experimental MI to test if inhibiting this receptor after the onset of injury in this CF-derived cell population is sufficient to impart protection against MI. *Htr2b*$^{fl/fl}$*Postn*$^{MCM/+}$ mice demonstrated comparable echocardiographic and morphometric improvements to the *Tcf21*-driven model. Functional outputs of EF and FS were improved; cardiac structure in both diastole and systole were preserved; and morphometric analysis confirmed an enhanced hypertrophic response in control animals that was prevented with myofibroblast 5-HT_{2B} ablation.

Utilizing these models, we have shown that 5-HT_{2B} expression in CFs, and specifically myofibroblasts, negatively contributes to wound healing response following MI. 5-HT_{2B} ablation in either of these cell types limits the structural and functional damage of MI and prevents cardiac hypertrophy.

Chapter 5

Cardiac Fibroblast Wound Healing is impaired by 5-HT$_{2B}$ Ablation

Text for Chapter 5 was adapted from **Snider JC**, Riley LA, Mallory NT, Bersi MR, Gautam R, Zhang Q, Mahadevan-Jansen A, Maroteaux L, Lal H, and Merryman WD. Targeting 5-HT$_{2B}$ Receptor Signaling Prevents Border Zone Expansion and Improves Microstructural Remodeling after Myocardial Infarction. *Submitted*

5.1 Abstract

Introduction: CFs participate in a plethora of functions following MI. They respond to cytokines, mechanical cues, and damaged-associated molecular patterns which cue them to initiate a wound healing response. Ultimately, CFs proliferate and infiltrate damaged tissue and then begin depositing and compacting ECM. 5-HT$_{2B}$ signaling has been shown to increase proliferation as well as myofibroblast activation in other disease models. We investigated the mechanism by which 5-HT$_{2B}$ ablation alters the scar formation process.

Methods: PDGFRα+ cells were isolated from scar tissue of *Htr2b*$^{fl/fl}$*Postn*$^{MCM/+}$ and *Htr2b*$^{fl/fl}$ animals seven days after MI and bulk RNA sequencing was performed. CFs were isolated from WT and 5-HT$_{2B}$ knockout mice for *in vitro* analysis of proliferation, migration, and remodeling capabilities.

Results: RNA sequencing revealed a decreased proliferative capacity with 5-HT$_{2B}$ ablation. This was confirmed with both immunostaining showing a decreased presence of myofibroblasts as well decreased proliferation of CFs *in vitro*. Mutant CFs also exhibited an impaired migratory capacity and impaired ability to contract collagen matrices.

Conclusions: 5-HT_{2B} ablation functions through decreased CF proliferation and matrix remodeling to limit fibrosis.

5.2 Introduction

CFs exhibit a diverse array of functions in the infarct setting. CFs are capable of responding to ROS, Toll-like receptor ligands, and IL-1β to produce proinflammatory cytokines and chemokines. In the early phases of inflammation after ischemic injury, these and other damage-associated molecular patterns released by dying cardiomyocytes activate a proinflammatory program in CFs [120]. It has recently been shown that CFs could stimulate leukocyte recruitment to infarcted tissue through secretion of granulocyte/macrophage colony stimulating factor [157]. They also secrete matrix metalloproteinases to degrade tissue and clear the myocardium of necrotic cells and debris [158]. It is difficult to parse out the relative contribution of these factors due to the fact that immune cells (the primary inflammation mediators), endothelial cells, and vascular mural cells are also capable of secreting proinflammatory cytokines such as tumor necrosis factor and IL-6 [159].

During the proliferative phase of infarct healing, CFs respond to multiple to cues acquire a matrix-synthetic phenotype through initiating myofibroblast activation, ECM secretion, and ECM compaction. Known factors that signal this transition include fibroblast growth factor, PDGF, AngII, and TGFβ [120]. Myofibroblast contractility stiffens ECM and activates latent TGFβ, creating positive feedback between myofibroblast activation and tissue remodeling [160]–[162]. TGFβ and fibroblast growth factor stimulate the migration of myofibroblasts into the infarct BZ where their persistence can cause infarct expansion [163], [164].

Myofibroblasts mediate scar maturation through secretion of structural ECM proteins, mainly collagen-1 and collagen-3. Lysyl oxidase expression crosslinks collagen fibers to impart

structural integrity to the final scar [134]. Myofibroblast density drastically decreases as the scar matures. It is believed that most myofibroblasts undergo apoptosis, but some myofibroblasts also acquire a more quiescent phenotype and lose expression of contractile proteins such as α-smooth muscle actin [13], [165].

Differences in cell phenotype when lacking 5-HT_{2B} have been reported. Several reports have shown regulation of cell proliferation through 5-HT_{2B} signaling [34], [48], [166]–[168]. Overexpression of 5-HT_{2B} increases mitochondrial enzymatic activity, indicative of an increased metabolic activity [87]. Activation of 5-HT_{2B} in valve cells increases secretory activity as seen in excessive deposition of glycosaminoglycans [42]. It also causes the α-smooth muscle actin-dependent formation of dystrophic calcific nodules in valve cells, formed by the overactivity of cell contraction and matrix remodeling [31]. 5-HT_{2B} also influences cell migration and invasion - antagonism prevented bone marrow-derived cell infiltration into pulmonary arterioles after hypoxic injury [33]. In cardiomyocytes, 5-HT_{2B} signaling imparts increased survival via the apoptosis regulator Bax [93]. In noncardiomyocytes, 5-HT_{2B} signaling induces the expression of IL-1β, IL-6, and TGFβ [35].

While a variety of cellular functions have been described to be regulated by 5-HT_{2B} signaling, downstream signaling cascades have not been well characterized for cardiopulmonary disease. 5-HT_{2B} antagonism has been shown to decrease the phosphorylation of the mitogen-activated protein kinase p38 upstream of myofibroblast activation [31]. This work was expanded upon when it was shown that TGFβ-mediated phosphorylation of p38 as well as cellular apoptosis susceptibility protein were dependent on the activation of the tyrosine kinase Src. 5-HT_{2B} antagonism arrested Src motility, preventing its downstream functions. This ultimately led to the decreased contractility of smooth muscle cells [67]. 5-HT_{2B} activation also causes activation of the mitogen-activated protein kinase ERK1/2 [29]. Non-canonical TGFβ

signaling has been shown to increase ERK1/2 phosphorylation and increase myofibroblast activation [169], [170].

We proceeded to investigate the mechanism by which 5-HT_{2B} ablation improved cardiac outcomes following MI. CFs were isolated seven days after MI, and RNA sequencing was performed to identify alterations in cellular functions in an unbiased manner. WT and 5-HT_{2B} knockout CFs were isolated and *in vitro* analyses performed to observe alterations in cell phenotype that are controlled by 5-HT_{2B}.

5.3 Methods

FACS

Isolation of CFs for RNA sequencing was performed via FACS. *Htr2b*$^{fl/fl}$*Postn*$^{MCM/+}$ and *Htr2b*$^{fl/fl}$ animals were given an MI as previously described. Seven days after injury, hearts were excised, and the atria and greater vessels were removed. The heart was cut transversely at the suture to isolate scar tissue which was then finely minced. Hearts were placed in > 175 units/mL collagenase type 2 (Worthington Biochemical, LS004202) at 37°C for 30 minutes, triturated, and replaced at 37°C for 15 minutes. Tissue was filtered through a 70 µm cell strainer, centrifuged at 350g at 4°C, and resuspended in 1x red blood cell lysis buffer for 10 minutes at room temperature. Tissue was filtered through a 40 µm cell strainer, centrifuged, and resuspended in FACS buffer with Fc block (1 µl/ 1 x 10^6 cells; BD Biosciences 553141) for 10 minutes on ice. Cells were then stained at 4°C for 30 minutes with DAPI (1:500,000), Ter-119 (1:400; violetFluor™ 450 clone; Tonbo Biosciences), and CD140a to identify CFs (PDGF Receptor α; 1:400; APC clone APA5; Invitrogen). Cells were analyzed using a BD LSRFortessa and DAPI-Ter119-PDGFRα+ cells were collected for RNA sequencing. In *Htr2b*$^{fl/fl}$*Postn*$^{MCM/+}$ animals, the percentage of tdTomato expressing cells was obtained.

RNA Sequencing

Cells were isolated from infarcted tissue one week after MI via FACS. Cells were homogenized in TRIzol reagent then RNA was isolated using the Zymo Direct-zol RNA Microprep kit (Zymo, R2060). RNA integrity was measured with an Agilent Bioanalyzer prior to library preparations.

The Vanderbilt Technologies for Advanced Genomics (VANTAGE) center performed library preparation, sequencing, and read alignment. Briefly, cDNA libraries were generated using NEBNext Ultra II Directional RNA Library Prep kits (New England BioLabs, E7760) then sequenced on an Illumina NovaSeq 6000 to an average depth of 84.7± 3.5 M reads per sample using 150bp paired-end chemistry. Sequencing quality was assessed using FastQC v. 1.0.0. Reads were aligned to mouse genome mm10 using a STAR based aligner and gene counts were quantified, both using Illumina's DRAGEN RNA Pipeline v. 3.6.3. Gene count data was imported to R using tximport for further analysis.

Differential gene expression analysis was performed using the R package DEseq2 using Cook's outliers to filter low gene counts and $\alpha = 0.05$. GO and KEGG over-representation analysis was performed with the R package clusterProfiler using the respective *enrich* function with default parameters. Gene sets were considered over-represented if $p_{adj} < 0.05$. Visualizations were generated using a combination of enrichplot and ggplot2 in R. RNA sequencing data generated in this manuscript have been deposited in GEO (Gene Expression Ominbus) of NCBI under accession code GSE157520.

Immunostaining

For periostin staining, seven μm tissue sections were brought to room temperature and OCT was removed with a PBS-/- wash, and for α-smooth muscle actin staining, polyacrylamide gels were rinsed of cell culture media. After fixation/permeabilization (4% paraformaldehyde and 0.1% Triton X-100), cells were blocked in 5% bovine serum albumin in PBS-/- for one hour. Cells were either stained with primary antibody against periostin (1:50; abcam, ab215199) overnight or α-smooth muscle actin conjugated to Cy3 (1:100; Sigma-Aldrich C6198) and phalloidin conjugated to AlexaFluor 488 (1:100; ThermoFisher; A12379) for one hour. Tissue was rinsed, stained with Alexa Fluor 647 secondary antibody (1:200; Invitrogen, A-21245) for one hour, then mounted in ProLong Gold with DAPI (Thermo-Fisher Scientific, P36941). Polyacrylamide gels were mounted in ProLong Gold with DAPI. Three fields of view in the infarcted area were taken per sample on an Olympus BX53 microscope equipped with a high resolution Qimaging Retiga 3000 camera at 20x magnification. Consistent imaging parameters were used, and no-stain and secondary-only stained controls can be seen in **Figure 5.1**. Quantitative image analysis was performed to extract area fractions using a previously described, custom MATLAB script [110], [171].

For the myofibroblast activation study, images were analyzed in a blinded manner. DAPI was used to identify nuclei and count total number of cells. Fully activated myofibroblasts were classified by expression of α-smooth muscle actin positive stress fibers which stretch the entire diameter of the cell. Partially activated myofibroblasts exhibited α-smooth muscle actin expression, but it was either limited to the cell periphery or the stress fibers were segmented and did not span the entire cell body. Phalloidin staining of F-actin was used to mark cell boundaries.

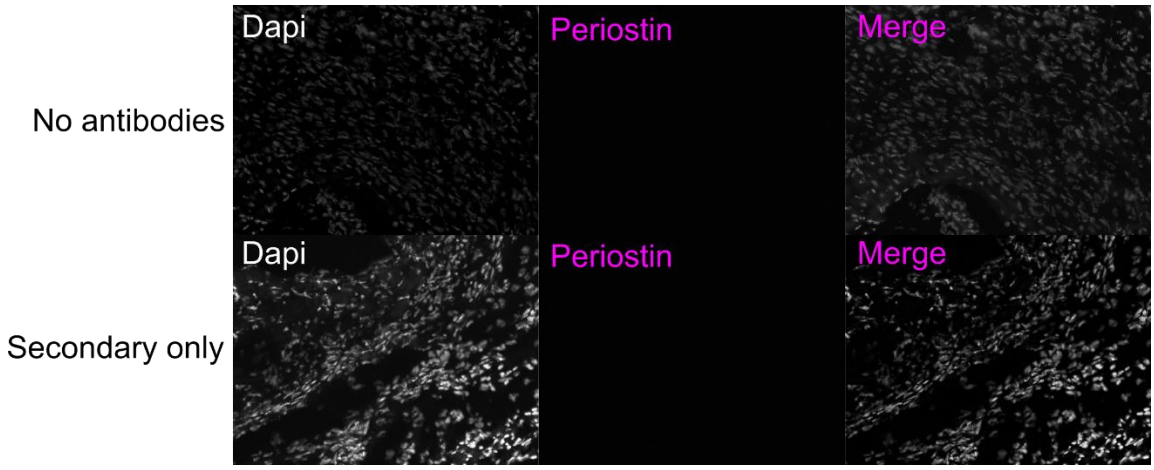

Figure 5.1. Controls for periostin immunostaining.
Unstained control (top) and secondary only control (bottom) imaged under identical settings as experimental samples.

Cell isolation and Culture

WT and *Htr2b*$^{-/-}$ animals were mated with mice harboring the *Immorto* gene to allow for serial cell-culture of littermate WT and *Htr2b*$^{-/-}$ knockout cell lines. CFs were isolated from eight-week-old mice. Hearts were excised, minced, and digested in > 175 units/mL collagenase type 2 (Worthington Biochemical, LS004202) at 37° with mixing for 45 minutes. Digested tissue was centrifuged, filtered through a 40 µm filter, and cells were plated on gelatin-coated dishes. Cells were cultured at 33°C in DMEM supplemented with 10% FBS, 1% penicillin/streptomycin, and 10 µg/mL recombinant murine interferon γ to induce activation of the simian virus 40 T antigen. Prior to experiments (overnight), cells were incubated at 37°C in the same media lacking interferon γ (complete media) to deactivate the T antigen that confers immortalization.

Collagen Gel Contraction

CFs suspended in complete media were used to create a 50:50 mixture with a bovine collagen solution (Advanced Biomatrix, 5005) for a final collagen concentration of 1.5 mg/mL

collagen and 200,000 cells/mL. 250 µL of solution was pipetted unto a Teflon ring within a suspension cell culture plate. Following 1.5 hours of polymerization, complete media was added ±1 ng/mL TGFβ1, and the collagen gel was released from both the Teflon mold and bottom of the plate. Gels were imaged immediately after release as well as six, 24, 48, and 72 hours following. Gel area was measured at each time point using ImageJ (NIH) and normalized to original gel area.

Polyacrylamide gel synthesis

Polyacrylamide gel synthesis was performed as previously described [172]. Briefly, Amino-silanated coverslips were prepared through evaporation of 0.1 M NaOH followed by a five-minute incubation in 3-aminopropyltriethoxysilane (Sigma-Aldrich 281778) to activate the coverslip to bond to the gel. Hydrophobic glass slides were prepared through a five-minute incubation in dichloromethylsilane (Sigma-Aldrich 440272) followed by rinsing. The 40 kPa polyacrylamide gel was formulated by an 8% polyacrylamide (Bio-Rad 161-0140) and 0.48% bis-acrylamide (Bio-Rad 161-0142) solution in PBS. The mixture was degassed and polymerization initiated through the addition of 1/100 volume of 10% (weight/volume) ammonium persulfate (Sigma-Aldrich A3678) and 1/1,000 volume of tetramethylethylenediamine (Sigma-Aldrich T7024). 50 µL of gel solution was pipetted onto the glass slide and a coverslip was placed on top. After polymerization, 500 µL of 0.2 mg/mL sulfo-SANPAH (Thermo Scientific 22589) was added to the gel, and the gels were exposed to 365 nm ultraviolet light at a distance of about 3 inches for 10 minutes. The gels were rinsed and incubated with 1 mg/mL fibronectin (Sigma-Aldrich F0895) overnight.

Cell Proliferation and Migration Assay

To measure cell proliferation, 5,000 cells/cm^2 were plated in a six-well dish for 24 hours. Cells were labeled with 5-bromo-2-deoxyuridine (**BrdU**; 1:1,000; GE Healthcare, RPN201) for two hours then fixed in 4% paraformaldehyde for 20 minutes at room temperature. Cell membranes were permeabilized using 0.05% Triton X-100 (Sigma-Aldrich, T8787) for 10 minutes followed by nuclear permeabilization using 2N HCl for 20 minutes. Cells were stained with anti-BrdU antibody (1:200; Santa Cruz Biotechnology, SC-32323) overnight. Coverslips were mounted in ProLong Gold with DAPI (Thermo-Fisher Scientific, P36941) in order to count total and BrdU+ nuclei.

Cell migration was quantified by first plating 15,000 cells/cm^2 in a 12-well dish and allowing them to adhere overnight and form a confluent monolayer. A 200 uL micropipette tip was dulled on the lid of the dish then used to create an artificial wound by dragging the tip down the center of the well. The center of the well was marked on the bottom of the dish to ensure imaging of a consistent area. Images were acquired at time of injury, and two, four, and six hours after injury. The cell front was measured and % closure was calculated over time using the ImageJ (NIH) software.

For both assays, three independent cell lines were used for each genotype and performed in triplicates.

Quantitative Polymerase Chain Reaction

A cohort of animals was set aside exclusively for qPCR as previously described in Chapter 3. Scar tissue was microdissected out at 7 days after MI and the primers listed in **Table 5-1** were used.

Table 5-1 qPCR primer sequences

Gene Target	Forward Primer (5' to 3')	Reverse Primer (5' to 3')
Gapdh	ATGACAATGAATACGGCTACAG	TCTCTTGCTCAGTGTCCTTG
Htr2b	TCAATAGGCATCGCCATCCCAG	CCATGATGGTGAGAGGTGCGAA
Il6	CAAAGCCAGAGTCCTTCAGAG	GAGCATTGGAAATTGGGGTAG
Tgfb1	CCTGGGTTGGAAGTGGATC	TTGGTTGTAGAGGGCAAGG
Sm22a	AGCCAGTGAAGGTGCCTGAGAAC	TGCCCAAAGCCATTAGAGTCCTC
Col1a1	CATAAAGGGTCATCGTGGCT	TTGAGTCCGTCTTTGCCAG
Col3a1	CCGAACTCAAGAGTGGAGAATAC	GGGCCATAGCTGAACTGAAA
Lox	CGATTTCCGCAAAGAGTGAAG	ATCAAGCAGGTCATAGTGGC
Mmp13	GATTATCCCCGCCTCATAGAAG	TCTCACAATGCGATTACTCCAG
Mmp2	GCGGCAGTGGTGTGTATTG	CGGCGATCCCCTTACTCTACT
Mmp9	AACCTCCAACCTCACGGACA	TGCTTCTCTCCCATCATCTGG

Western blot

Cells were lysed in RIPA buffer and frozen at -80°C. Protein lysates were denatured via β-mercaptoethanol and heat (five minutes at 95°C). 10% polyacrylamide gels were used for gel electrophoresis to separate proteins. Proteins were transferred to nitrocellulose membranes (LI-COR 926) and blocked with Odyssey Blocking Buffer (LI-COR 927) to prevent non-specific antibody binding. Membranes were incubated serially in primary antibody followed by fluorescently tagged secondary antibodies. LI-COR odyssey fluorescent scanner was used to image membranes and Image Studio Lite was used to analyze the images and perform the densitometry. Antibodies used were αTubulin for normalizing total protein and pErk1/2 (Cell Signaling Technology; 4370S).

Statistical Analysis

Statistical analysis was performed using SigmaPlot version 11. Shapiro-Wilk test was used to test for data normality. Subsequent statistical analyses used either a 2-way ANOVA with Holm-Sidak post hoc or a Kruskal-Wallis rank-sum test with Conover-Iman post hoc test for nonparametric data. A two-tailed Student *t* test was used for comparisons of two normally distributed groups. Applicable tests and significance are labeled in figure captions with $P<0.05$ as the cutoff for data to be considered significantly different.

5.4 Results

5.4.1 5-HT$_{2B}$ ablation in periostin-expressing cells have altered gene expression detected by RNA sequencing

In order to investigate how periostin-driven ablation of 5-HT$_{2B}$ imparts beneficial outcomes following MI, we performed RNA sequencing on PDGFRα+ cells isolated from the scar tissue of infarcted hearts seven days after MI (**Figure 5.2**). Quality RNA isolation and alignment of the short sequencing reads to the reference genome were successfully performed, however, only about 20% of PDGFRα+ cells were tdTomato+ in the *Htr2b*$^{fl/fl}$*Postn*$^{MCM/+}$ group (indicating 5-HT$_{2B}$ knockout; **Table 5-1**). Despite incomplete penetrance of 5-HT$_{2B}$ ablation, differential expression of several genes controlling cell proliferation and cell adhesion and migration was observed compared to control animals (**Figure 5.3**). The gene ontology (**GO**) terms associated with the altered transcripts were overwhelmingly associated with mitotic processes (**Table 5-2**). For a full list of genes that were deferentially expressed at a significant level, see **Appendix A**.

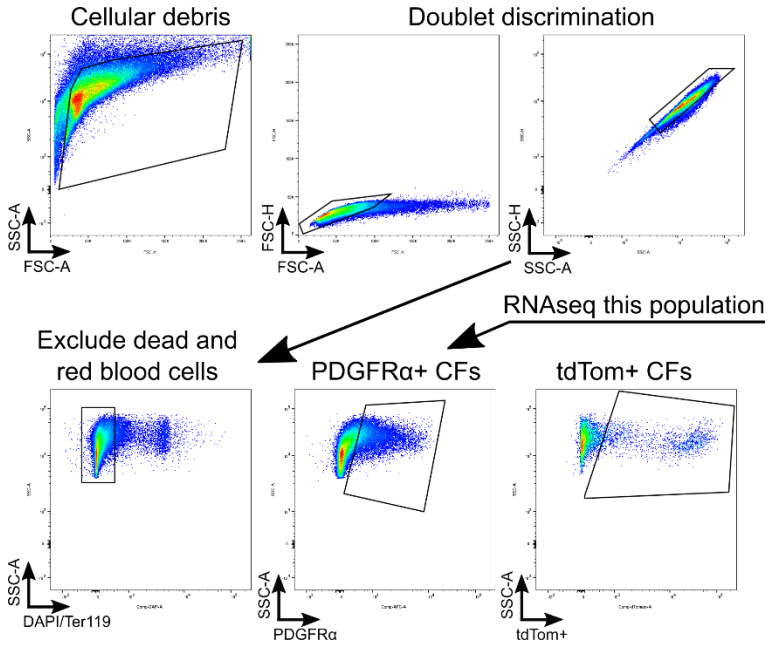

Figure 5.2. PDGFRα+ cell sorting.
PDGFRα+ cells were isolated from infarcted tissue of *Htr2b*$^{fl/fl}$ and *Htr2b*$^{fl/fl}$*Postn*$^{MCM/+}$ mice seven days after MI for subsequent RNA sequencing.

Table 5-2 Quality of RNA integrity number (RIN), alignment efficiency, and the percentage of cells with a recombined *Htr2b* allele which underwent RNA sequencing.

Mouse ID	RIN	Total Reads	Mapped Reads	Percent Aligned	Percent tdTom+
Htr2b$^{fl/fl}$					
6	9.3	70826758	69942731	98.75	0.00
5	9.2	93422980	91778498	98.24	0.00
Htr2b$^{fl/fl}$*Postn*$^{MCM/+}$					
7	9.6	90420754	87771218	97.07	14.20
4	8.6	89413414	83571864	93.47	23.50
1	6.6	78616202	73991839	94.12	14.40
2	5.9	85407778	83312403	97.55	24.30
Summary					
Average	8.2	84684648	81728092	96.53	19.10
SEM	0.6	3468970	3377296	0.90	2.78

Table 5-3 Significantly altered GO terms from RNA sequencing (BP = biological process, CC = cellular component).

ID	ONTOLOGY	Description
GO:0098813	BP	nuclear chromosome segregation
GO:0000819	BP	sister chromatid segregation
GO:0033047	BP	regulation of mitotic sister chromatid segregation
GO:0033045	BP	regulation of sister chromatid segregation
GO:0007059	BP	chromosome segregation
GO:0000070	BP	mitotic sister chromatid segregation
GO:0051983	BP	regulation of chromosome segregation
GO:0000793	CC	condensed chromosome
GO:0000779	CC	condensed chromosome, centromeric region
GO:0000775	CC	chromosome, centromeric region
GO:0000780	CC	condensed nuclear chromosome, centromeric region
GO:0098687	CC	chromosomal region
GO:0000777	CC	condensed chromosome kinetochore
GO:0000940	CC	condensed chromosome outer kinetochore
GO:0000778	CC	condensed nuclear chromosome kinetochore
GO:0000776	CC	kinetochore

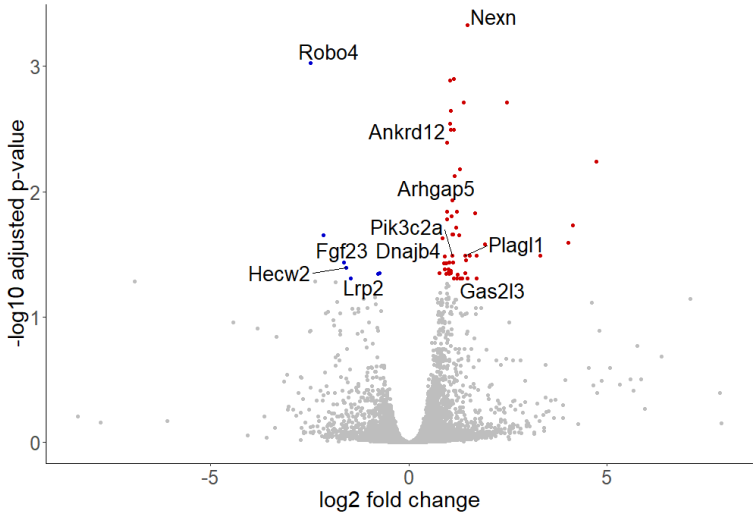

Figure 5.3. Volcano plot illustrating RNA sequencing results.
Significantly differentially regulated genes (blue/red) in PDGFRα+ cells isolated from *Htr2b*$^{fl/fl}$*Postn*$^{MCM/+}$ compared to *Htr2b*$^{fl/fl}$ animals.

5.4.2 5-HT$_{2B}$ controls myofibroblast proliferation

RNA sequencing pointed to an alteration in myofibroblast proliferation following MI. We observed a decreased area fraction of periostin staining in the infarct of SB-treated mice one

week after injury, indicative of decreased myofibroblast proliferation and infiltration (**Figure 5.4A**). To confirm these findings, *in vitro* analysis of 5-$HT_{2B}^{-/-}$ CFs revealed a decreased proliferative capacity as seen by fewer cells incorporating BrdU compared to WT CFs. (**Figure 5.4B**).

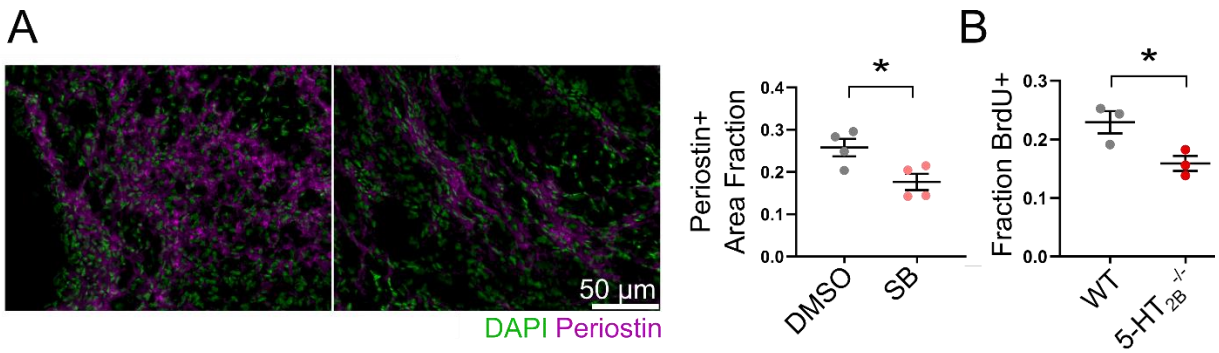

Figure 5.4. *Htr2b* deletion impairs proliferative capabilities.
A, Periostin immunostaining reveals a decrease in myofibroblast presence in damaged tissue one week after MI. **B**, 5-HT_{2B}-knockout CFs exhibit decrease proliferation measured by BrdU incorporation. Mean ± SEM, *P<0.05, following 2-tailed Student *t* test.

5.4.3 Ablation of 5-HT_{2B} limits CF migration and ECM remodeling in vitro

Multiple transcripts were identified from RNA sequencing which influence behavior of CFs during the wound healing process (*Nexn*, *Gas2l3*, *Lrp2*, *Fgf23*, and *Robo4*). Therefore, we investigated the migratory capacity of WT and 5-$HT_{2B}^{-/-}$ CFs *in vitro* to assess the capability to respond and migrate into an artificial wound. CFs lacking 5-HT_{2B} demonstrated an approximate 50% decrease in migratory capacity (**Figure 5.5**).

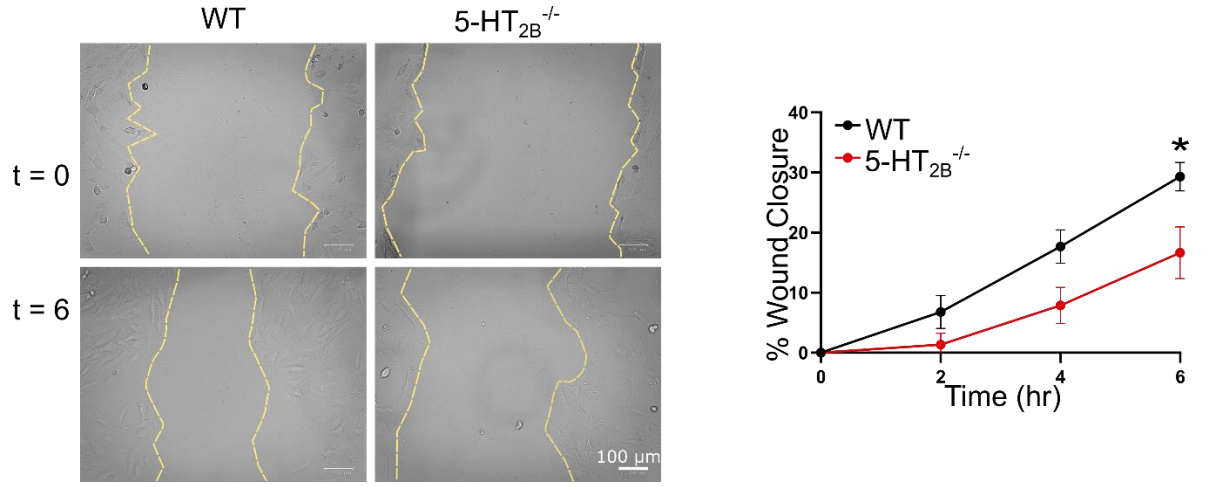

Figure 5.5. *Htr2b* deletion impairs migratory wound healing response.
5-HT$_{2B}$-knockout CFs are less migratory than WT counterparts (N=3). Mean ± SEM, *P<0.05, following 2-tailed Student *t* test.

CFs were seeded into free-floating collagen gels in order to test their ability to remodel a collagen matrix. In 3D collagen gels seeded with 5-HT$_{2B}^{-/-}$ CFs, gel contraction was significantly hindered. Even with the administration of TGFβ, the contractile response in 5-HT$_{2B}$-knockout cells could not be replicated (**Figure 5.6**). These results point to a mechanism of 5-HT$_{2B}$-mediated myofibroblast proliferation and matrix remodeling leading to adverse scar formation following MI.

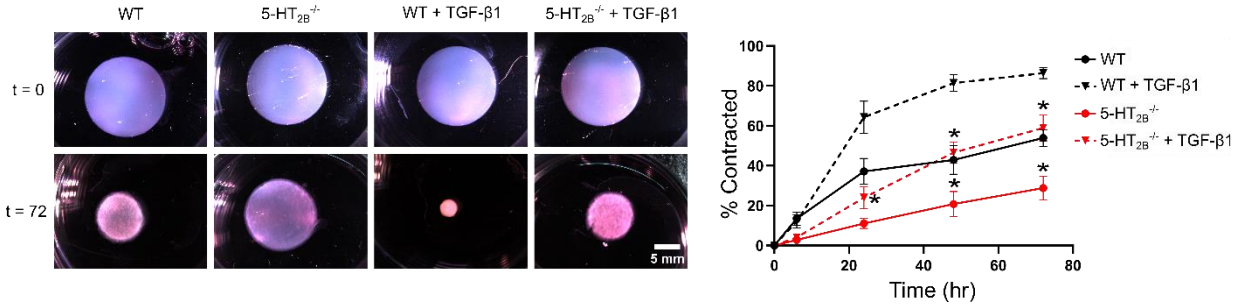

Figure 5.6. 5-HT$_{2B}$ deletion impairs 3D collagen matrix compaction.
5-HT$_{2B}$-knockout CFs contract free-floating collagen gels less compared to WT (N=6). Treatment with TGFβ1 caused nearly complete contraction of the gel by WT cells but does not rescue contraction in 5-HT$_{2B}$ knockouts. Mean ± SEM, *P<0.05, following 2-way ANOVA and Holm-Sidak post hoc test.

We next investigated the activation of CFs into myofibroblasts by observing the expression of α-smooth muscle actin positive stress fibers with TGFβ treatment. We seeded

CFs onto 40 kPa polyacrylamide gels to prevent mechanically-induced myofibroblast activation normally observed when cells are plated on stiff, tissue culture plastic even without a stimulus. We observed a decreased proportion of both partially and fully activated myofibroblasts with 5-HT_{2B} knockout prior to treatment. Upon treatment with TGFβ, the number of fully activated WT CFs was dramatically increased over 5-HT_{2B} knockout CFs. However, there were more mutant CFs that were partially activated, indicating an impaired ability to fully form mature stress fibers when lacking 5-HT_{2B} (**Figure 5.7**).

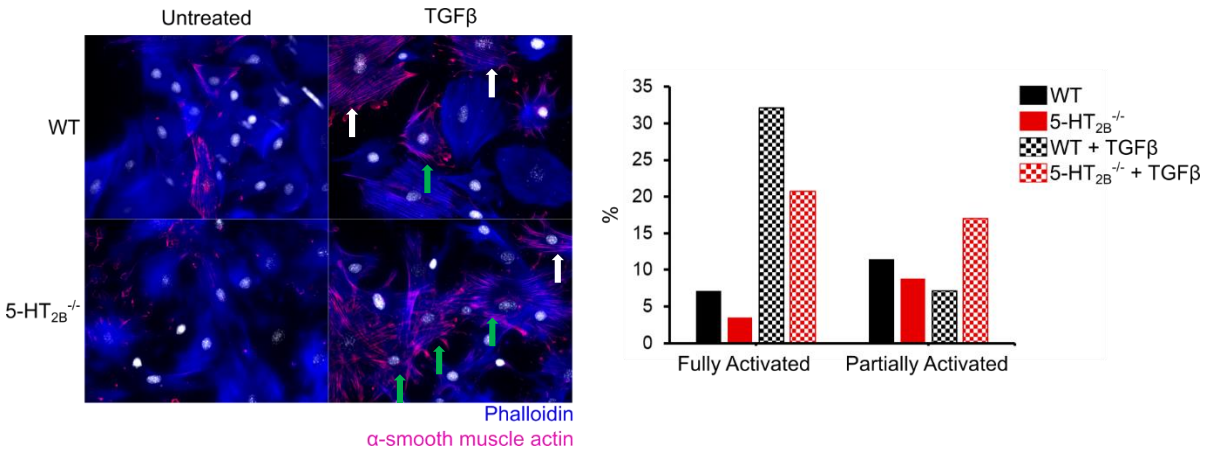

Figure 5.7. 5-HT_{2B} deletion impairs stress fiber formation.
WT CFs seeded on 40 kPa polyacrylamide gels transform more completely into myofibroblasts by expressing fully formed stress fibers marked by α-smooth muscle actin (white arrow). 5-HT_{2B} knockout CFs have more partially activated myofibroblasts (green arrow) demonstrating an impaired ability to fully assemble their contractile machinery. Expressed as a percentage of cells counted (N=53-70 cells counted per group).

5.4.4 Transcriptional and kinase regulation in scar tissue with 5-HT_{2B} antagonism

After observing phenotypic changes in CFs lacking 5-HT_{2B}, we performed qPCR analysis from scar tissue removed seven days following MI. We investigated alterations in *Il6* (shown to decrease with 5-HT_{2B} ablation in noncardiomyocytes and decrease cardiac hypertrophy), the pro-fibrotic gene encoding TGFβ, the contractile marker *Sm22α*, and the two major collagen molecules that make up the scar, namely *Col1a1* and *Col3a1*. In mice treated with RS, we saw no change in expression for the gene encoding 5-HT_{2B}. We saw significant downregulation of *Il6*

and *Tgfb1* which could indicate a decreased fibrotic environment. Decreased expression of the contractile marker *Sm22a* could explain the decreased contractility of our CFs. Lastly, decreased expression of collagen-encoding genes could be indicative of muted scar formation (**Figure 5.8A**). We repeated this analysis in scar tissue of mice treated with SB, but the results were not conserved (**Figure 5.8B**).

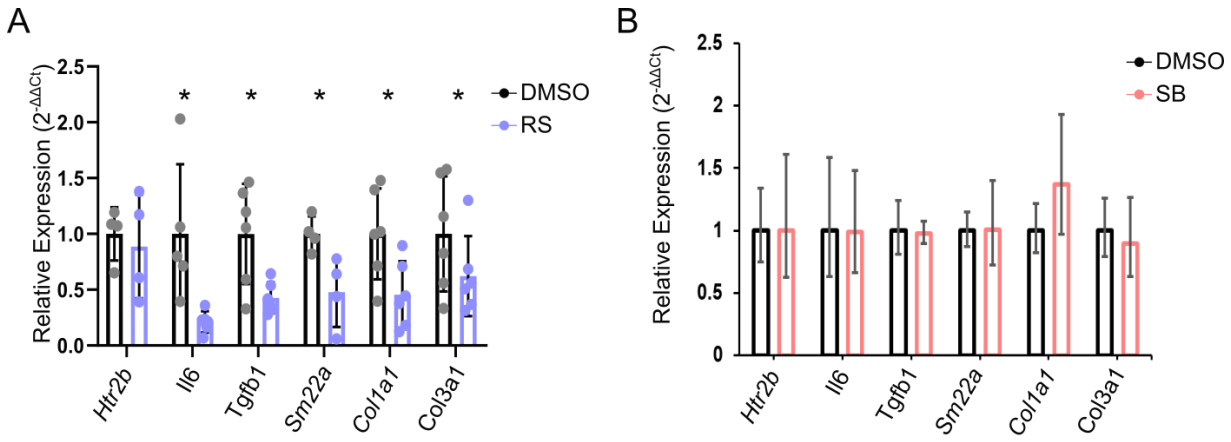

Figure 5.8. 5-HT$_{2B}$ antagonism yields disparate results for fibrotic gene transcription. RS treatment downregulates gene transcription of fibrotic markers of disease in scars seven days after MI which are not conserved in SB-treated animals (N=4). *P<0.05, following 2-tailed Student *t* test.

After observing the discrepancies between our antagonism treatments, we isolated RNA from CFs as a cleaner model system to look at baseline alterations of collagen transcripts. Both *Col1a1* and *Col3a1* appear to be decreased in 5-HT$_{2B}^{-/-}$ CFs compared to WT (**Figure 5.9**).

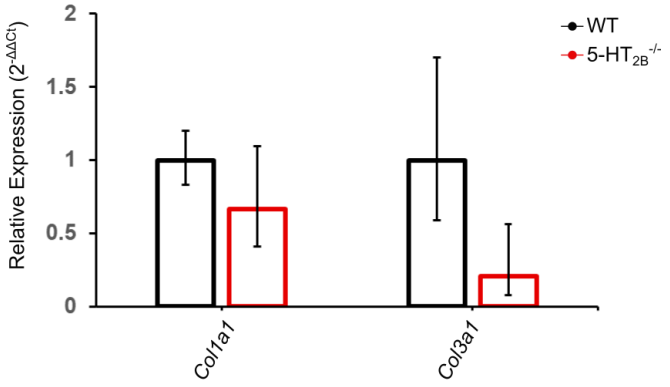

Figure 5.9. 5-HT$_{2B}$ ablation appears to alter collagen expression in isolated CFs.
5-HT$_{2B}^{-/-}$ CFs have decreased expression of collagen transcripts *in vitro* (N=3 independent cell lines).

Since we saw alterations in collagen processing and tissue stiffness as outlined in Chapter 3, we investigated potential alterations in expression of transcripts for proteins that participate in ECM remodeling. *Lox* encodes the protein which crosslinks collagen. *Mmp13* is the murine gene analogous to *MMP1* in humans which encodes a matrix metalloproteinase (**MMP**) functioning to cleave collagens type I and III. MMP2 is a gelatinase that is present in tissue injury to degrade denature collagen, and MMP9 is the most extensively studied MMP post-MI with substrates including collagen I and fibronectin [173]. After administration of RS, scars seven days after MI appear to have some decreases in *Lox* and the aforementioned MMPs, most notably *Mmp13* (**Figure 5.10**). While none of these results were statistically significant, they do warrant further investigation into collagen processing.

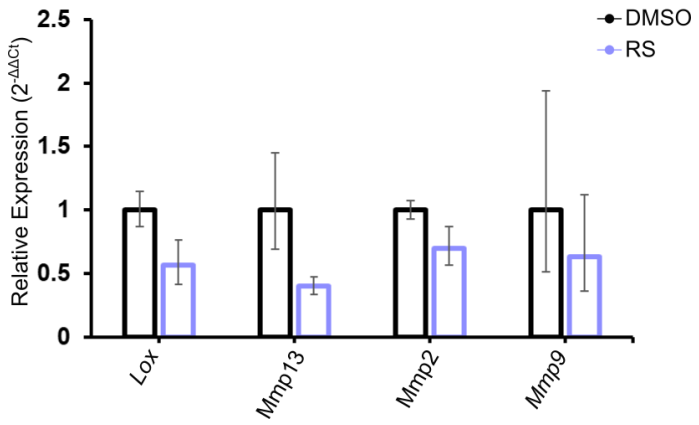

Figure 5.10. 5-HT$_{2B}$ antagonism with RS alters collagen processing transcripts.
RS treatment for 7 days following MI partially reduces expression of genes encoding proteins responsible for collagen cross-linking as well as degradation and remodeling (N=4).

Lastly, we investigated the phosphorylation of the mitogen-activated protein kinase Erk1/2 as a known downstream target of 5-HT$_{2B}$ activation implicated in cellular remodeling. While baseline levels of phosphorylation of this kinase were identical, treatment with the 5-HT$_{2B}$ agonist BW723C86 induced approximately 13-fold increase in Erk1/2 phosphorylation compared to only about 6-fold activation in 5-HT$_{2B}^{-/-}$ CFs (**Figure 5.11**).

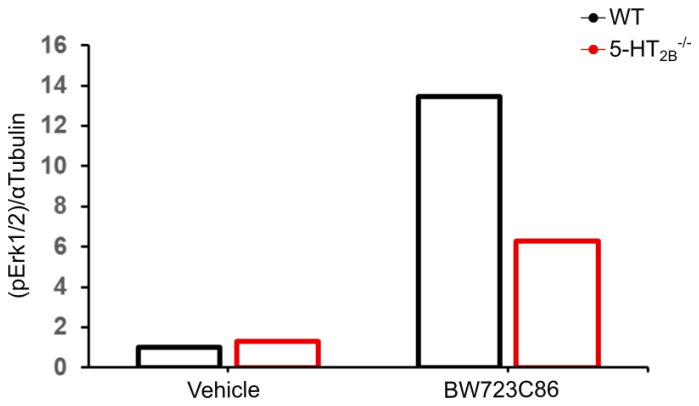

Figure 5.11. 5-HT$_{2B}^{-/-}$ CFs have decreased Erk1/2 activation upon 5-HT$_{2B}$ activation.
Activation of the 5-HT$_{2B}$ receptor with BW723C86 induces drastic activation of pErk1/2 with only about half the phosphorylation levels seen in 5-HT$_{2B}^{-/-}$ CFs (N=2).

5.5 Discussion

After MI, rapid infiltration and proliferation of CFs into the injured tissue are necessary for the fibrotic wound healing response. This process plays a significant role in the quantity and composition of ECM deposition that will eventually form the mature scar [174], [175]. We utilized RNA sequencing as an unbiased technique to reveal specific genetic aberrations with myofibroblast-targeted 5-HT_{2B} deletion seven days following MI. Our approach was limited by the inability to isolate a pure population of cells that are directly comparable to our control animals with periostin-driven 5-HT_{2B} knockout. Since the tdTomato reporter was under the control of Cre expression, we were unable to sort based on expression of this fluorescent reporter. We utilized the surrogate CF marker PDGFRα to select for CFs [176]–[178]. Despite only about 20% of these cells displaying the tdTomato fluorescent reporter in the *Htr2b*$^{fl/fl}$*Postn*$^{MCM/+}$ group, we still observed differential regulation of multiple genes in myofibroblasts with 5-HT_{2B} ablation. We saw upregulation of genes such as *Plagl1* which inhibits cell growth and proliferation, potentially through PPARγ [179], *Nexn* whose loss is associated with dilated cardiomyopathy [180], and the tumor suppressor *Dnajb4* which is a member of the heat shock protein 40 family known to arrest cell cycle [181]. Several interesting transcripts were also downregulated: *Lrp2* which increases proliferation of epicardial cells (CF precursors) [182], *Fgf23* which demonstrates broad mitogenic and cell survival actions specifically in the heart [183], and *Robo4* which is associated with increased matrix metalloproteinase expression and predisposition for aortic valve disease [184]. These genes, as well as the associated GO terms, point to 5-HT_{2B} control of fundamental processes in scar formation after MI.

The alterations in the aforementioned genes as well as others listed in Appendix A directed our investigation to characterize CF phenotype in relation to 5-HT_{2B} control of proliferation and matrix remodeling. CFs lacking 5-HT_{2B} clearly exhibited a phenotype indicative

of decreased cardiac remodeling. Myofibroblasts were sparser in damaged tissue of SB-treated animals. We believe this is due to a decrease in cell migratory and proliferative capacity. This finding could explain the decreased scar thickness due to a decrease in ECM deposition. It could also explain the presence of thinner, less mature collagen fibers if myofibroblasts were less prevalent and unable to compact and remodel collagen fibers. To confirm these results, we isolated 5-HT_{2B} knockout CFs and observed proliferation *in vitro*. Without expression of 5-HT_{2B}, CFs were significantly less proliferative.

Subsequently, we investigated CF migration and collagen matrix remodeling *in vitro*. After subjecting a cell monolayer to an artificial wound, 5-HT_{2B} knockout CFs migrated into the wound at only half the rate of WT controls. We also embedded CFs into free-floating collagen matrices to assess the contractile and remodeling capacity of a 3D collagen matrix. 5-HT_{2B} knockout significantly reduced gel compaction. Even under the potent fibrotic stimulus of TGFβ, gel contraction could not be rescued. To further investigate alterations into this contractile phenotype, CFs were seeded on 40 kPa polyacrylamide gels since plating CFs on stiff substrates such as tissue culture plastic mechanically induces a strong myofibroblast phenotype [146]. We used a phalloidin stain to mark F-actin to observe cell boundaries and α-smooth muscle actin to observe the formation of contractile stress fibers as a surrogate of myofibroblast activation. In untreated cells, WT CFs were more likely to form full stress fibers which stretched the diameter of the cell. This difference was more dramatic when treated with TGFβ. 5-HT_{2B} knockout CFs were more likely to be partially activated into myofibroblasts and exhibit segments of stress fibers which did not stretch the full diameter of the cell or were localized to the cell periphery. This decreased ability to fully transform into myofibroblasts could account for the decreased contractility and remodeling capability when 5-HT_{2B} signaling is impaired.

We investigated the scar tissue of 5-HT_{2B} antagonized mice for further evidence of transcriptional regulation of scar formation. In RS-treated animals, we saw significant decreases

in genes which influence the fibrotic activity of CFs, including *Il6*, *Tgfb1*, and *Sm22a*. Furthermore, the collagen transcripts *Col1a1* and *Col3a1* were downregulated. These data would give further insight into how 5-HT_{2B} control fibrosis post-MI through decreased presence of fibrotic cytokines and decreased expression of contractile machinery. However, when we attempted to confirm these results with SB treatment, we observed no differences. One possible explanation would be the microdissection process. Different proportions of myocardium could have been included when isolating scar tissue, which would decrease the fraction of CF RNA in the pool of RNA which qPCR was performed on. Laser microdissection should be conducted as a more accurate way to isolate scar tissue and determine how 5-HT_{2B} antagonism alters transcription. In an effort to reconcile these results, we performed qPCR on isolated CFs. We observed a nonsignificant decrease in collagen transcription of both *Col1a1* and *Col3a1* in 5-HT_{2B} knockout CFs. This result seems to implicate a decreased secretory phenotype of CFs which lack 5-HT_{2B} signaling.

To understand if collagen processing was altered, we observed transcriptional regulation of the collagen-crosslinker *Lox* and the collagenases and gelatinases *Mmp13*, *Mmp2*, and *Mmp9* with RS treatment. While downregulation was not significant, there did appear to be some decrease in transcription of *Lox* and *Mmp13*. This would indicate a decreased maturation and stiffening of the collagen matrix through cross-linking of collagen fibers, as well as a decreased ability to remodel the tissue. Since we saw incremental changes in our histological analyses - improving outcomes without preventing sufficient scar formation - these marginal transcriptional changes could indicate a hindered yet not prevented remodeling response in CFs. Lastly, we looked into activation of downstream protein kinases known to signal myofibroblast activation. While there were no alterations in phosphorylation of p38 or Src in 5-HT_{2B} knockout CFs (data not shown), we did demonstrate that ablation of 5-HT_{2B} inhibits the 5-HT_{2B}-mediated activation of Erk1/2. While not completely prevented (due to the lack of

specificity of BW723C86), this result is supported by previous studies and a potential avenue to further explore the molecular mechanism of 5-HT_{2B}-mediated fibrosis [29], [57].

Using RNA sequencing and supportive *in vitro* analyses, these studies point to 5-HT_{2B} control over CF proliferation, migration, and matrix remodeling. There is preliminary evidence of 5-HT_{2B} ablation decreasing remodeling capabilities through a decrease in myofibroblast activation and collagen deposition and processing. In the context of MI, these mechanistic alterations support a decrease in fibrotic scar formation, expansion, and ECM remodeling observed *in vivo*.

Chapter 6

Summary, broader impacts, and future directions

6.1 Summary and broader impact

This work investigated the role of 5-HT_{2B} in the context of MI. Cardiovascular disease is the leading cause of death worldwide, and there is no indication that its prevalence is decreasing. Despite this fact, acute mortality following MI has improved. One consequence of this improvement is the increased rate of heart failure cases due to the permanent loss of contractile cardiomyocytes after ischemic injury. This motivated us to investigate the healing process post-MI with the goal of influencing scar formation in a manner that preserves cardiac structure and function to impart lasting therapeutic benefits. Since cardiac fibrosis is a hallmark of a wide variety of cardiovascular pathologies, we believed that targeting the fibrotic response could be a viable avenue to achieve these goals. Following MI, most pharmacological interventions (ACE inhibitors, ARBs, statins, etc.) function through wide-spread mechanisms of actions that do not offer specific control over the healing process in MI. While they have proven useful, the results obtained with these strategies can be improved.

To address these challenges, we utilized highly specific and selective 5-HT_{2B} antagonists to address a single receptor and its role in the healing process after MI. We utilized two independent antagonists which were administered globally and tracked cardiac structure and function over a six-week time-course. We observed an initial preservation of cardiac structure as measured by EF and FS, and systolic dimensions were significantly improved with the SB antagonist. For both antagonists, we removed treatment after three weeks in order to determine if the differences observed were due to the initial wound healing response and if they

persisted for the following three weeks after removal of the antagonist. Indeed, this is what was observed indicating an improved scar formation process, creating a tissue environment that conveyed functional benefits without the need of constant perturbation. We also utilized a speckle-tracking algorithm to quantify the strain generated in the LV and track its evolution over time. While the strains were initially similar one week after injury, we observed a stabilized deformation of the LV in our 5-HT_{2B} antagonist groups, indicative of preserved myocardial contractility. In our control treated groups, this metric decreased over the six-week experiment, pointing to decreased cardiac function and a potential progression into heart failure.

Naturally, we proceeded to investigate the histological changes associated with our echocardiographic observations. We first observed a decrease in scar thickness with 5-HT_{2B} antagonism without an increase in mortality. We concluded that the fibrotic process was muted but not to the extent that a functional scar was not formed. To our knowledge, we are the first to mathematically define the BZ region, and using that definition, we calculated this transition region was smaller in our treatment group which would decrease the disruption of the myocardial syncytium. There were no differences in interstitial fibrosis, further pointing to altered scar formation as the driver of improved outcomes.

To further investigate the changes in the deposition of scar tissue, we employed multiple imaging techniques that are not commonly applied to assessing scar formation following MI. These techniques provided further insight into how alterations in collagen structure can improve outcomes after MI. First, we imaged PSR staining under polarized light to quantify collagen fiber thickness. This analysis revealed an increase in the proportion of thin, immature collagen fibers in the BZ of SB-treated animals. These collagen fibers are less likely to be cross-linked and formed into a dense matrix that is unable to be contracted. Secondly, SHG analysis revealed an increased anisotropic distribution of collagen fibers in the BZ of SB-treated animals. Collagen fibers will undergo elastic deformation preferentially along the length of the fiber. Deformation

perpendicular to the fiber is limited. The higher BZ anisotropy would impart an increased contractile phenotype as the collagen fibers have a dominant alignment allowing them to deform in a more uniform manner along the direction of cardiomyocyte contraction.

Continuing to assess alterations to regional tissue properties, we used AFM to quantify the mechanical properties of both scar and BZ tissue. Upon treatment with a 5-HT_{2B} antagonist, scar and BZ stiffness were significantly decreased, further supporting the differences we observed in collagen architecture. Since tissue stiffness is a mechanical driver of fibrosis, and specifically drives hypertrophy in the heart, we quantified cardiomyocyte area in noninfarcted tissue to observe any remodeling of the cardiomyocytes in response to increased tissue stiffness. The cross-sectional area of these cells was higher in the control group which may be predictive of cardiac hypertrophy proceeding to heart failure. Also supporting this finding was an increased expression of the myocardial injury marker *Nppb*.

After extensive characterization of structural, molecular, and mechanical changes mediated by 5-HT_{2B} antagonism, we sought out to identify the cell population responsible for these changes. After eliminating bone marrow-derived cells, we developed two novel genetic knockout models to test 5-HT_{2B} ablation in CFs and CF-derived populations. Inducible, resident CF-targeted ablation of 5-HT_{2B} successfully recapitulated results observed with 5-HT_{2B} antagonism. The genetic model had more striking effects, preserving both systolic and diastolic cardiac dimensions, as well as decreasing relative heart weight. With the success of the resident CF knockout model, we generated a model targeting activated myofibroblasts to investigate changes in a cell population present after the onset of injury. This model revealed nearly identical results to the resident CF model, further solidifying the CF and its derivatives as drivers of 5-HT_{2B}-mediated maladaptive remodeling after MI.

Our last goal was to identify a cellular mechanism in these cell populations. RNA sequencing provided a robust, unbiased investigation into transcriptional changes in cells with

5-HT_{2B} ablated in myofibroblasts. While the cell isolation approach could have potentially masked some results, we still identified changes in the proliferative phenotype of myofibroblasts lacking 5-HT_{2B}. Genes strongly linked to matrix remodeling were also identified as being differentially regulated. To further support these findings, we identified that within the injured tissue of 5-HT_{2B} antagonized hearts, fewer myofibroblasts were present. We believed this is due to the decreased proliferative and migratory phenotypes which were observed *in vitro* using 5-HT_{2B} knockout CFs. Collagen matrix remodeling was also decreased using an *in vitro* 3D gel contraction assay, further highlighting a cell phenotype with limited fibrotic capabilities.

In conclusion, due to the complexities associated with the intricate coordination involved in the inflammatory response post-MI [21], we set out to target the effector cells of fibrosis (i.e. CFs) to control the initial reparative response and limit adverse fibrotic remodeling. Previous reports have shown targeting CFs can control scar mechanics and limit fibrosis without affecting scar stability [185], [186]. This study has identified a novel role of the 5-HT_{2B} receptor in regulating fibrotic remodeling post-MI. Inhibiting the activity of this receptor has an acute benefit that is sustained well beyond the initial healing phase and even demonstrates that cardiac hypertrophy subsequent to an ischemic event can be curtailed. Taken together, this work has identified 5-HT_{2B} as a potential therapeutic target for muting the overactivity of myofibroblasts following MI to preserve cardiac phenotype and prevent the initiation and progression of cardiac fibrosis and heart failure.

6.2 Future directions

The present work advanced our understanding of 5-HT_{2B} in the context of MI and fibrotic remodeling but also raised important questions that can be used to direct future research into this topic. In particular, this research should be expanded by investigating the mechanism of altered collagen deposition and processing. While we did begin investigation into alterations in

the transcription of *Lox* and various MMPs, this avenue is the most likely culprit of altered deposition and assembly of collagen that should be explored further. The collagen cross-linking ratio has recently been used to quantify the amount of collagen cross-linking by dividing the abundance of Lox (obtained through Western blot) by the amount of various collagen isoforms [187]. As cross-linker increases per unit of collagen, the ratio increases indicating more matrix remodeling. Mass spectrometry is a technique that can be applied to identify collagen abundance and modifications in a more complete fashion that could motivate further downstream exploration [188]. This analysis could reveal how formation of the scar is altered by 5-HT_{2B} antagonism. Furthermore, we could use novel techniques for *in vitro* assays to determine if collagen architecture is a primary cause for imparting improved scar mechanics or if it is a downstream consequence. It has been recently shown that fiber alignment in collagen matrices can be controlled to influence matrix pore size and stiffness [189]. We could employ this technique to create anisotropic, less stiff collagen matrices and then seed our WT CFs on them. We could then repeat our gel contraction assay to determine if WT CFs contract more like the 5-HT_{2B} knockout cells when on a more favorable matrix. If they do, we can infer that that an initial fibrotic formation is altered between the cells which is perpetuated by improved matrix properties. If the WT cells do not behave differently than the knockouts, this would inform us that the inherent remodeling capabilities of the cells are different. These collagen gel matrices could also provide more relevant *in vitro* environments to repeat some of the other studies including myofibroblast activation, gene expression, and explore collagen deposition.

Future experiments should also include determining the timing of drug administration that is required to achieve improved cardiac outcomes. We should administer 5-HT_{2B} antagonists starting at various times throughout the wound healing process and for various lengths. In our studies, drug was given beginning day of injury and maintained for three weeks. We showed that even upon removal of drug at three weeks, the outcomes persisted out to six

weeks. This led us to conclude that the early stages of wound healing were improved and sufficient to sustain cardiac improvements. Therefore, we should investigate exactly when the drug should be administered and for how long it needs to be administered. These experiments would also help us understand the mechanism of how ablation of 5-HT_{2B} in *Tcf21*- and *Postn*-expressing cells functions to improve cardiac outcomes. If drug administration is only required in the proliferative phase of wound healing (days 3-5 after injury), our mechanism would likely be a decreased presence and proliferation of CFs leads to improved scar formation. If the drug is required only during the scar maturation phase (days 5-7 after injury), then the mechanism would likely be altered collagen deposition and processing. Potentially, the antagonist would need to be administered throughout the first week to incrementally alter both phases but could be removed after one week after the initial scar has been formed.

Pericyte biology is a relatively understudied field. These cells play a key role in vascular integrity as well as angiogenesis. It has been shown that pericyte ablation contributes to MI as well as fibrosis through modulating myofibroblast collagen secretion [190]. Pericytes have been shown to secrete ECM proteins, including collagen 1 under wound healing conditions in the heart [191], [192]. Pericytes participate in both the inflammatory process and have been reported to give rise to myofibroblasts [9], [193]. Purified human skeletal pericytes have been shown to improve cardiac contractility, reduce fibrosis, and attenuate LV dilation in a mouse model of MI [194]. This result is interesting as it would contradict the hypothesized contribution of pericytes to increased myofibroblast presence and function. We know that *Tcf21* is expressed by this stromal cell population with mesenchymal properties, which would include them in our cell-specific exploration into 5-HT_{2B} function described in this dissertation [135], [195]. Pericytes can be marked with platelet-derived growth factor β allowing for the specific study of their contribution to 5-HT_{2B}-mediated cardiac remodeling [196]. The multiplicity of pericyte control of endothelial cells, vascular integrity, cytokine secretion of immune cells, fibroblast function, and

collagen secretion could explain the results we have observed with 5-HT_{2B} inhibition and warrant specific investigation. Since it is known several cues can influence myofibroblast activation and tissue fibrosis, this under-studied cell type which plays a role in a variety of these cues should not be ignored.

Identifying the specific molecular targets downstream of 5-HT_{2B} would provide greater mechanistic insight into its regulation of fibrosis. While RNA sequencing revealed a pool of candidate genes and our *in vitro* experiments showed phenotypic changes, it is worth pursuing the molecular mediators of these changes to fully characterize the mechanism. We could begin by confirming alterations in these genes with qPCR following MI and 5-HT_{2B} antagonism. Our preliminary data points to the activation of the mitogen-activated protein kinase Erk1/2 downstream of 5-HT_{2B} activation. Blocking activation of this kinase with the inhibitor U0126 is one method to see if we get similar effects as with SB treatment. Since Erk1/2 is a ubiquitous signal transducer with built-in redundancies, it would not be a feasible therapeutic target, but the specificity of 5-HT_{2B} antagonism would prove a useful target [197]. While we did not observe alterations in phosphorylation of the tyrosine kinase Src, we did not test its transportation within the cell as it has been shown that 5-HT_{2B} antagonism arrests Src motility [31].

Upstream activators of 5-HT_{2B} signaling also need to be explored. The literature is sparse when it comes to the role of serotonin in MI, with most research focusing on clotting response mediated by platelet activation and the relationship with selective serotonin reuptake inhibitors and depression. We have cited reports of cross-talk between 5-HT_{2B} and AT_1R in a model of cardiac hypertrophy, and it is known that AngII is increased after MI. Our collagen gel contraction assay also reveals a muted response to TGFβ1, possibly the most well-characterized regulator of fibrosis. With all of these potential activators of 5-HT_{2B} signaling, a future experiment identifying which molecule most potently activates 5-HT_{2B} would be a worthy study. A starting experiment could involve the administration of the 5-HT_{2B} agonist BW723C86

and see if the injury response is worsened. Losartan is an ARB commonly given to reduce blood pressure after MI to reduce the load on the heart. Some therapeutic benefits have been noted with this drug, and since 5-HT_{2B} and AT_1R cross-talk has been noted, an interesting study could investigate if losartan administration post-MI achieves similar results as 5-HT_{2B} inhibition. This experiment could reveal a common signaling mechanism for further exploitation.

The sex-specific role of 5-HT_{2B} signaling is another route to further expand this research. As previously stated, it is known that developmental deficiency of 5-HT_{2B} is less catastrophic in females than in males, as seen by fewer fibrotic lesions and less severe diastolic dysfunction [85]. Sex-specific outcomes in cardiac disease are also well-documented. For example, aged female rats have functionally favorable tissue properties such as preserved cardiomyocyte density and greater compliance when compare to males [198]. While it is thought that estrogen is protective against heart disease, two trials investigating the effect of estrogen and progestin hormone replacement revealed either no protection or increased risk of cardiovascular disease with hormone replacement therapy [199], [200]. Conversely, gene expression analysis in female versus male mice revealed higher levels of gene induction in females relative to males related to patterns associated with overall better outcomes [201]. Testosterone has also been shown to enhance cardiac remodeling after MI which leads to deterioration of cardiac function [202]. 5-HT_{2B} has been linked to testosterone levels and function [203], [204]. Therefore, in the context of myocardial remodeling, it would be worth exploration into the role 5-HT_{2B} plays in sex-specific outcomes. Is estrogen protective or testosterone detrimental? We could explore testosterone levels in mice lacking 5-HT_{2B} to determine if it confers protection in this manner. We could also administer a 5-HT_{2B} agonist to females to see if we can induce increased testosterone levels and worsen cardiac outcomes. Conversely, we could explore a link between estrogen and 5-HT_{2B} to understand why females are inherently protected against the detrimental effects of 5-HT_{2B} alterations.

Limitations of the work described in this dissertation could be addressed with a variety of studies to directly and incrementally expand the data presented. First, blood pressure measurements of infarcted mice treated with a 5-HT_{2B} antagonist could be obtained. Since vascular tone is susceptible to AngII; 5-HT_{2B} and AT_1R potentially have a shared mechanism; and afterload on the heart has a significant contribution to cardiac contractility, investigation into 5-HT_{2B}'s effect on blood pressure is warranted as a potential mechanism into improved contractility [35], [205]. Decreased blood pressure could also provide a mechanical cue for the formation of a thinner, softer scar if the LV wall needs less reinforcement as less pressure must be generated to overcome the afterload. Furthermore, more invasive measurements of LV pressure as a result of cardiac contractility and relaxation could be obtained through LV catheterization. It would be worthwhile to confirm GLS measurements of contractility through another method especially since there were discrepancies in the echocardiographic data where GLS decreased over time but EF and the structural metrics did not. Mice should also be allowed to survive greater than 6 weeks after the initial injury to allow for cardiac decompensation to occur to further confirm that improved scar formation is sufficient to prevent heart failure. Histological evaluation of the genetic ablation models should be performed to corroborate the findings in the antagonist studies. Seeing that echocardiographic analyses revealed an even stronger protective response in the genetic models, we would expect similar if not greater differences in our histological analyses.

In terms of RNA sequencing, we would like to have an improved selection of the target cell population with 5-HT_{2B} ablation to see if we could detect more subtle changes. Since we only partially diminished the fibrotic response, we are not looking for a complete cessation of transcription related to fibrosis, and therefore may need a more homogenous population to identify minor but significant changes. One potential approach could be generating a mouse with the fluorescent reporter constitutively active in cells with the *Htr2b*$^{fl/fl}$ allele. This would allow

us to sort for 5-HT_{2B}-expressing cells with negative selection for CD45+ hematopoietic cells and CD31+ endothelial cells. We could also alter our breeding strategy such that our control animals express *Tcf21*^{MCM} and the *Rosa26* tdTomato reporter but do not have the *Htr2b*$^{fl/fl}$ allele. This would ensure that all *Tcf21*+ CFs are fluorescent in both the control and experimental groups, but only the experimental group lacks *Htr2b* expression.

Another research question to investigate is the reversibility of 5-HT_{2B} ablation. Tamoxifen administration could be given several days after injury in the periostin Cre model to induce 5-HT_{2B} ablation after the onset of injury. Since our studies show acute changes in scar properties, it is likely that the benefits observed are due to early changes in CF activity. In order to determine temporal requirements to this approach, either late induction in the periostin model or later administration of the 5-HT_{2B} antagonist could be performed.

Since 5-HT signaling plays such a significant role in neurological processes controlling appetite and depression, a systemically restricted antagonist would need to be developed before this 5-HT_{2B} antagonism could proceed as a viable therapy.

Based on our findings of altered collagen processing, a future direction related to 5-HT_{2B} signaling could be to investigate collagen formation and cross-linking in the context of diabetes. It is well established that diabetes results in the formation of advanced glycation end products which function to cross-link proteins and stiffen tissue mechanics [206]. Could this process be inhibited by 5-HT_{2B} antagonism? On a related topic, cross-link breakers have been discovered which reverse the results of advanced glycation end product cross-linking [207]. In our MI models, could we see a relaxation of tissue stiffness through the administration of one such cross-link breaker? If 5-HT_{2B} antagonism is playing a role in collagen cross-linking, it would be interesting to see if the tissue relaxation in these mice would be less than control animals. We would investigate if the mechanics of the cardiac tissue could be improved through alterations in

scar architecture using *ex vivo* mechanical testing such as inflating hearts to measure the strain in the wall or biaxial tissue testing [208]–[211].

Another potential avenue of research would be the role of 5-HT_{2B} in vascular remodeling. Our lab has shown that neointima formation following femoral artery injury is limited by 5-HT_{2B} antagonism (**Figure 6.1**). This result is especially relevant since the femoral injury model provides information about the remodeling process associated with stent placement. Since MI is frequently addressed with initial percutaneous coronary intervention and stent placement, limiting the fibrotic response to stent placement would be an added benefit of 5-HT_{2B} therapy. The wound healing response is generally through to be mediated by smooth muscle cells influenced by inflammatory infiltrate, so this preliminary finding could reveal a novel function of 5-HT_{2B}.

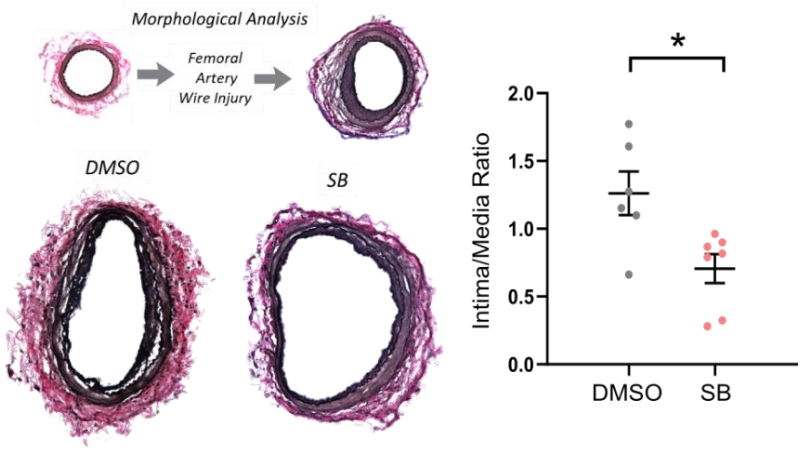

Figure 6.1. 5-HT_{2B} antagonism limits vascular remodeling.
Femoral wire injury causes neointima formation and constriction of the vessel, which is limited by administration of SB.

Collectively, the work presented in this dissertation contributes to the understanding of 5-HT_{2B} function in cardiovascular pathologies, specifically MI. This work applies a variety of tools to garner a better understanding of scar formation which could be applied to other fibrotic

processes. It defines a method to describe the BZ, which is an understudied yet highly important tissue in the context of MI. Lastly, it provides an avenue to investigate a potential therapeutic approach to improve healing after MI with lasting effects.

REFERENCES

[1] S. S. Virani *et al.*, “Heart Disease and Stroke Statistics—2020 Update: A Report From the American Heart Association,” *Circulation*, vol. 141, no. 9, Mar. 2020.

[2] S. Barquera *et al.*, “Global Overview of the Epidemiology of Atherosclerotic Cardiovascular Disease,” *Arch. Med. Res.*, vol. 46, no. 5, pp. 328–338, Jul. 2015.

[3] S. Boateng and T. Sanborn, “Acute myocardial infarction,” *Disease-a-Month*, vol. 59, no. 3, pp. 83–96, Mar. 2013.

[4] M. P. Thomas and E. R. Bates, “Update on primary PCI for patients with STEMI,” *Trends in Cardiovascular Medicine*, vol. 27, no. 2. Elsevier Inc., pp. 95–102, 01-Feb-2017.

[5] D. S. Menees *et al.*, “Door-to-balloon time and mortality among patients undergoing primary PCI,” *N. Engl. J. Med.*, vol. 369, no. 10, pp. 901–909, 2013.

[6] J. O. Mudd and D. A. Kass, “Tackling heart failure in the twenty-first century,” *Nature*, vol. 451, no. 7181, pp. 919–928, Feb. 2008.

[7] S. Doroudgar *et al.*, “S100A4 protects the myocardium against ischemic stress,” *J. Mol. Cell. Cardiol.*, vol. 100, pp. 54–63, Nov. 2016.

[8] L. N. Sanders *et al.*, “BMP Antagonist Gremlin 2 Limits Inflammation After Myocardial Infarction.,” *Circ. Res.*, vol. 119, no. 3, pp. 434–49, Jul. 2016.

[9] S. D. Prabhu and N. G. Frangogiannis, “The Biological Basis for Cardiac Repair After Myocardial Infarction: From Inflammation to Fibrosis.,” *Circ. Res.*, vol. 119, no. 1, pp. 91–112, Jun. 2016.

[10] K. D. Boudoulas and A. K. Hatzopoulos, “Cardiac repair and regeneration: the Rubik’s cube of cell therapy for heart disease.,” *Dis. Model. Mech.*, vol. 2, pp. 344–358, 2009.

[11] A. V Shinde and N. G. Frangogiannis, “Fibroblasts in myocardial infarction: a role in inflammation and repair.,” *J. Mol. Cell. Cardiol.*, vol. 70, pp. 74–82, May 2014.

[12] A. K. Schroer *et al.*, “Cadherin-11 blockade reduces inflammation-driven fibrotic remodeling and improves outcomes after myocardial infarction,” *JCI Insight*, vol. 4, no. 18, Sep. 2019.

[13] X. Fu *et al.*, “Specialized fibroblast differentiated states underlie scar formation in the infarcted mouse heart,” *J. Clin. Invest.*, vol. 128, no. 5, pp. 2127–2143, May 2018.

[14] M. J. Daseke, M. A. A. Tenkorang, U. Chalise, S. R. Konfrst, and M. L. Lindsey, “Cardiac fibroblast activation during myocardial infarction wound healing,” *Matrix Biol.*, vol. 91–92, pp. 109–116, Sep. 2020.

[15] L. Li, Q. Zhao, and W. Kong, “Extracellular matrix remodeling and cardiac fibrosis,” *Matrix Biol.*, vol. 68–69, pp. 490–506, Aug. 2018.

[16] V. Talman and H. Ruskoaho, “Cardiac fibrosis in myocardial infarction—from repair and remodeling to regeneration,” *Cell Tissue Res.*, vol. 365, no. 3, pp. 563–581, Sep. 2016.

[17] B. M. Jackson *et al.*, “Border zone geometry increases wall stress after myocardial infarction: contrast echocardiographic assessment,” *Am. J. Physiol. Circ. Physiol.*, vol. 284, no. 2, pp. H475–H479, Feb. 2003.

[18] P. M. Ridker *et al.*, “Antiinflammatory Therapy with Canakinumab for Atherosclerotic Disease,” *N. Engl. J. Med.*, vol. 377, no. 12, pp. 1119–1131, Sep. 2017.

[19] P. W. Armstrong *et al.*, “PexeLizumab for Acute ST-elevation myocardial infarction in patients undergoing primary percutaneous coronary intervention: A randomized controlled trial,” *J. Am. Med. Assoc.*, vol. 297, no. 1, pp. 43–51, Jan. 2007.

[20] S. J. Nicholls *et al.*, “Varespladib and cardiovascular events in patients with an acute coronary syndrome: The VISTA-16 randomized clinical trial,” *JAMA - J. Am. Med. Assoc.*, vol. 311, no. 3, pp. 252–262, Jan. 2014.

[21] C. B. Granger and A. Kochar, “Understanding and Targeting Inflammation in Acute Myocardial Infarction: An Elusive Goal ∗,” *Journal of the American College of Cardiology*, vol. 72, no. 2. Elsevier USA, pp. 199–201, 10-Jul-2018.

[22] P. T. O’Gara *et al.*, “2013 ACCF/AHA guideline for the management of ST-elevation myocardial infarction: Executive summary: A report of the American College of Cardiology Foundation/American Heart Association Task Force on practice guidelines,” *Circulation*, vol. 127, no. 4. Lippincott Williams & Wilkins Hagerstown, MD, pp. 529–555, 29-Jan-2013.

[23] K. T. Weber, Y. Sun, S. K. Bhattacharya, R. A. Ahokas, and I. C. Gerling, “Myofibroblast-mediated mechanisms of pathological remodelling of the heart,” *Nat. Rev. Cardiol.*, vol. 10, no. 1, pp. 15–26, Jan. 2013.

[24] S. Mann, A. Bajulaiye, K. Sturgeon, A. Sabri, G. Muthukumaran, and J. R. Libonati, “Effects of acute angiotensin II on ischemia reperfusion injury following myocardial infarction,” *J. Renin-Angiotensin-Aldosterone Syst.*, vol. 16, no. 1, pp. 13–22, Mar. 2015.

[25] W. C. Winkelmayer, M. A. Fischer, S. Schneeweiss, R. Levin, and J. Avorn, “Angiotensin inhibition after myocardial infarction: does drug class matter?,” *J. Gen. Intern. Med.*, vol. 21, no. 12, pp. 1242–7, Dec. 2006.

[26] J. H. Lee *et al.*, “Angiotensin II type 1 receptor blockers as a first choice in patients with acute myocardial infarction.,” *Korean J. Intern. Med.*, vol. 31, no. 2, pp. 267–76, Mar. 2016.

[27] J. J. Park *et al.*, “Effect of β-Blockers Beyond 3 Years After Acute Myocardial Infarction,” *J. Am. Heart Assoc.*, vol. 7, no. 5, p. e007567, Mar. 2018.

[28] R. B. Rothman *et al.*, “Evidence for Possible Involvement of 5-HT $_{2B}$ Receptors in the Cardiac Valvulopathy Associated With Fenfluramine and Other Serotonergic Medications,” *Circulation*, vol. 102, no. 23, pp. 2836–2841, Dec. 2000.

[29] B. L. Roth, “Drugs and Valvular Heart Disease,” *N. Engl. J. Med.*, vol. 356, no. 1, pp. 6–9, Jan. 2007.

[30] C. S. Elangbam *et al.*, “5-Hydroxytryptamine (5HT)-induced valvulopathy: Compositional valvular alterations are associated with 5HT2B receptor and 5HT transporter transcript changes in Sprague-Dawley rats,” *Exp. Toxicol. Pathol.*, vol. 60, pp. 253–262, 2008.

[31] J. D. Hutcheson, L. M. Ryzhova, V. Setola, and W. D. Merryman, “5-HT(2B) antagonism arrests non-canonical TGF-β1-induced valvular myofibroblast differentiation.,” *J. Mol. Cell. Cardiol.*, vol. 53, no. 5, pp. 707–14, Nov. 2012.

[32] J.-M. Launay *et al.*, “Serotonin 5-HT2B receptors are required for bone-marrow

contribution to pulmonary arterial hypertension," *Blood*, vol. 119, no. 7, 2012.

[33] N. C. Bloodworth *et al.*, "Bone Marrow–Derived Proangiogenic Cells Mediate Pulmonary Arteriole Stiffening via Serotonin 2B Receptor Dependent Mechanism," *Circ. Res.*, vol. 123, no. 12, pp. e51–e64, Dec. 2018.

[34] C. G. Nebigil *et al.*, "Serotonin 2B receptor is required for heart development.," *Proc. Natl. Acad. Sci. U. S. A.*, vol. 97, no. 17, pp. 9508–13, Aug. 2000.

[35] F. Jaffré *et al.*, "Serotonin and angiotensin receptors in cardiac fibroblasts coregulate adrenergic-dependent cardiac hypertrophy," *Circ. Res.*, vol. 104, no. 1, pp. 113–123, 2009.

[36] B. I. Gustafsson, O. Hauso, I. Drozdov, M. Kidd, and I. M. Modlin, "Carcinoid heart disease," *Int. J. Cardiol.*, vol. 129, no. 3, pp. 318–324, Oct. 2008.

[37] P. A. Robiolio *et al.*, "Carcinoid Heart Disease," *Circulation*, vol. 92, no. 4, pp. 790–795, Aug. 1995.

[38] J. Davar *et al.*, "Diagnosing and Managing Carcinoid Heart Disease in Patients With Neuroendocrine Tumors," *J. Am. Coll. Cardiol.*, vol. 69, no. 10, pp. 1288–1304, Mar. 2017.

[39] M. Yen and M. B. Ewald, "Toxicity of Weight Loss Agents," *J. Med. Toxicol.*, vol. 8, no. 2, pp. 145–152, Jun. 2012.

[40] H. M. Connolly *et al.*, "Valvular Heart Disease Associated with Fenfluramine–Phentermine," *N. Engl. J. Med.*, vol. 337, no. 9, pp. 581–588, Aug. 1997.

[41] M. A. Khan *et al.*, "The Prevalence of Cardiac Valvular Insufficiency Assessed by Transthoracic Echocardiography in Obese Patients Treated with Appetite-Suppressant Drugs," *N. Engl. J. Med.*, vol. 339, no. 11, pp. 713–718, Sep. 1998.

[42] E. Ayme-Dietrich, R. Lawson, B. Gasser, R. Dallemand, N. Bischoff, and L. Monassier, "Mitral bioprosthesis hypertrophic scaring and native aortic valve fibrosis during benfluorex therapy," *Fundam. Clin. Pharmacol.*, vol. 26, no. 2, pp. 215–218, Apr. 2012.

[43] L. W. Fitzgerald *et al.*, "Possible Role of Valvular Serotonin 5-HT2B Receptors in the Cardiopathy Associated with Fenfluramine," *Mol. Pharmacol.*, vol. 57, no. 1, pp. 75–81, 2000.

[44] J. D. Hutcheson, V. Setola, B. L. Roth, and W. D. Merryman, "Serotonin receptors and heart valve disease--it was meant 2B.," *Pharmacol. Ther.*, vol. 132, no. 2, pp. 146–57, Nov. 2011.

[45] J. Horvath *et al.*, "Severe multivalvular heart disease: A new complication of the ergot derivative dopamine agonists," *Mov. Disord.*, vol. 19, no. 6, pp. 656–662, Jun. 2004.

[46] A. Antonini and W. Poewe, "Fibrotic heart-valve reactions to dopamine-agonist treatment in Parkinson's disease," *Lancet Neurol.*, vol. 6, no. 9, pp. 826–829, Sep. 2007.

[47] R. Zanettini, A. Antonini, G. Gatto, R. Gentile, S. Tesei, and G. Pezzoli, "Valvular Heart Disease and the Use of Dopamine Agonists for Parkinson's Disease," *N. Engl. J. Med.*, vol. 356, no. 1, pp. 39–46, Jan. 2007.

[48] L. Maroteaux *et al.*, "New therapeutic opportunities for 5-HT2 receptor ligands," *Pharmacol. Ther.*, vol. 170, pp. 14–36, 2017.

[49] V. Setola *et al.*, “3,4-methylenedioxymethamphetamine (MDMA, "Ecstasy") induces fenfluramine-like proliferative actions on human cardiac valvular interstitial cells in vitro.,” *Mol. Pharmacol.*, vol. 63, no. 6, pp. 1223–9, Jun. 2003.

[50] M. Weintraub, J. D. Hasday, A. I. Mushlin, and D. H. Lockwood, “A Double-blind Clinical Trial in Weight Control,” *Arch. Intern. Med.*, vol. 144, no. 6, p. 1143, Jun. 1984.

[51] P. K. Chugh and S. Sharma, “Recent advances in the pathophysiology and pharmacological treatment of obesity,” *J. Clin. Pharm. Ther.*, vol. 37, no. 5, pp. 525–535, Oct. 2012.

[52] K. Schmuck, C. Ullmer, H. O. Kalkman, A. Probst, and H. Lübbert, “Activation of Meningeal 5-HT $_{2B}$ Receptors: An Early Step in the Generation of Migraine Headache?,” *Eur. J. Neurosci.*, vol. 8, no. 5, pp. 959–967, May 1996.

[53] K. W. Johnson *et al.*, “Neurogenic dural protein extravasation induced by meta-chlorophenylpiperazine (mCPP) involves nitric oxide and 5-HT 2B receptor activation,” *Cephalalgia*, vol. 23, pp. 117–123, 2003.

[54] A. Antonini, W. Poewe, and C. Perfezionamento, “Fibrotic heart-valve reactions to dopamine-agonist treatment in Parkinson ’ s disease,” vol. 6, no. September, pp. 4–7, 2007.

[55] B. I. Gustafsson *et al.*, “Long-Term Serotonin Administration Induces Heart Valve Disease in Rats,” *Circulation*, vol. 111, no. 12, pp. 1517–1522, Mar. 2005.

[56] S. E. Cremer *et al.*, “Alpha-smooth muscle actin and serotonin receptors 2A and 2B in dogs with myxomatous mitral valve disease,” *Res. Vet. Sci.*, vol. 100, pp. 197–206, 2015.

[57] K. H. Driesbaugh *et al.*, “Serotonin receptor 2B signaling with interstitial cell activation and leaflet remodeling in degenerative mitral regurgitation,” *J. Mol. Cell. Cardiol.*, vol. 115, pp. 94–103, 2018.

[58] M. G. George, L. J. Schieb, C. Ayala, A. Talwalkar, and S. Levant, “Pulmonary Hypertension Surveillance,” *Chest*, vol. 146, no. 2, p. 476, Aug. 2014.

[59] I. R. Preston, “Properly Diagnosing Pulmonary Arterial Hypertension,” *Am. J. Cardiol.*, vol. 111, no. 8, pp. 2C-9C, Apr. 2013.

[60] M. R. MacLean and Y. Dempsie, “The Serotonin Hypothesis of Pulmonary Hypertension Revisited,” Humana Press, Totowa, NJ, 2010, pp. 309–322.

[61] M. Humbert *et al.*, “Survival in incident and prevalent cohorts of patients with pulmonary arterial hypertension,” *Eur. Respir. J.*, vol. 36, no. 3, pp. 549–555, Sep. 2010.

[62] T. Thenappan, J. J. Ryan, and S. L. Archer, “Evolving Epidemiology of Pulmonary Arterial Hypertension,” *Am. J. Respir. Crit. Care Med.*, vol. 186, no. 8, pp. 707–709, Oct. 2012.

[63] J. Gomez-Arroyo *et al.*, “The monocrotaline model of pulmonary hypertension in perspective,” *Am. J. Physiol. Cell. Mol. Physiol.*, vol. 302, no. 4, pp. L363–L369, Feb. 2012.

[64] J. Gomez-Arroyo *et al.*, “A brief overview of mouse models of pulmonary arterial hypertension: problems and prospects,” *Am. J. Physiol. Cell. Mol. Physiol.*, vol. 302, no. 10, pp. L977–L991, May 2012.

[65] N. D. Tsihlis, C. S. Oustwani, A. K. Vavra, Q. Jiang, L. K. Keefer, and M. R. Kibbe, “Nitric

Oxide Inhibits Vascular Smooth Muscle Cell Proliferation and Neointimal Hyperplasia by Increasing the Ubiquitination and Degradation of UbcH10," *Cell Biochem. Biophys.*, vol. 60, no. 1–2, pp. 89–97, Jun. 2011.

[66] D. Montani *et al.*, "Targeted therapies in pulmonary arterial hypertension," *Pharmacol. Ther.*, vol. 141, no. 2, pp. 172–191, Feb. 2014.

[67] J. D. West *et al.*, "Serotonin 2B Receptor Antagonism Prevents Heritable Pulmonary Arterial Hypertension.," *PLoS One*, vol. 11, no. 2, p. e0148657, 2016.

[68] E. Soon *et al.*, "Elevated Levels of Inflammatory Cytokines Predict Survival in Idiopathic and Familial Pulmonary Arterial Hypertension," *Circulation*, vol. 122, no. 9, pp. 920–927, Aug. 2010.

[69] H. Matsubara and A. Ogawa, "Treatment of idiopathic/hereditary pulmonary arterial hypertension," *J. Cardiol.*, vol. 64, no. 4, pp. 243–249, Oct. 2014.

[70] A. Macchia *et al.*, "Systematic review of trials using vasodilators in pulmonary arterial hypertension: Why a new approach is needed," *Am. Heart J.*, vol. 159, no. 2, pp. 245–257, Feb. 2010.

[71] A. Macchia *et al.*, "A meta-analysis of trials of pulmonary hypertension: A clinical condition looking for drugs and research methodology," *Am. Heart J.*, vol. 153, no. 6, pp. 1037–1047, Jun. 2007.

[72] M. de Caestecker, "Serotonin Signaling in Pulmonary Hypertension," *Circ. Res.*, vol. 98, no. 10, pp. 1229–1231, May 2006.

[73] J. M. Esteve, J.-M. Launay, O. Kellermann, and L. Maroteaux, "Functions of serotonin in hypoxic pulmonary vascular remodeling," *Cell Biochem. Biophys.*, vol. 47, no. 1, pp. 33–43, Jan. 2007.

[74] P. Herve, C. Dosquet, J.-M. Launay, G. Simonneau, J. Caen, and P. Duroux, "Primary Pulmonary Hypertension in a Patient with a Familial Platelet Storage Pool Disease: Role of Serotonin," *Am. J. Med.*, vol. 89, no. 1, pp. 117–120, 1990.

[75] H. W. Farber and J. Loscalzo, "Pulmonary Arterial Hypertension," *N. Engl. J. Med.*, vol. 351, no. 16, pp. 1655–1665, Oct. 2004.

[76] J.-M. Launay *et al.*, "Function of the serotonin 5-hydroxytryptamine 2B receptor in pulmonary hypertension," *Nat. Med.*, vol. 8, no. 10, pp. 1129–1135, Oct. 2002.

[77] S. Rich, L. Rubin, A. M. Walker, S. Schneeweiss, and L. Abenhaim, "Anorexigens and Pulmonary Hypertension in the United States," *Chest*, vol. 117, no. 3, pp. 870–874, Mar. 2000.

[78] L. Abenhaim *et al.*, "Appetite-Suppressant Drugs and the Risk of Primary Pulmonary Hypertension," *N. Engl. J. Med.*, vol. 335, no. 9, pp. 609–616, Aug. 1996.

[79] C. Guignabert *et al.*, "Serotonin Transporter Inhibition Prevents and Reverses Monocrotaline-Induced Pulmonary Hypertension in Rats," *Circulation*, vol. 111, no. 21, pp. 2812–2819, May 2005.

[80] S. L. Porvasnik *et al.*, "PRX-08066, a novel 5-hydroxytryptamine receptor 2B antagonist, reduces monocrotaline-induced pulmonary arterial hypertension and right ventricular hypertrophy in rats.," *J. Pharmacol. Exp. Ther.*, vol. 334, no. 2, pp. 364–72, Aug. 2010.

[81] D. A. Zopf, L. A. A. das Neves, K. J. Nikula, J. Huang, P. B. Senese, and M. R. Gralinski, “C-122, a novel antagonist of serotonin receptor 5-HT2B, prevents monocrotaline-induced pulmonary arterial hypertension in rats,” *Eur. J. Pharmacol.*, vol. 670, no. 1, pp. 195–203, Nov. 2011.

[82] S. J. Callebert *et al.*, “Evidence for a Control of Plasma Serotonin Levels by 5-Hydroxytryptamine 2B Receptors in Mice,” *J. Pharmacol. Exp. Ther.*, vol. 317, no. 2, pp. 724–731, 2006.

[83] J. M. Launay, S. Loric, V. Mutel, and O. Kellermann, “The 5-HT2B Receptor Controls the Overall 5-HT Transport System in the 1C11 Serotonergic Cell Line,” *Ann. N. Y. Acad. Sci.*, vol. 861, no. 1 ADVANCES IN S, pp. 247–247, Dec. 1998.

[84] M. S. Yavarone, D. L. Shuey, H. Tamir, T. W. Sadler, and J. M. Lauder, “Serotonin and cardiac morphogenesis in the mouse embryo,” *Teratology*, vol. 47, no. 6, pp. 573–584, Jun. 1993.

[85] C. G. Nebigil *et al.*, “Ablation of serotonin 5-HT(2B) receptors in mice leads to abnormal cardiac structure and function.,” *Circulation*, vol. 103, no. 24, pp. 2973–9, Jun. 2001.

[86] C. G. Nebigil, J.-M. Launay, P. Hickel, C. Tournois, and L. Maroteaux, “5-Hydroxytryptamine 2B receptor regulates cell-cycle progression: Cross-talk with tyrosine kinase pathways,” *Proc. Natl. Acad. Sci.*, vol. 97, no. 6, pp. 2591–2596, Mar. 2000.

[87] C. G. Nebigil *et al.*, “Overexpression of the Serotonin 5-HT 2B Receptor in Heart Leads to Abnormal Mitochondrial Function and Cardiac Hypertrophy,” *Circulation*, vol. 107, no. 25, pp. 3223–3229, Jul. 2003.

[88] C. G. Nebigil and L. Maroteaux, “Functional Consequence of Serotonin/5-HT 2B Receptor Signaling in Heart,” *Circulation*, vol. 108, no. 7, pp. 902–908, Aug. 2003.

[89] E. Calama, M. M. Fernández, A. Morán, M. Martín, and L. San Román, “Vasodilator and vasoconstrictor responses induced by 5-hydroxytryptamine in the in situ blood autoperfused hindquarters of the anesthetized rat,” *Naunyn. Schmiedebergs. Arch. Pharmacol.*, vol. 366, pp. 110–116, 2002.

[90] S. W. Watts and G. D. Fink, “5-HT $_{2B}$ -receptor antagonist LY-272015 is antihypertensive in DOCA-salt-hypertensive rats,” *Am. J. Physiol. Circ. Physiol.*, vol. 276, no. 3, pp. H944–H952, Mar. 1999.

[91] Y. Liu *et al.*, “Inhibition of 5-Hydroxytryptamine Receptor 2B Reduced Vascular Restenosis and Mitigated the β-Arrestin2-Mammalian Target of Rapamycin/p70S6K Pathway.,” *J. Am. Heart Assoc.*, vol. 7, no. 3, p. e006810, Jan. 2018.

[92] F. Jaffré *et al.*, “Involvement of the serotonin 5-HT2B receptor in cardiac hypertrophy linked to sympathetic stimulation: control of interleukin-6, interleukin-1beta, and tumor necrosis factor-alpha cytokine production by ventricular fibroblasts.,” *Circulation*, vol. 110, no. 8, pp. 969–74, Aug. 2004.

[93] C.-F. Bai *et al.*, “Role of 5-HT2B receptors in cardiomyocyte apoptosis in noradrenaline-induced cardiomyopathy in rats,” *Clin. Exp. Pharmacol. Physiol.*, vol. 37, no. 7, pp. e145–e151, Mar. 2010.

[94] L. Monassier, M.-A. Laplante, F. Jaffré, P. Bousquet, L. Maroteaux, and J. de Champlain, “Serotonin 5-HT(2B) receptor blockade prevents reactive oxygen species-induced cardiac hypertrophy in mice.,” *Hypertens. (Dallas, Tex. 1979)*, vol. 52, no. 2, pp. 301–7, Aug.

2008.

[95] W. Janssen *et al.*, “5-HT2B Receptor Antagonists Inhibit Fibrosis and Protect from RV Heart Failure,” *Biomed Res. Int.*, vol. 2015, pp. 1–8, 2015.

[96] Y. Liang *et al.*, “Mechanical stress enhances serotonin 2B receptor modulating brain natriuretic peptide through nuclear factor-κB in cardiomyocytes,” *Cardiovasc. Res.*, vol. 72, no. 2, pp. 303–312, Nov. 2006.

[97] E. Ayme-Dietrich *et al.*, “Contribution of serotonin to cardiac remodeling associated with hypertensive diastolic ventricular dysfunction in rats,” *J. Hypertens.*, vol. 33, no. 11, pp. 2310–2321, Nov. 2015.

[98] P. Manivet *et al.*, “The serotonin binding site of human and murine 5-HT2B receptors: molecular modeling and site-directed mutagenesis.,” *J. Biol. Chem.*, vol. 277, no. 19, pp. 17170–8, May 2002.

[99] R. B. Rothman *et al.*, “Evidence for Possible Involvement of 5-HT $_{2B}$ Receptors in the Cardiac Valvulopathy Associated With Fenfluramine and Other Serotonergic Medications,” *Circulation*, vol. 102, no. 23, pp. 2836–2841, Dec. 2000.

[100] H. Feng *et al.*, “Activation of Rac1 by Src-dependent phosphorylation of Dock180(Y1811) mediates PDGFRα-stimulated glioma tumorigenesis in mice and humans.,” *J. Clin. Invest.*, vol. 121, no. 12, pp. 4670–84, Dec. 2011.

[101] Q. Shen *et al.*, “MUC1 Initiates Src-CrkL-Rac1/Cdc42-Mediated Actin Cytoskeletal Protrusive Motility after Ligating Intercellular Adhesion Molecule-1,” *Mol. Cancer Res.*, vol. 6, no. 4, pp. 555–567, Mar. 2008.

[102] J. D. Molkentin *et al.*, “Fibroblast-Specific Genetic Manipulation of p38 Mitogen-Activated Protein Kinase In Vivo Reveals Its Central Regulatory Role in Fibrosis.,” *Circulation*, vol. 136, no. 6, pp. 549–561, Aug. 2017.

[103] M. J. Daseke, F. M. Valerio, W. J. Kalusche, Y. Ma, K. Y. DeLeon-Pennell, and M. L. Lindsey, “Neutrophil proteome shifts over the myocardial infarction time continuum,” *Basic Res. Cardiol.*, vol. 114, no. 5, p. 37, Sep. 2019.

[104] G. Bajpai *et al.*, “Tissue Resident CCR2− and CCR2+ Cardiac Macrophages Differentially Orchestrate Monocyte Recruitment and Fate Specification Following Myocardial Injury,” *Circ. Res.*, vol. 124, no. 2, pp. 263–278, Jan. 2019.

[105] E. Gao *et al.*, “A Novel and Efficient Model of Coronary Artery Ligation and Myocardial Infarction in the Mouse,” *Circ. Res.*, vol. 107, no. 12, pp. 1445–1453, Dec. 2010.

[106] L. Wu *et al.*, “IL-10–producing B cells are enriched in murine pericardial adipose tissues and ameliorate the outcome of acute myocardial infarction,” *Proc. Natl. Acad. Sci. U. S. A.*, vol. 116, no. 43, pp. 21673–21684, Oct. 2019.

[107] H. Lal *et al.*, “Cardiac fibroblast glycogen synthase kinase-3β regulates ventricular remodeling and dysfunction in ischemic heart.,” *Circulation*, vol. 130, no. 5, pp. 419–30, Jul. 2014.

[108] D. W. Bonhaus *et al.*, “RS-127445: a selective, high affinity, orally bioavailable 5-HT 2B receptor antagonist,” *Br. J. Pharmacol.*, vol. 127, no. 5, pp. 1075–1082, Jul. 1999.

[109] A. J. Yezzi and J. L. Prince, “An Eulerian PDE Approach for Computing Tissue

Thickness," *IEEE Trans. Med. Imaging*, vol. 22, no. 10, pp. 1332–1339, Oct. 2003.

[110] M. R. Bersi, R. Khosravi, A. J. Wujciak, D. G. Harrison, and J. D. Humphrey, "Differential cell-matrix mechanoadaptations and inflammation drive regional propensities to aortic fibrosis, aneurysm or dissection in hypertension," *J. R. Soc. Interface*, vol. 14, no. 136, p. 20170327, Nov. 2017.

[111] G. Cox, E. Kable, A. Jones, I. Fraser, F. Manconi, and M. D. Gorrell, "3-Dimensional imaging of collagen using second harmonic generation," *J. Struct. Biol.*, vol. 141, no. 1, pp. 53–62, Jan. 2003.

[112] S. R. Watson, P. Liu, E. A. Peña, M. A. Sutton, J. F. Eberth, and S. M. Lessner, "Comparison of Aortic Collagen Fiber Angle Distribution in Mouse Models of Atherosclerosis Using Second-Harmonic Generation (SHG) Microscopy," *Microsc. Microanal.*, vol. 22, no. 1, pp. 55–62, Feb. 2016.

[113] W. Adams *et al.*, "Multimodal Nonlinear Optical and Thermal Imaging Platform for Label-Free Characterization of Biological Tissue," *bioRxiv*, p. Preprint posted online August 28, 2020, Apr. 2020.

[114] Z. Püspöki, M. Storath, D. Sage, and M. Unser, "Transforms and operators for directional bioimage analysis: A survey," *Adv. Anat. Embryol. Cell Biol.*, vol. 219, pp. 69–93, 2016.

[115] X. Chen, O. Nadiarynkh, S. Plotnikov, and P. J. Campagnola, "Second harmonic generation microscopy for quantitative analysis of collagen fibrillar structure," *Nat. Protoc.*, vol. 7, no. 4, pp. 654–669, Apr. 2012.

[116] A. J. Schriefl, H. Wolinski, P. Regitnig, S. D. Kohlwein, and G. A. Holzapfel, "An automated approach for three-dimensional quantification of fibrillar structures in optically cleared soft biological tissues," *J. R. Soc. Interface*, vol. 10, no. 80, pp. 20120760–20120760, Dec. 2012.

[117] T. R. Jones *et al.*, "CellProfiler Analyst: Data exploration and analysis software for complex image-based screens," *BMC Bioinformatics*, vol. 9, no. 1, p. 482, Nov. 2008.

[118] E. B. Schelbert, J. Butler, and J. Diez, "Why Clinicians Should Care About the Cardiac Interstitium," *JACC Cardiovasc. Imaging*, vol. 12, no. 11, pp. 2305–2318, Nov. 2019.

[119] F. K. Swirski and M. Nahrendorf, "Cardioimmunology: the immune system in cardiac homeostasis and disease," *Nat. Rev. Immunol.*, p. 1, Sep. 2018.

[120] C. Humeres and N. G. Frangogiannis, "Fibroblasts in the Infarcted, Remodeling, and Failing Heart.," *JACC. Basic to Transl. Sci.*, vol. 4, no. 3, pp. 449–467, Jun. 2019.

[121] M. Reindl *et al.*, "Global longitudinal strain by feature tracking for optimized prediction of adverse remodeling after ST-elevation myocardial infarction," *Clin. Res. Cardiol.*, pp. 1–11, Apr. 2020.

[122] M. Reindl *et al.*, "Prognostic Implications of Global Longitudinal Strain by Feature-Tracking Cardiac Magnetic Resonance in ST-Elevation Myocardial Infarction.," *Circ. Cardiovasc. Imaging*, vol. 12, no. 11, p. e009404, Nov. 2019.

[123] A. Gonzalez, B. Lopez, S. Ravassa, G. San Jose, and J. Diez, "The complex dynamics of myocardial interstitial fibrosis in heart failure. Focus on collagen cross-linking," *BBA - Mol. Cell Res.*, vol. 1866, no. 9, pp. 1421–1432, 2019.

[124] K. Toischer *et al.*, “Differential cardiac remodeling in preload versus afterload,” *Circulation*, vol. 122, no. 10, pp. 993–1003, Sep. 2010.

[125] M. Jung *et al.*, “IL-10 improves cardiac remodeling after myocardial infarction by stimulating M2 macrophage polarization and fibroblast activation,” *Basic Res. Cardiol.*, vol. 112, no. 3, p. 33, May 2017.

[126] F. Ahmad *et al.*, “Cardiomyocyte-Specific Deletion of Gsk3α Mitigates Post–Myocardial Infarction Remodeling, Contractile Dysfunction, and Heart Failure,” *J. Am. Coll. Cardiol.*, vol. 64, no. 7, pp. 696–706, 2014.

[127] S. A. Dick *et al.*, “Self-renewing resident cardiac macrophages limit adverse remodeling following myocardial infarction,” *Nat. Immunol.*, vol. 20, no. 1, pp. 29–39, Jan. 2019.

[128] A. Fabre *et al.*, “Modulation of bleomycin-induced lung fibrosis by serotonin receptor antagonists in mice,” *Eur. Respir. J.*, vol. 32, no. 2, pp. 426–436, Aug. 2008.

[129] M. P. E. Wenger, L. Bozec, M. A. Horton, and P. Mesquidaz, “Mechanical properties of collagen fibrils,” *Biophys. J.*, vol. 93, no. 4, pp. 1255–1263, Aug. 2007.

[130] J. W. Holmes, Z. Laksman, L. Gepstein, and J. Holmes, “Making Better Scar: Emerging Approaches for Modifying Mechanical and Electrical Properties Following Infarction and Ablation HHS Public Access,” *Prog Biophys Mol Biol. Prog Biophys Mol Biol*, vol. 120, no. 3, pp. 134–148, 2016.

[131] G. M. Fomovsky and J. W. Holmes, “Evolution of scar structure, mechanics, and ventricular function after myocardial infarction in the rat.,” *Am. J. Physiol. Heart Circ. Physiol.*, vol. 298, no. 1, pp. H221-8, Jan. 2010.

[132] A. R. Pinto *et al.*, “Revisiting Cardiac Cellular Composition,” *Circ. Res.*, vol. 118, no. 3, pp. 400–409, Feb. 2016.

[133] I. Valiente-Alandi *et al.*, “Inhibiting Fibronectin Attenuates Fibrosis and Improves Cardiac Function in a Model of Heart Failure,” *Circulation*, vol. 138, no. 12, pp. 1236–1252, Sep. 2018.

[134] C. K. Nagaraju *et al.*, “Global fibroblast activation throughout the left ventricle but localized fibrosis after myocardial infarction,” *Sci. Reports 2017 71*, vol. 7, no. 1, p. 10801, Sep. 2017.

[135] A. Acharya *et al.*, “The bHLH transcription factor Tcf21 is required for lineage-specific EMT of cardiac fibroblast progenitors.,” *Development*, vol. 139, no. 12, pp. 2139–49, Jun. 2012.

[136] A. Wessels *et al.*, “Epicardially derived fibroblasts preferentially contribute to the parietal leaflets of the atrioventricular valves in the murine heart,” *Dev. Biol.*, vol. 366, no. 2, pp. 111–124, Jun. 2012.

[137] C.-L. Cai *et al.*, “A myocardial lineage derives from Tbx18 epicardial cells,” *Nature*, vol. 454, no. 7200, pp. 104–108, Jul. 2008.

[138] P. Snider, K. N. Standley, J. Wang, M. Azhar, T. Doetschman, and S. J. Conway, “Origin of cardiac fibroblasts and the role of periostin.,” *Circ. Res.*, vol. 105, no. 10, pp. 934–47, Nov. 2009.

[139] O. Kanisicak *et al.*, “Genetic lineage tracing defines myofibroblast origin and function in

the injured heart.," *Nat. Commun.*, vol. 7, p. 12260, 2016.

[140] D. A. Chistiakov, A. N. Orekhov, and Y. V. Bobryshev, "The role of cardiac fibroblasts in post-myocardial heart tissue repair," *Exp. Mol. Pathol.*, vol. 101, no. 2, pp. 231–240, Oct. 2016.

[141] D. T. Paik *et al.*, "Wnt10b gain-of-function improves cardiac repair by arteriole formation and attenuation of fibrosis," *Circ. Res.*, vol. 117, no. 9, pp. 804–816, Oct. 2015.

[142] S. van Putten, Y. Shafieyan, and B. Hinz, "Mechanical control of cardiac myofibroblasts," *J. Mol. Cell. Cardiol.*, vol. 93, pp. 133–142, 2016.

[143] A. Belmer *et al.*, "Positive regulation of raphe serotonin neurons by serotonin 2B receptors," *Neuropsychopharmacology*, vol. 43, no. 7, pp. 1623–1632, Jun. 2018.

[144] A. Acharya, S. T. Baek, S. Banfi, B. Eskiocak, and M. D. Tallquist, "Efficient inducible Cre-mediated recombination in Tcf21cell lineages in the heart and kidney," *genesis*, vol. 49, no. 11, pp. 870–877, Nov. 2011.

[145] J. Davis *et al.*, "MBNL1-mediated regulation of differentiation RNAs promotes myofibroblast transformation and the fibrotic response," *Nat. Commun.*, vol. 6, no. 1, pp. 1–14, Dec. 2015.

[146] R. B. Driesen *et al.*, "Reversible and irreversible differentiation of cardiac fibroblasts.," *Cardiovasc. Res.*, vol. 101, no. 3, pp. 411–22, Mar. 2014.

[147] K. M. Herum, J. Choppe, A. Kumar, A. J. Engler, and A. D. McCulloch, "Mechanical regulation of cardiac fibroblast profibrotic phenotypes," *Mol. Biol. Cell*, vol. 28, no. 14, pp. 1871–1882, Jul. 2017.

[148] D. S. Sohal *et al.*, "Temporally Regulated and Tissue-Specific Gene Manipulations in the Adult and Embryonic Heart Using a Tamoxifen-Inducible Cre Protein," *Circ. Res.*, vol. 89, no. 1, pp. 20–25, Jul. 2001.

[149] T. Doetschman and M. Azhar, "Cardiac-specific inducible and conditional gene targeting in mice," *Circulation Research*, vol. 110, no. 11. Lippincott Williams & WilkinsHagerstown, MD, pp. 1498–1512, 25-May-2012.

[150] E. Ayme-Dietrich *et al.*, "The role of 5-HT $_{2B}$ receptors in mitral valvulopathy: bone marrow mobilization of endothelial progenitors," *Br. J. Pharmacol.*, vol. 174, no. 22, pp. 4123–4139, Nov. 2017.

[151] J. Patel, G. Douglas, A. G. Kerr, A. B. Hale, and K. M. Channon, "Effect of irradiation and bone marrow transplantation on angiotensin II-induced aortic inflammation in ApoE knockout mice.," *Atherosclerosis*, vol. 276, pp. 74–82, Jul. 2018.

[152] T. Moore-Morris *et al.*, "Infarct Fibroblasts Do Not Derive From Bone Marrow Lineages," *Circ. Res.*, vol. 122, no. 4, pp. 583–590, Feb. 2018.

[153] E. Kolaczkowska and P. Kubes, "Neutrophil recruitment and function in health and inflammation," *Nature Reviews Immunology*, vol. 13, no. 3. Nature Publishing Group, pp. 159–175, 25-Mar-2013.

[154] L. He *et al.*, "Preexisting endothelial cells mediate cardiac neovascularization after injury," *J. Clin. Invest.*, vol. 127, no. 8, pp. 2968–2981, Jun. 2017.

[155] O. Aisagbonhi, M. Rai, S. Ryzhov, N. Atria, I. Feoktistov, and A. K. Hatzopoulos,

"Experimental myocardial infarction triggers canonical Wnt signaling and endothelial-to-mesenchymal transition.," *Dis. Model. Mech.*, vol. 4, no. 4, pp. 469–483, 2011.

[156] P. V. Avdonin, A. D. Nadeev, G. Y. Mironova, I. L. Zharkikh, P. P. Avdonin, and N. V. Goncharov, "Enhancement by Hydrogen Peroxide of Calcium Signals in Endothelial Cells Induced by 5-HT1B and 5-HT2B Receptor Agonists," *Oxid. Med. Cell. Longev.*, vol. 2019, 2019.

[157] A. Anzai *et al.*, "The infarcted myocardium solicits GM-CSF for the detrimental oversupply of inflammatory leukocytes," *J. Exp. Med.*, vol. 214, no. 11, pp. 3293–3310, Nov. 2017.

[158] A. Saxena *et al.*, "IL-1 induces proinflammatory leukocyte infiltration and regulates fibroblast phenotype in the infarcted myocardium.," *J. Immunol.*, vol. 191, no. 9, pp. 4838–48, Nov. 2013.

[159] N. G. Frangogiannis *et al.*, "Resident Cardiac Mast Cells Degranulate and Release Preformed TNF-α, Initiating the Cytokine Cascade in Experimental Canine Myocardial Ischemia/Reperfusion," *Circulation*, vol. 98, no. 7, pp. 699–710, Aug. 1998.

[160] J. Davis and J. D. Molkentin, "Myofibroblasts: Trust your heart and let fate decide," *J. Mol. Cell. Cardiol.*, vol. 70, pp. 9–18, 2014.

[161] A. Petersen, P. Joly, C. Bergmann, G. Korus, and G. N. Duda, "The Impact of Substrate Stiffness and Mechanical Loading on Fibroblast-Induced Scaffold Remodeling," *Tissue Eng. Part A*, vol. 18, no. 17–18, pp. 1804–1817, 2012.

[162] B. Hinz, "It has to be the αv: myofibroblast integrins activate latent TGF-β1," *Nat. Med.*, vol. 19, no. 12, pp. 1567–1568, 2013.

[163] K. A. Detillieux, F. Sheikh, E. Kardami, and P. A. Cattini, "Biological activities of fibroblast growth factor-2 in the adult myocardium," *Cardiovascular Research*, vol. 57, no. 1. Oxford Academic, pp. 8–19, 01-Jan-2003.

[164] P. Stawowy *et al.*, "Regulation of matrix metalloproteinase MT1-MMP/MMP-2 in cardiac fibroblasts by TGF-β1 involves furin-convertase," *Cardiovasc. Res.*, vol. 63, no. 1, pp. 87–97, Jul. 2004.

[165] K. Hayakawa *et al.*, "Inhibition of granulation tissue cell apoptosis during the subacute stage of myocardial infarction improves cardiac remodeling and dysfunction at the chronic stage," *Circulation*, vol. 108, no. 1, pp. 104–109, Jul. 2003.

[166] A. Slominski, A. Pisarchik, B. Zbytek, D. J. Tobin, S. Kauser, and J. Wortsman, "Functional activity of serotoninergic and melatoninergic systems expressed in the skin," *J. Cell. Physiol.*, vol. 196, no. 1, pp. 144–153, Jul. 2003.

[167] M. R. Ebrahimkhani *et al.*, "Stimulating healthy tissue regeneration by targeting the 5-HT 2B receptor in chronic liver disease," *Nat. Med.*, vol. 17, no. 12, pp. 1668–1673, Dec. 2011.

[168] I. Moutkine, E. L. Collins, C. Béchade, and L. Maroteaux, "Evolutionary considerations on 5-HT2 receptors," *Pharmacol. Res.*, vol. 140, pp. 14–20, Feb. 2019.

[169] R. M. Gallucci, E. G. Lee, and J. J. Tomasek, "IL-6 Modulates Alpha-Smooth Muscle Actin Expression in Dermal Fibroblasts from IL-6-Deficient Mice," *J. Invest. Dermatol.*, vol. 126, no. 3, pp. 561–568, 2006.

[170] M. Chatzifrangkeskou *et al.*, “ERK1/2 directly acts on CTGF/CCN2 expression to mediate myocardial fibrosis in cardiomyopathy caused by mutations in the lamin A/C gene,” *Hum. Mol. Genet.*, vol. 25, no. 11, pp. 2220–2233, Jun. 2016.

[171] J. E. Joll II, C. R. Clark, C. S. Peters, M. A. Raddatz, M. R. Bersi, and W. D. Merryman, “Genetic ablation of serotonin receptor 2B improves aortic valve hemodynamics in a high-cholesterol diet mouse model,” *bioRxiv*, p. Preprint posted online August 18, 2020, Aug. 2020.

[172] J. R. Tse, A. J. Engler, J. R. Tse, and A. J. Engler, “Preparation of Hydrogel Substrates with Tunable Mechanical Properties,” in *Current Protocols in Cell Biology*, Hoboken, NJ, USA: John Wiley & Sons, Inc., 2010, pp. 10.16.1-10.16.16.

[173] M. L. Lindsey, “Assigning matrix metalloproteinase roles in ischaemic cardiac remodelling,” *Nature Reviews Cardiology*, vol. 15, no. 8. Nature Publishing Group, pp. 471–479, 01-Aug-2018.

[174] M. Dobaczewski *et al.*, “Smad3 signaling critically regulates fibroblast phenotype and function in healing myocardial infarction.,” *Circ. Res.*, vol. 107, no. 3, pp. 418–28, Aug. 2010.

[175] M. J. Ivey, J. T. Kuwabara, J. T. Pai, R. E. Moore, Z. Sun, and M. D. Tallquist, “Resident fibroblast expansion during cardiac growth and remodeling,” *J. Mol. Cell. Cardiol.*, vol. 114, pp. 161–174, Jan. 2018.

[176] S. R. Ali *et al.*, “Developmental Heterogeneity of Cardiac Fibroblasts Does Not Predict Pathological Proliferation and Activation,” *Circ. Res.*, vol. 115, no. 7, pp. 625–635, Sep. 2014.

[177] M. Nakaya *et al.*, “Cardiac myofibroblast engulfment of dead cells facilitates recovery after myocardial infarction,” *J. Clin. Invest.*, vol. 127, no. 1, pp. 383–401, Dec. 2016.

[178] J. M. Swonger, J. S. Liu, M. J. Ivey, and M. D. Tallquist, “Genetic tools for identifying and manipulating fibroblasts in the mouse.,” *Differentiation*, vol. 92, no. 3, pp. 66–83, Sep. 2016.

[179] A. F. Vega-Benedetti *et al.*, “PLAGL1 gene function during hepatoma cells proliferation,” *Oncotarget*, vol. 9, no. 67, pp. 32775–32794, Aug. 2018.

[180] D. Hassel *et al.*, “Nexilin mutations destabilize cardiac Z-disks and lead to dilated cardiomyopathy,” *Nat. Med.*, vol. 15, no. 11, pp. 1281–1288, 2009.

[181] T. Acun *et al.*, “HLJ1 (DNAJB4) Gene Is a Novel Biomarker Candidate in Breast Cancer,” *Omi. A J. Integr. Biol.*, vol. 21, no. 5, pp. 257–265, May 2017.

[182] M. E. Baardman *et al.*, “Common arterial trunk and ventricular non-compaction in Lrp2 knockout mice indicate a crucial role of LRP2 in cardiac development,” *DMM Dis. Model. Mech.*, vol. 9, no. 4, pp. 413–425, Apr. 2016.

[183] C. Faul, “Cardiac actions of fibroblast growth factor 23,” *Bone*, vol. 100. Elsevier Inc., pp. 69–79, 01-Jul-2017.

[184] R. A. Gould *et al.*, “ROBO4 variants predispose individuals to bicuspid aortic valve and thoracic aortic aneurysm,” *Nature Genetics*, vol. 51, no. 1. Nature Publishing Group, pp. 42–50, 01-Jan-2019.

[185] H. Kaur *et al.*, “Targeted Ablation of Periostin-Expressing Activated Fibroblasts Prevents Adverse Cardiac Remodeling in Mice,” *Circ. Res.*, vol. 118, no. 12, pp. 1906–1917, Jun. 2016.

[186] S. Thavapalachandran *et al.*, “Platelet-derived growth factor-AB improves scar mechanics and vascularity after myocardial infarction,” *Sci. Transl. Med.*, vol. 12, no. 524, p. eaay2140, Jan. 2020.

[187] C. A. Meschiari *et al.*, “Macrophage overexpression of matrix metalloproteinase-9 in aged mice improves diastolic physiology and cardiac wound healing after myocardial infarction,” *Am. J. Physiol. Circ. Physiol.*, vol. 314, no. 2, pp. H224–H235, Feb. 2018.

[188] N. A. van Huizen, J. N. M. Ijzermans, P. C. Burgers, and T. M. Luider, “Collagen analysis with mass spectrometry,” *Mass Spectrometry Reviews*, vol. 39, no. 4. John Wiley and Sons Inc., pp. 309–335, 01-Jul-2020.

[189] P. V. Taufalele, J. A. VanderBurgh, A. Muñoz, M. R. Zanotelli, and C. A. Reinhart-King, “Fiber alignment drives changes in architectural and mechanical features in collagen matrices,” *PLoS One*, vol. 14, no. 5, p. e0216537, May 2019.

[190] L. L. Lee and V. Chintalgattu, “Pericytes in the heart,” in *Advances in Experimental Medicine and Biology*, vol. 1122, Springer, Cham, 2019, pp. 187–210.

[191] S. Nees *et al.*, “Isolation, bulk cultivation, and characterization of coronary microvascular pericytes: The second most frequent myocardial cell type in vitro,” *Am. J. Physiol. - Hear. Circ. Physiol.*, vol. 302, no. 1, Jan. 2012.

[192] R. M. Weiss, J. D. Miller, and D. D. Heistad, “Fibrocalcific aortic valve disease: Opportunity to understand disease mechanisms using mouse models,” *Circ. Res.*, vol. 113, no. 2, pp. 209–222, Jul. 2013.

[193] B. Hinz, S. H. Phan, V. J. Thannickal, A. Galli, M.-L. Bochaton-Piallat, and G. Gabbiani, “The Myofibroblast: One Function, Multiple Origins,” *Am. J. Pathol.*, vol. 170, no. 6, pp. 1807–1816, Jun. 2007.

[194] C. W. Chen *et al.*, “Human pericytes for ischemic heart repair,” *Stem Cells*, vol. 31, no. 2, pp. 305–316, Feb. 2013.

[195] S. Cui, L. Schwartz, and S. E. Quaggin, “Pod1 is required in stromal cells for glomerulogenesis,” *Dev. Dyn.*, vol. 226, no. 3, pp. 512–522, Mar. 2003.

[196] T. Moore-Morris *et al.*, “Resident fibroblast lineages mediate pressure overload–induced cardiac fibrosis,” *J. Clin. Invest.*, vol. 124, no. 7, pp. 2921–2934, Jul. 2014.

[197] C. Frémin, M. K. Saba-El-Leil, K. Lévesque, S. L. Ang, and S. Meloche, “Functional redundancy of ERK1 and ERK2 MAP kinases during development,” *Cell Rep.*, vol. 12, no. 6, pp. 913–921, Aug. 2015.

[198] E. I. Dedkov *et al.*, “Sex-related differences in intrinsic myocardial properties influence cardiac function in middle-aged rats during infarction-induced left ventricular remodeling,” *Physiol. Rep.*, vol. 4, no. 11, p. e12822, Jun. 2016.

[199] D. Grady *et al.*, “Cardiovascular disease outcomes during 6.8 years of hormone therapy: Heart and estrogen/progestin replacement study follow-up (HERS II),” *J. Am. Med. Assoc.*, vol. 288, no. 1, pp. 49–57, Jul. 2002.

[200] J. E. Rossouw *et al.*, “Risks and benefits of estrogen plus progestin in healthy postmenopausal women: Principal results from the women’s health initiative randomized controlled trial,” *J. Am. Med. Assoc.*, vol. 288, no. 3, pp. 321–333, Jul. 2002.

[201] Q. Chen, R. Williams, C. L. Healy, C. D. Wright, S. C. Wu, and T. D. O’Connell, “An association between gene expression and better survival in female mice following myocardial infarction,” *J. Mol. Cell. Cardiol.*, vol. 49, no. 5, pp. 801–811, Nov. 2010.

[202] M. A. Cavasin, Z. Y. Tao, A. L. Yu, and X. P. Yang, “Testosterone enhances early cardiac remodeling after myocardial infarction, causing rupture and degrading cardiac function,” *Am. J. Physiol. - Hear. Circ. Physiol.*, vol. 290, no. 5, May 2006.

[203] T. Songtachalert, C. Roomruangwong, A. F. Carvalho, M. Bourin, and M. Maes, “Anxiety Disorders: Sex Differences in Serotonin and Tryptophan Metabolism,” *Curr. Top. Med. Chem.*, vol. 18, no. 19, pp. 1704–1715, Nov. 2018.

[204] M. Giammanco, G. Tabacchi, S. Giammanco, D. Di Majo, and M. La Guardia, “Testosterone and aggressiveness,” *Medical Science Monitor*, vol. 11, no. 4. Med Sci Monit, Apr-2005.

[205] E. Ayme-Dietrich *et al.*, “Contribution of serotonin to cardiac remodeling associated with hypertensive diastolic ventricular dysfunction in rats.,” *J. Hypertens.*, vol. 33, no. 11, pp. 2310–21, Nov. 2015.

[206] M. Asif *et al.*, “An advanced glycation endproduct cross-link breaker can reverse age-related increases in myocardial stiffness.,” *Proc. Natl. Acad. Sci. U. S. A.*, vol. 97, no. 6, pp. 2809–13, Mar. 2000.

[207] D. Susic, “Cross-link breakers as a new therapeutic approach to cardiovascular disease,” in *Biochemical Society Transactions*, 2007, vol. 35, no. 5, pp. 853–856.

[208] K. L. Fujimoto *et al.*, “An Elastic, Biodegradable Cardiac Patch Induces Contractile Smooth Muscle and Improves Cardiac Remodeling and Function in Subacute Myocardial Infarction,” *J. Am. Coll. Cardiol.*, vol. 49, no. 23, pp. 2292–2300, Jun. 2007.

[209] S. M. Boronyak and W. D. Merryman, “In vitro assessment of a combined radiofrequency ablation and cryo-anchoring catheter for treatment of mitral valve prolapse,” *J. Biomech.*, vol. 47, no. 5, pp. 973–980, 2014.

[210] S. L. Price, C. G. Norwood, J. L. Williams, H. T. McElderry, and W. D. Merryman, “Radiofrequency Ablation Directionally Alters Geometry and Biomechanical Compliance of Mitral Valve Leaflets: Refinement of a Novel Percutaneous Treatment Strategy,” *Cardiovasc. Eng. Technol.*, vol. 1, no. 3, pp. 194–201, Sep. 2010.

[211] S. M. Boronyak and W. D. Merryman, “Development of a Simultaneous Cryo-Anchoring and Radiofrequency Ablation Catheter for Percutaneous Treatment of Mitral Valve Prolapse,” *Ann. Biomed. Eng.*, vol. 40, no. 9, pp. 1971–1981, Sep. 2012.

APPENDIX A

Differentially regulated genes

RNA sequencing revealed a total of 63 differentially regulated genes in PDGFRα+ cells seven days post-MI between *Htr2b*$^{fl/fl}$*Postn*$^{MCM/+}$ mice compared to *Htr2b*$^{fl/fl}$ controls. These genes are listed below, sorted by P-value.

Gene symbol	log2 fold change	P-value
Nexn	1.471576	1.2E-07
Robo4	-2.474	4.39E-07
Jmjd1c	1.138789	8.06E-07
Rock1	1.044832	9.08E-07
Lysmd3	1.386306	1.52E-06
Rbm46	2.472345	1.61E-06
Nktr	1.06835	2.15E-06
Smc5	1.041086	2.94E-06
Cenpf	1.139837	3.74E-06
Ankrd12	1.054677	3.85E-06
Dek	0.971351	5.16E-06
Lmtk3	4.733398	7.69E-06
Zfp948	1.290178	9.29E-06
Arhgap5	1.158358	1.09E-05
Fgl2	1.100437	1.92E-05
Atrx	0.956775	2.46E-05
Zfp280d	1.219905	2.56E-05
Kntc1	1.67433	2.74E-05
Snx13	1.077254	2.96E-05
Osbpl8	0.957838	3.34E-05
Nrip3	4.136591	3.85E-05
Sema4a	1.194405	4.14E-05
Cenpe	1.091765	5.02E-05
Gcc2	1.125511	5.16E-05
Rasal1	-2.15257	5.59E-05
Aspn	1.276485	5.66E-05
Mier1	0.856401	6.09E-05
Glrb	4.026224	6.81E-05
Tmem26	1.920824	7.13E-05
Resf1	1.091209	9.51E-05
Pik3c2a	1.091179	9.68E-05

Plagl1	1.414272	9.93E-05
Mis18bp1	1.529537	9.94E-05
Mybl1	1.699491	0.000104
Lrat	3.31384	0.000104
Dnajb4	0.911883	0.000108
Esco2	1.44808	0.000119
Fgf23	-1.64058	0.000126
Lrrcc1	1.120165	0.000131
Cip2a	1.016491	0.000131
ND4L	0.938987	0.000135
Pcmtd1	0.895613	0.000136
Hecw2	-1.57896	0.000151
Tmed5	1.009144	0.00016
Fnip1	0.90586	0.000163
Sema3d	1.06457	0.000171
Rbm39	0.77975	0.000182
Zfp942	1.422534	0.000183
Vps37a	1.052524	0.000186
Clk1	0.977222	0.00019
Rps3a1	-0.7444	0.000193
H2-Q6	-0.77723	0.000199
Cspp1	1.025785	0.000199
Smc2	0.942901	0.000203
Angpt1	1.229603	0.00021
Gas2l3	1.291994	0.000229
Fam126b	1.470598	0.000233
Ccp110	1.210643	0.000234
Gen1	1.714732	0.000236
Brwd3	1.131081	0.000244
Rn7s1	1.346248	0.000245
Lrp2	-1.47023	0.000246
Ints6	1.469984	0.000249